UNDERSTANDING MESOSCOPIC CHEMO-MECHANICAL DISTRESS AND MITIGATION MECHANISMS OF CONCRETE SUBJECT TO ASR

by

Md Asif Rahman

A thesis

submitted in partial fulfillment

of the requirements for the degree of

Master of Science in Civil Engineering

Boise State University

December 2020

BOISE STATE UNIVERSITY GRADUATE COLLEGE

DEFENSE COMMITTEE AND FINAL READING APPROVALS

of the thesis submitted by

Md Asif Rahman

Thesis Title: Understanding Mesoscopic Chemo-Mechanical Distress and Mitigation Mechanisms of Concrete Subject to ASR

Date of Final Oral Examination: 19 November 2020

The following individuals read and discussed the thesis submitted by student Md Asif Rahman, and they evaluated his presentation and response to questions during the final oral examination. They found that the student passed the final oral examination.

Yang Lu, Ph.D.	Chair, Supervisory Committee
Mojtaba Sadegh, Ph.D.	Member, Supervisory Committee
Arvin Farid, Ph.D.	Member, Supervisory Committee

The final reading approval of the thesis was granted by Yang Lu, Ph.D., Chair of the Supervisory Committee. The thesis was approved by the Graduate College.

DEDICATION

Dedicated to all the researchers who come out of their comfort zone to flourish the world with innovative idea and development.

ACKNOWLEDGEMENTS

I would like to express my gratitude for many suggestions and constructive comments I have received from people throughout the journey of my Masters in Civil Engineering at Boise State University. I am strongly indebted to them for their consistent support which ultimately helped me to complete my research project and thesis work successfully.

I would like to thank my supervisor Dr. Yang Lu for giving me the platform to work, gather experience and expertise in the field of research and innovation on concrete materials. His patience and technical support have developed my academic writing as well as professional presentation skills. I really appreciate his welcoming vibe, flexible mentality, timely feedback, guidance, and critical commentary on my work which have continuously helped me to grow as a confident and productive researcher.

I would like to express special thanks to my thesis committee members: Dr. Mojtaba Sadegh and Dr. Arvin Farid for guiding me with their valuable knowledge and expertise in the versatile fields of Civil Engineering. I also would like to address my gratitude to all my course instructors at Boise State University for supporting me with their knowledge and technical details. I would like to acknowledge the support of Dr. Arvin Farid and Dr. Clare Fitzpatrick on the concepts of finite element modeling, Dr. Stephen Brill on the fundamentals of partial differential equations based modeling, and Dr. Trevor J. Lujan on the base knowledge of continuum theory and modeling.

I would like to thank all the members of my research group for motivating me and providing me with technical supports on my research projects. I shall not forget the friendly vibe of Aidin Golrokh, Aminul Islam, Md. Fazle Rabbi, Md Jibon, Mahmudul Hasan, Shahjalal Chowdhury, Mostofa Najmus Sakib, and other graduate students of the Civil Engineering Department at Boise State University.

Finally, I would like to thank the Boise International Student Community for their amazing hospitality and support throughout my journey at Boise State. I will always remember all these people and memories for the rest of my life.

ABSTRACT

Alkali-silica reaction (ASR) is one of the common sources of concrete damage worldwide. The surrounding environment, namely, temperature and humidity greatly influence the alkali-silica reaction induced expansion. Global warming (GW) has caused frequent change in the climate and initiated extreme weather events in recent years. These extreme events anticipate random change in temperature and humidity, and convey potential threats to the concrete infrastructure. Moreover, external loading conditions also affect the service life of concrete. Thus, complex mechanisms of ASR under the impact of seasonal change and global warming require a precise quantitative assessment to guide the durable infrastructure materials design practices. Despite decades of phenological observation study, the expansion behavior of ASR under these situations remains to be understood for capturing the ASR damage properly. Within this context this research focuses on the mathematical model development to quantify and mitigate ASR-induced damage. Mesoscale characteristics of ASR concrete was captured in the virtual cement-concrete lab where the ASR gel-induced expansion zone was added as a uniform thickness shell. Finite element method (FEM) was used to solve the ASR formation and expansion evolution. The results of this study are presented in the form of one conference and their journal manuscripts.

The first manuscript focuses on the development of the governing equations based on the chemical formulas of alkali-silica reaction to account for the ASR kinetics and swelling pressure exerted by the ASR expansion. There is a fluid flow and mass transfer in

the concrete domain due to ASR gel associated from ASR kinetics. This paper involves derivation of the mass and momentum balance equation in terms of the thermo-hygro-mechanical (THM) model. THM model accounts for thermal expansion and hygroscopic swelling in addition to traffic loads to represent volumetric change in the concrete domain.

The second manuscript is a case study based on different cement-aggregate proportions and alkali hydroxide concentrations. It is important to know how ASR evolves under variable concentration of the chemical species. The simulated results show that high concentration of hydroxide ion in concrete initiates more reaction and damage in concrete. Also chemical reaction moves to the right direction with low cement to aggregate ratio which means ASR expansion depends on the availability of the reactive aggregates in the concrete domain.

The third manuscript attempts to develop a simplified ASR model that integrates chemo-physio-mechanical damage under stochastic weather impact. Stochasicity incorporates the random behavior of surrounding nature in the model. The simulated results elucidate that ASR expansion is more severe under the influence of global warming and climate change. This will support long-term damage forecasts of concrete subjected to extreme weather events.

The fourth manuscript focuses on the quantification of mechanical damage under ASR expansion and a dedicated mitigation scheme to minimize it. Added creep loads and physics identify the role of creep damage on ASR expansion. The results from this paper confirms that the ASR-induced damage significantly minimize the load carrying capacity of concrete. It directly affects the compressive strength, tensile strength, and modulus of elasticity of concrete. Damage in aggregates domain is more than the mortar phase under

the creep loadings. Among many supplementary materials, fly ash is the most effective in minimizing ASR expansion and damage. This work also includes a petrographic comparison between different mineral types collected from different locations to identify the reactivity of certain aggregates.

Thus, the final outcome of this research is a complete model which is a conclusive solution to the long-term ASR damage prediction. The validated model provides better understanding of ASR kinetics from mesoscale perspective. The developed model can potentially accelerate the precise prediction of concrete service life and mitigation schemes as well as can be used as an alternative scope to the costly laboratory tests methods.

TABLE OF CONTENTS

LIST OF TABLES

LIST OF FIGURES

CHAPTER ONE: INTRODUCTION AND BACKGROUND

Problem Statement

Damage to concrete infrastructure has become more frequent nowadays. Almost all types of concrete structures are being affected by this damage, e.g. pavements, bridges, buildings, and hydraulic dams etc. Aging and detrimental chemical reaction are the major sources of concrete damage in recent years. These are causing billions of dollars in damages every year in the United States. Alkali-silica reaction (ASR) is a frequently occurring undesirable phenomena for concrete damage worldwide.

Portland cement is a widely used construction material. It is frequently used and preferred over other materials because of its durability, great economy, and long service life. Cement is used in the construction of concrete materials. It is a binding agent which reacts with water and aggregates to form the hard skeleton of concrete. However, there are some undesirable chemical reactions in concrete that can lead to early damage to concrete. Alkali-aggregate reaction is one of these kinds that is responsible for concrete degradation. It happens due to the chemical reaction between different components of cement and reactive aggregates. There are two major types of alkali-aggregate reaction: alkali-carbonate reaction (ACR) and alkali-silica reaction (ASR). ACR mostly occurs with dolomitic or ACR-susceptible aggregates which are hardly seen in a few restricted regions, and thus, concrete damage due to ACR is very rare. On the other hand, ASR is a common problem which starts with the chemical contact between reactive aggregates and alkali hydroxides in concrete. Silica from reactive aggregates reacts with alkali hydroxide of

Portland cement to form alkali silica gel in a solid form [1]. This gel further absorbs water from the surrounding and swells which induces increasing internal pressure in the cementitious matrix of concrete structure [2]. This pressure can break the coherence between the components of concrete structure and develop cracks in the concrete domain with the progression of time. Damage from alkali-silica reaction is very significant across the United States.

The concrete ASR problem can be influenced by many factors: surrounding environment, concrete properties, mechanical loadings, aggregate/mineral types, use of supplementary materials etc. Surrounding environment greatly influences the kinetics of alkali-silica reaction and damage mechanisms. Effects of ambient temperature and humidity on the evolution of ASR expansion are clear [3, 4]. High temperature and humidity lead chemical reaction to the right direction and thus, initiate the ASR gel production. Moreover, extreme weather events in recent years have increased the complexity of ASR kinetics to some extent. Extreme weather is the sudden change in temperature or relative humidity. Climate change and global warming can alter the environment and initiate many extreme weather events, i.e. heat waves, rainfall, humidity or air vapor, snowfall during the winter etc. A small change in global warming can boost the intensity of many extreme events like heat waves and rainfall [5]. These weather events have already warmed the United States faster than the global rate since the late 1970s [6]. Heat waves contain warmer air which supplies more water vapor than the cooler air. Human-induced warming has also increased the amount of available water vapor in the atmosphere [7-8]. Moreover, some regions can show heavy snowfall during the winter season. The intensity of snowstorms has increased since the 1950s [9], and become more

frequent across the northern part of the United States [10-11]. Thus, the occurrence of extreme weather events is an emerging problem to the world. However, ASR kinetics and its evolution under these extreme events are yet to be justified.

Strength defines the load carrying capacity of concrete which depends on the interaction and bonding between mortar and aggregate phases of concrete. ASR expansion and induced-damage reduce the concrete strength significantly. ASR damage reduces the compressive strength of concrete [12]. Expansion from the alkali-aggregate reaction can reduce the flexural capacity of concrete [13-15]. Tensile strength of concrete is more likely to be affected by the ASR phenomena [16, 17]. ASR expansion also reduces the dynamic modulus of elasticity [15] and Young's modulus [18] of concrete.

Alkali-silica reaction is also greatly influenced by the type or reactivity of aggregates. Reactivity of an aggregate depends on its irregular crystallinity as well as the amount of energy stored in the crystal structure [19]. The swelling behavior of ASR gel determines the extent of damage to concrete structures, and the mitigation of this damage depends solely on the preventive measures to gel formation as well as its corresponding swelling [20]. Several research studies have been conducted to identify ASR mechanisms and evolution since the 1940s. The mechanism and properties of ASR kinetics under surrounding environment, extreme weather events, service loadings, and the use of supplementary materials should be clearly understood to make judicious choice of materials. The research effort documented in the current master's thesis focused on the development of a multiphysics model to capture the ASR mechanisms under these factors and precisely predict and mitigate ASR-induced expansion as well as damage.

Background

Manuscript - 1

Complex mechanisms of ASR kinetics works on three variables: sufficient alkali from cement, silica from reactive aggregates and sufficient moisture from the surrounding area [21]. Alkalies (K^+ and Na^+) from cement reacts with the pore water in concrete and thus, it produces high pH in the pore solution. This high pH solution breaks the silica bonds of reactive aggregates and forms alkali-silica gel. Aggregate's reactivity to alkalis are greatly influenced by its irregular crystallinity. Sometimes non-crystalline silicate structures are formed by irregular tetrahedral arrangements which make it more porous than crystalline silicate and thus, more susceptible to reaction. Moisture in concrete facilitates the flow of ions in concrete. When hard ASR gel absorbs water it goes through hygroscopic swelling and subsequent expansion. A minimum relative humidity of 80 percent is required to set out alkali-silica reaction and cause significant expansion [22]. Much research has been conducted to assess ASR related problems through lab experiments and numerical models [23-26]. However, a detailed study on the chemical species transport as well as ASR evolution in rigid pavement under traffic loads and the surrounding environment remain to be explored to predict damage in concrete pavements and other structures.

This manuscript (Chapter 2 of this thesis) evaluates the ASR kinetics on a representative concrete block as a middle portion of a rigid pavement slab. Analysis is done through a multiphysics model that combines ASR kinetics, traffic loads, and environmental conditions in the same platform. Analysis is performed considering four key steps: chemical ingress, traffic loadings, hygroscopic swelling & thermal expansion, and concrete

damage model to predict the service life of concrete. There are six chemical species that are involved in the ASR kinetics. A finite-element method (FEM) is used to approximate partial differential equation (PDE)-based governing equation sets that combines two major fields of transport mechanism: mass balance and momentum balance. This determines the concentration of each chemical species with the progression of time. A time-dependent function based on equivalent single axle load (ESAL) data of highway I084 is developed to apply traffic loads in the model following the Idaho Transportation Manual (ITD) from years 2018 to 2048 [27]. Other equation sets were developed to introduce temperature and moisture variation. Thus, ASR expansion and damage under the impact of chemical species, traffic loads, and environment are explored.

Manuscript - 2

Aggregates are more or less chemically inactive. However, some reactive aggregates react with the alkalis in concrete that causes expansion and damage over a long time. Aggregates consist of stone, gravel, and sands that lie in the concrete matrix. The mortar or cement paste contain the alkali rich pore solution. Thus, ASR expansion significantly depends on the proportion of aggregates and availability of alkali hydroxides in concrete. Moreover, external loading can affect the ASR expansion. A case by case study is needed to assess these phenomena accurately. Chemophysical mechanism of ASR under different case studies from the meso-scale perspective is yet to be analyzed.

This manuscript (Chapter 3 of this thesis) attempts to predict ASR- induced damage in concrete porous media on a case by case basis. A representative 2D concrete block is considered as a middle portion of a concrete structure. It includes a time-dependent chemo-mechanical model for different geometric proportions of cement and aggregate particles,

and hydroxile ion concentrations. Modeling is conducted considering four key steps: a case study on mesoscale geometry, a case study on chemical species, solid mechanics, and concrete damage. Five sets of concrete geometry are introduced to simulate variable cement-aggregate proportions in concrete. Two different concentrations of alkali hydroxide content are considered to simulate variance in concentration of chemical species. This work identifies the mechanical deterioration in concrete due to ASR in terms of the volume change, strain, and stress on a case by case basis. The added flexibility to change cement-aggregate ratio per concrete mix, and alkali hydroxide and siloxane concentrations per cement-aggregate mineralogy provides with in depth understanding of ASR evolution and damage.

Manuscript - 3

Extreme weather events can initiate frequent change in certain environmental conditions like temperature and humidity which will adversely affect the concrete infrastructures. Climate change and global warming can maximize or minimize the intensity of temperature and humidity surrounding the concrete structures. This random change in environmental parameters creates uncertainty in ASR kinetics, expansion and associated damage. There is also sharp change in the degree of saturation of porous media due to ongoing extreme weather events. This will generate frequent expansion and shrinkage in the tiny pores of the concrete porous media. Thus, extreme weather events are a potential source of damage to the ASR occupied concrete structures. However, impact of extreme weather events on concrete structures have been frequently underestimated. Moreover saturated porous media and constant environmental conditions assumption can lead to over or under conservative design practices. To capture the evolution of alkali-silica

reaction precisely the effects of uncertain environmental and extreme weather conditions on concrete porous media must be evaluated accurately.

Within this context, this manuscript (Chapter 4 of this thesis) develops a simplified alkali silica reaction model to capture the uncertainties involved in the transport of the chemical species in the variably saturated porous media of concrete under the impacts of seasonal variation and extreme weather events in terms of a stochastic process. The proposed model incorporates global warming impact-induced weather data and its stochastic representation as input parameters, and provides a new perspective of ASR evolution and damage under a real-world scenario.

Manuscript - 4

Alkali silica reaction deteriorates the concrete service life by reducing the load carrying capacity of concrete. Study [28] performed lab tests on the ASR affected concrete prism to record the ASR-induced mechanical damage with time. According to this study, there are noticeable reductions in the compressive strength, tensile capacity, and Young's modulus of concrete due to the alkali-silica reaction, especially under the high temperature and alkali content. Moreover, random distribution of aggregate particles from different mineral sites adds complexity to ASR mechanisms.

The mitigation process of ASR damage is also a very challenging job. Several lab experiments have been conducted to evaluate the effectiveness of supplementary materials in mitigation measures [29-31]. These lab tests are mostly limited to certain test set ups and fixed weather conditions which are costly and time consuming in many cases. No promising work has been developed so far to assess the mitigation measures in a modeling

platform. A robust numerical model can potentially predict chemo-mechanical damage of ASR and incorporate the mitigation scheme to minimize it.

This manuscript (Chapter 5 of this thesis) proposes a new modeling approach to track the mechanical damage in concrete with the progress of alkali-silica reaction as well as a mitigation module to minimize concrete damage. This work determines mechanical properties of ASR affected concrete in terms of a modified strength model. It includes a case study to evaluate the change in compressive strength, tensile strength, and Young's modulus of concrete with the progression of time under the impacts of ASR and creep loadings. 17 different types of coarse aggregate are considered in the model as part of the petrographic analysis. Added mitigation schemes define the applicability of different supplementary materials, i.e. fly ash, slag and silica fumes in minimizing ASR expansion.

Research Objectives, Tasks, and Thesis Preparation

The main objective of this master's thesis research was to develop numerical model to quantify alkali-silica reaction damage in concrete pavement and structures in terms of ASR kinetics, disparate geometry and chemical species concentrations, global warming, climate change and stochastic weather events, service loadings, and mitigation schemes. The research work has been reported in the form of four different manuscripts.

This Master's thesis document includes six chapters in it. Chapter 2 contains manuscript # 1, titled "A Meso-Scale Multiphysics Model for Predicting Concrete Pavement Performance Subject to ASR Degradation". The primary objective of this manuscript was to evaluate ASR expansion and damage in a concrete pavement under all chemical species involved in the ASR kinetics. A 3D concrete geometry was developed to replicate the middle portion of a rigid pavement, and also developed governing equation

sets incorporating complex chemophysics of ASR and traffic loadings into the pavement model. Findings from these tasks have been detailed in Chapter 2 of this thesis.

Chapter 3 contains manuscript # 2, titled “A Time-Dependent Chemo-Mechanical Analysis of Alkali-Silica Reaction for The Disparate Geometry of Concrete Meso-Structure”. The primary objective of this manuscript was to introduce disparate geometry and compositions in the ASR model to quantify ASR damage in terms of different cement-aggregate proportions and alkali hydroxide concentrations. A 2D meso-scale geometry was used as a representative concrete block to run case studies on the ASR model based on the governing equation sets. Findings from these tasks have been detailed in Chapter 3 of this thesis.

Chapter 4 includes manuscript # 3, titled “A Stochastic Model to Evaluate Alkali-Silica Reaction (ASR) in Concrete Subject to Global Warming and Climate Change Impacts”. The main objective of this manuscript was to evaluate the impacts of weather uncertainty on the mechanism of ASR expansion. A stochastic approach was used to produce randomized temperature and relative humidity data from climate change and global warming effects. Thus, the 2D meso-scale model simulated ASR evolution under extreme weather events. Findings from these tasks have been presented in Chapter 4 of this thesis.

Chapter 5 includes manuscript # 4, titled “Mitigation Schemes for The Alkali-Silica Reaction (ASR)-induced Damage: A Mineralogical Study on Concrete”. The main purpose of this manuscript was to develop a robust model that can predict and mitigate mechanical damage of concrete structures under the impacts of alkali-silica reaction and creep loadings. A strength based mechanical model and different supplementary materials based

mitigation scheme were developed to analyze ASR damage for 17 types of coarse aggregate in a 2D meso-scale geometry. Findings from these tasks have been presented in Chapter 5 of this thesis.

Finally, chapter 6 summarizes all the results and findings from these four manuscripts, and presents potential scopes for future research and innovation. Table 1-1 summarizes all the individual tasks which were carried out under the scope of this master's thesis, and correlates each of the tasks to the technical manuscripts prepared.

Table 1-1 Individual tasks from technical manuscript

	Tasks	Manuscript
1	Analysis of complex ASR chemophysics under chemical species transport and traffic loadings in a concrete pavement	Manuscript #1
2	Case studies on the ASR model in terms of different cement-aggregate proportions and alkali hydroxide concentrations	Manuscript #2
3	Evaluation of the impacts of extreme weather events on the ASR kinetics and expansion	Manuscript #3
4	Prediction and mitigation schemes for the mechanical damage of ASR affected concrete structures	Manuscript #4

References

[1]. Alexander, M. and S. Mindess. Aggregates in Concrete: Modern Concrete Technology 13. Taylor & Francis, London and New York, 2010.

[2]. Prezzi, M., P. J. M. Monteiro, and G. Sposito. The Alkali-Silica Reaction, Part I: Use of The Double-Layer. ACI Materials Journal, 1997. January-February: 10-16.

[3]. Poyet, S., A. Sellier, B. Capra, G. Thèvenin-Foray, J. M. Torrenti, H. Tournier-Cognon, and E. Bourdarot. Influence of Water on Alkali-Silica Reaction: Experimental Study and Numerical Simulations. Journal of Materials in Civil Engineering, 2006. 18: 588-596.

[4]. Leger, P., P. Cote, and R. Tinawi. Finite Element Analysis of Concrete Swelling Due to Alkali-Aggregate Reactions in Dams. Computers & Structures, 1996. 60: 601-611.

[5]. Noah S. Diffenbaugh. Verification of extreme event attribution: Using out-of-sample observations to assess changes in probabilities of unprecedented events. Science Advances 18 Mar 2020:Vol. 6, no. 12, eaay2368. DOI: 10.1126/sciadv.aay2368.

[6]. NOAA (National Oceanic and Atmospheric Administration). 2016. National Centers for Environmental Information. Accessed February 2016. www.ncei.noaa.gov.

[7]. Dai, A., 2006: Recent climatology, variability, and trends in global surface humidity. Journal of Climate, 19, 3589-3606, doi:10.1175/JCLI3816.1.

[8]. Willett, K. M., P. D. Jones, N. P. Gillett, and P. W. Thorne, 2008: Recent changes in surface humidity: Development of the HadCRUH dataset. Journal of Climate, 21, 5364-5383, doi:10.1175/2008JCLI2274.1.

[9]. Vose, R. S. et al., 2013: Monitoring and understanding changes in extremes: Extratropical storms, winds, and waves. Bulletin of the American Meteorological Society, in press, doi:10.1175/BAMS-D-12-00162.1.

[10]. Wang, X. L., Y. Feng, G. P. Compo, V. R. Swail, F. W. Zwiers, R. J. Allan, and P. D. Sardeshmukh, 2012: Trends and low frequency variability of extra-tropical cyclone activity in the ensemble of twentieth century reanalysis. Climate Dynamics, 40, 2775-2800, doi:10.1007/s00382-012-1450-9.

[11]. Wang, X. L., V. R. Swail, and F. W. Zwiers, 2006: Climatology and changes of extratropical cyclone activity: Comparison of ERA-40 with NCEP-NCAR reanalysis for 1958-2001. Journal of Climate, 19, 3145-3166, doi:10.1175/JCLI3781.1.

[12]. Ono K (1990). "Strength and stiffness of alkali silica reaction concrete and concrete members." structural engineering review 2: pp121-125.

[13]. Swamy R.N (1992). "Testing for alkali-silica reaction in concrete." the alkali silica reaction in concrete ed R N Swamy, Blackie, Van Nostrand Reinhold: pp54-95.

[14]. Swamy R.N, a. A.-A. M. M. (1986). "Influence of Alkali silica reaction on the engineering properties of concrete." Alkalis in concrete, ASTM STP 930, Ed, V.H. Dodson, American society for testinfg and materials Journal, Philadelphia: pp69-86.

[15]. Monette L.J, G. N. J., Grattan-Bellew P.E, (2000). "Structural effects of the alkali aggregate reactions on non-loaded and loaded reinforced concrete beams." 11th international conference on alkali aggregate reaction: pp999-1008.

[16]. Al-Asali, S. a. (1988). "Engineering properties of concrete affected by alkali silica reactions." ACI materials Journal: pp367-374.

[17]. Charlwood R.G (1992). "A review of alkali-aggregate reactions in hydro-electric plants and dams." International conference on Alkali aggregate reactions in hydro-electric plants and dams, fredericton, New brunswick, Canada.

[18]. Larive C (1998). "apports combinés de l'expérimentation et de la modélisation à la compréhension de l'alcali réaction et de ses effets mécaniques." LCPC thèse: 395pages.

[19]. Touma, W. E., D. F. Fowler, and R. L. Carrasquillo. Alkali-Silica Reaction in Portland Cement Concrete: Testing Methods and Mitigation Alternatives. Research Report ICAR 301-1F. International Center for Aggregates Research (ICAR), The University of Texas at Austin, 2001.

[20]. Gholizadeh Vayghan, A. Characterization Of the Rheological and Swelling Properties of Synthetic Alkali Silicate Gels in Order to Predict Their Behavior in ASR Damaged Concrete. Doctoral dissertation, Civil and Environmental Engineering, The Pennsylvania State University, USA, 2017.

[21]. Mukhopadhyay, A. K. An Effective Approach to Utilize Recycled Aggregates (RAs) From Alkali-Silica Reaction (ASR) Affected Portland Cement Concrete. In Handbook of Recycled Concrete and Demolition Waste (F. Pacheco-Torgal, V. W. Y. Tam, J. A. Labrincha, Y. Ding, and J. de Brito), Woodhead Publishing Limited, Cambridge, UK, 2013. pp. 555-568.

[22]. Thomas, M. D. A., B. Fournier, and K. J. Folliard. Alkali-Aggregate Reactivity (AAR) Facts Book. Publication FHWA-HIF-13-019. FHWA, U.S. Department of Transportation, 2013.

[23]. Ulm, F.J., O. Coussy, L. Kefei, and C. Larive. Thermo-Chemo-Mechanics of ASR Expansion in Concrete Structures. Journal of Engineering Mechanics, 2000. 126: 233-242.

[24]. Hobbs, D. W. The Alkali-Silica Reaction - A Model For Predicting Expansion in Mortar. Magazine of Concrete Research, 1981. 33 (117): 208 - 220.

[25]. Saouma, V. E., R.A. Martin, M. A. Hariri-Ardebili, and T. Katayama. A Mathematical Model For The Kinetics of The Alkali–Silica Chemical Reaction. Cement and Concrete Research, 2015. 68:184-195.

[26]. Balbo, F. A. N., G. A. Pianezzer, L. M. Gramani, E. Kaviski, and M. R. Teixeira. An Application to the Diffusion Equation in a Model For The Damage in Concrete Due to Alkali-Silica Reaction. Applied Mathematical Sciences, 2015. 9: 4135-4147.

[27]. Pavement Design, ITD Manual, Section 500, http://apps.itd.idaho.gov/apps/manuals/Materials/Sec%20500.pdf

[28]. Ben Haha, M. Mechanical Effects of Alkali Silica Reaction in Concrete Studied by SEM-Image Analysis. Doctoral dissertation, École Polytechnique Fédérale de Lausanne. À La Faculté Sciences Et Techniques De L'ingénieur, France, 2006.

[29]. Yi, C.K., C.P. Ostertag. Mechanical approach in mitigating alkali-silica reaction. Cement and Concrete Research, 2005. 35(1): 67-75.

[30]. Javier Malvar, L., Lary R. Lenke. Efficiency of Fly Ash in Mitigating Alkali-Silica Reaction Based on Chemical Composition. ACI Materials Journal, 2006. 103(5): 319-326.

[31]. Folliard , K. J., Ryan Barborak, Thano Drimalas, Dr. Lianxiang Du, Sabrina Garber, Jason Ideker, Tyler Ley, Stephanie Williams, Maria Juenger, Benoit Fournier, and M.D.A. Thomas. Preventing ASR/DEF in New Concrete: Final Report. Publication FHWA/TX-06/0-4085-5. FHWA, U.S. Department of Transportation, 2006.

CHAPTER 2: MANUSCRIPT ONE – A MESO-SCALE MULTIPHYSICS MODEL FOR PREDICTING CONCRETE PAVEMENT PERFORMANCE SUBJECT TO ASR DEGRADATION[1]

Abstract

Alkali-silica reaction (ASR) is a major concern as aggregates commonly contain reactive silica materials and react with alkali hydroxide in concrete. Environmental conditions, namely, temperature and humidity levels amplify ASR progression and evolution. Complex mechanisms of alkali-silica reaction in Portland cement concrete significantly deteriorates concrete service life and requires quantitative assessment. Despite decades of phenological observation study, the expansion mechanism of ASR from the mesoscale perspectives remains to be understood for clearly capturing the ASR induced damage processes. Mesoscale characteristics of ASR concrete was captured using a 3-D virtual concrete model, where the ASR gel-induced expansion zone was added as a uniform thickness shell. A novel set of governing equations according to chemical formulas was derived and proposed to account for ASR kinetics and swelling pressure exerted by the ASR reaction. Based on the governing equations of ASR expansion, finite element method (FEM) was used to solve the ASR formation and expansion evolution. The multiphysics

[1] This chapter includes results already published in the following publication. Contribution of the coauthor is sincerely acknowledged: Rahman, M. A., and Lu, Y. “A Meso-Scale Multiphysics Model for Predicting Concrete Pavement Performance Subject to ASR Degradation”, Transportation Research Board (TRB) Annual Meeting Paper, 2019, 19–03839R1.

model which involves multiple simultaneous physical phenomena was used to develop a thermo-hygro-mechanical (THM) model. THM model accounts for thermal expansion and hygroscopic swelling in addition to traffic loads to represent volumetric change in the concrete domain. The validated model provided a new perspective from meso-scale physics for a better understanding of ASR kinetics. This multiphysics scenario-based model can serve as a concrete transportation infrastructure management system and as an accurate tool to predict the service life of concrete, as well as on time maintenance decision.

Keywords: ASR kinetics, ASR mechanisms, Concrete damage model

1. Introduction

Portland cement concrete is a widely used construction material due to its durability, long service life and great economy. The mechanism and properties related to chemical kinetics under variable environmental conditions should be clearly understood to effectively control the use of concrete in construction and make judicious choices of materials. Cement acts as a binding agent when mixed with water and aggregates will react chemically with each other to form concrete. However, in concrete many chemical components of reactive aggregate & cement lead to undesirable chemical reaction which has detrimental effects to concrete. One of the major sources of this deterioration is the alkali-aggregate reaction. Since the 1940s, several research studies have been conducted to identify chemical reaction between cement and aggregate that contribute to concrete degradation. Though aggregates are chemically inert to a certain extent, reactive aggregate particles make chemical contact with the alkali hydroxides in concrete, degrading coherence between concrete materials and developing cracks in concrete structure over a period of many years. The two major types of alkali-aggregate reaction are alkali-carbonate

reaction (ACR) and alkali-silica reaction (ASR). Incidences of ACR are hardly seen and generally formed with dolomitic or ACR-susceptible aggregates which are restricted to a few isolated regions. In ASR, aggregates containing silica will react with alkali hydroxide in concrete which form alkali silica gel in a solid form *(1)*. This gel further swells when it absorbs water from surrounding cement paste or the environment and induces increasing internal pressure in the cementitious matrix of concrete structure *(2)*. This pressure may initiate expansion and develop cracks in concrete materials. Unlike ACR, ASR is considerably more widespread and is of more significance in the United States.

The mechanisms governing ASR are quite complex *(3)*. ASR kinetics depends on three variables: (1) sufficient pH and alkalies from cement; (2) reactive silica from aggregates and (3) sufficient moisture/water *(4)*. Each of these criteria must be met for the reaction to occur *(5)*. The alkali-silica reaction takes place between silica and hydroxides. Alkalies (namely K^+ and Na^+) coming from cement ultimately reside in the concrete pore solution *(6)*. Cement reacts with mixing water and thus concrete pore solutions are associated with hydroxyl ion (OH^-) which produces high pH in the pore solution *(7)*. Reactive silica in aggregate tends to breakdown due to the high alkalinity of pore solution in concrete and subsequently react with alkali-hydroxides to form ASR gel. Not all aggregates containing silica are susceptible to react with hydroxides. There may be two forms of silica in natural aggregates: crystalline or non-crystalline. In a crystalline silicate structure like quartz (SiO_2) there are no complete tetrahedron formed on the surface and structural impermeability of such structures allow it to react only on the surface, and thus, they are less reactive *(8)*. Unlike crystalline silicate, non-crystalline silicate structures are formed by irregular tetrahedral arrangements which make it more porous with greater

surface area and thus, they are more susceptible to reaction *(8)*. Hence, aggregate's reactivity to alkalis are greatly influenced by its irregular crystallinity. Sufficient moisture is important for potential ASR reaction *(4)*. Moisture facilitates the flow of ions in the porous media and allows hygroscopic gel to swell when it absorbs water. Expansion is directly related to the percentage of relative humidity in concrete. Many researchers have reported increasing ASR expansions as the relative humidity tends to increase *(9)*. A minimum relative humidity of 80 percent is required to set out alkali-silica reaction and cause significant expansion *(10)*. Moreover, increased temperature accelerates the alkali-silica reactions to some extent *(11)*. Much research has been conducted to figure out ASR problems and develop numerical models to predict expansion caused by alkali-silica reactions *(6, 12-16)*. Existing research shows versatility in the field of ASR analysis and modeling.

However, the mechanism of ASR from the mesoscale perspectives remains to be understood for clearly capturing ASR induced damage processes. In this work, a multiphysics model was developed that combines ASR kinetics, traffic loads, and hygroscopic and thermal expansion. Analysis was performed considering four key steps: chemical ingress, traffic loadings, hygroscopic swelling & thermal expansion, and a concrete damage model to predict the service life of concrete. First, finite-element method (FEM) was employed to model the ingress of multiple chemical species into a variably saturated concrete matrix. For chemical kinetics it was assumed that there was enough moisture to stimulate chemical reaction. Several sets of governing equations were established to simulate ASR kinetics. Second, traffic loads were applied to concrete slab. Third, we introduced temperature and moisture variation. Two separate sets of governing

equations were established to simulate temperature and moisture effects on concrete. Finally, we developed a damage model in terms of changing volume to predict damage in concrete structure. A representative concrete block was considered as a middle portion of a rigid pavement slab and assumed to be situated in highway.

2. ASR Mechanisms

The alkali-silica reaction in Portland cement concrete occurs in multi steps *(17)*. It is believed that the process starts with the attacking of siliceous components on the surface of the aggregate particles. Though researchers have studied the mechanisms governing alkali-silica reaction since the mid-1900s, doubts remain for the expansion mechanisms. In general, the chemical reactions involved in ASR mechanisms can be treated as acid-base reactions where silica in aggregate is acid reactant, hydroxides (K^+ or Na^+) remaining in the pore solution are basic reactants, water is the reaction medium and calcium potassium (or sodium) silicate hydrate are the reaction product *(18)*. In this study the ASR mechanism is divided into three stages: (1) Hydration, (2) Neutralization and (3) Osmosis. Equations (1), (2), and (3) were considered to depict chemical reactions that represent three stages, respectively *(15)*. In the first stage hydrolysis of the reactive silica (siloxane) by hydroxyl ions (OH^-) takes place. The siloxanes on reactive aggregate are attacked by the hydroxyl ions that remain dissolved in the pore solution with high pH. This attack on silicate core structure breaks down siloxane bonds (≡Si–O–Si≡) and alkali cations participate in doing the charge balance, which forms silanol bonds (≡Si–O–H) and alkali-silicate gel (≡Si–O–R) as illustrated by Eq. (1). This is a slow process where aggregate participates very slowly in the chemical reaction. In the second stage, weak silanol bonds (≡Si–O–H) further react with hydroxyl ions to generate alkali-silicate gel. Thus, readily available alkaline cations

(K^+ or Na^+) diffuse in the gel to balance the negatively charged species and thus neutralize the basic pore solution *(2)*. This stage can be defined as a charge neutralization process. At the last stage hydrophilic alkali-silicate gel formed in the earlier stages imbibes water or moisture from hydrated cement paste or the surrounding environment due to osmotic pressure and increases in volume. Osmotic pressure is generated by the difference between the mole fractions of water inside and outside of the membrane or the reaction rim *(17)*. Concrete structures subject to alkali-silica degradation typically show at least one of the following degradation: cracking, expansion of concrete block, misalignments of structural components, or gel 'pop-outs' *(19)*.

It is noteworthy that less viscous Na-K rich gel generated inside the reactive aggregates first followed by aggregate cracking and then cracking in paste. Thus, gel flows along the cracks from the aggregate through the cement paste. When gel flows through the fine crack, it participates in ion-exchange reaction and absorb Ca from the nearby cement paste and produces relatively Ca-rich gel which is more expansive than the gel originally formed inside aggregate. However, very slow ionic exchange by mutual diffusion between alkalis in ASR gel and calcium in cement paste results in the conversion of expansive alkali-rich ASR gel into non-expansive calcium silicate gel (CSH gel) per Eq. (4) *(15)*. This may happen during repeated drying and wetting or the freeze/thaw cycles which limit the ASR expansion. C–S–H mechanism is not considered in the chemical model of this study.

$$\underbrace{\equiv Si–O–Si\equiv}_{\text{Siloxane}} + \underbrace{R^+ + OH^-}_{\text{ROH}} \longrightarrow \underbrace{\equiv Si–O–R}_{\text{ASR gel}} + \underbrace{H–O–Si\equiv}_{\text{Silanol}} \quad (1)$$

$$\underbrace{H–O–Si\equiv}_{\text{Silanol}} + \underbrace{R^+ + OH^-}_{\text{ROH}} \longrightarrow \underbrace{\equiv Si–O^-R^+}_{\text{ASR gel}} + \underbrace{H2O}_{\text{Water}} \quad (2)$$

$$\underbrace{\equiv Si–O–R}_{\text{ASR gel}} + \underbrace{nH2O}_{\text{Water}} \longrightarrow \underbrace{\equiv Si–O^- + (H_2O)_n + R^+}_{\text{Expanded ASR gel}} \quad (3)$$

$$\underbrace{\equiv Si–O^- + (H2O)_n + R^+}_{\text{Expanded ASR gel}} + \underbrace{\frac{1}{2}Ca^{2+}}_{\text{Calcium Ions}} \longrightarrow \underbrace{\equiv Si–O^- + \frac{1}{2}Ca + (H_2O)_n}_{\text{C-S-H gel}} + \underbrace{R^+}_{\text{Excluded Alkali}} \quad (4)$$

where, R^+ denotes an alkali ion (K^+ or Na^+).

ASR kinetics is the study of reaction rates related to ASR mechanisms. Reaction rate is different for each stage *(15)*. Reaction rates, k_1, k_2, and k_3 were assigned to first, second and third stages respectively. The reaction rates are dependent on temperature through the Arrhenius equation *(20)* given as Eq. (5).

$$k = Ae^{-E_a/(RgT)} \quad (5)$$

where k is reaction rate, A is the frequency factor, E_a is activation energy, R_g is the gas constant and T represents temperature.

The rate of change of concentration for each of the six species can be expressed in the group Eq. (6) according to study *(15)*.

$$\frac{d[\text{Siloxane}]}{dt} = -k_1[\text{Siloxane}][\text{ROH}]$$

$$\frac{d[\text{ROH}]}{dt} = -k_1[\text{Siloxane}][\text{ROH}] - k_2[\text{Silanol}][\text{ROH}]$$

$$\frac{d[\text{ASR gel}]}{dt} = k_1[\text{Siloxane}][\text{ROH}] + k_2[\text{Silanol}][\text{ROH}] - k_3[\text{ASR gel}][\text{H2O}]$$

$$\frac{d[\text{Silanol}]}{dt} = k_1[\text{Siloxane}][\text{ROH}] - k_2[\text{Silanol}][\text{ROH}]$$

$$\frac{d[\text{H2O}]}{dt} = k_2[\text{Silanol}][\text{ROH}] - k_3[\text{ASR gel}][\text{H2O}]$$

$$\frac{d[\text{Expanded ASR gel}]}{dt} = k_3[\text{ASR gel}][\text{H2O}] \quad (6)$$

where [Siloxane], [ROH], [ASR gel], [Silanol], [H2O], and [Expanded ASR gel] represents concentration of each species, respectively.

To solve ASR kinetics a system of six coupled governing equations is required that will account for diffusion of the species and concentration of each species. For a realistic simulation ASR model is needed to couple with mechanical loading as well as temperature and moisture variation.

3. Mathematical Models

3.1. ASR Model

ASR mechanisms progress with the change in concentration of chemical species, gel formation and penetration of gel into the pores. In this study, finite-element method (FEM) was used to compute numerical approximation of PDEs and predict ASR-induced expansion. There are six reacting species that participate in the ASR mechanisms according to chemical kinetics discussed previously in section 2. To predict the concentration of each relevant species in the different steps of ASR, this work developed a comprehensive FEM model which couples the major relevant physics fields (transport mechanisms) based on the principles of mass balance and momentum balance. The basic principle used in the

modeling of a chemical engineering process is the concept of balance of momentum, mass and energy, which can be expressed in a general form as eq. (7) according to study *(21)*.

$$A = I+G-O-C \qquad (7)$$

where, A is the accumulation built-up within system, I is input entering through system surface, G means generation produced in system volume, O means output leaving through system boundary and C is the consumption used in system volume.

Coupled Equation

One of the fundamental laws of physics states that mass can neither be produced nor destroyed, that is, mass is conserved. Mass balance equation was developed using the principle of Fick's law. According to Fick's 2nd law per Eq. (8), the accumulation rate is proportional to the diffusivity and the 2nd derivative (or curvature) of the mass fraction (or in this study in terms of concentration).

$$\frac{\partial}{\partial t}(c_i) = \nabla \cdot (D_i \nabla c_i) \qquad (8)$$

$$\text{Or, } \frac{\partial}{\partial t}(c_i) - \nabla \cdot (D_i \nabla c_i) = 0 \qquad (9)$$

where, $\frac{\partial}{\partial t}(c_i)$ is the accumulation rate, D_i is diffusivity, and $\nabla \bullet (\nabla c_i)$ indicates the 2nd derivative of the concentration of each species I, i.e. c_i. In this study, local rule for accumulation was expressed by Fick's 2nd law of diffusion to simulate concrete as an isotropic material.

On the other hand, momentum of a particle can be defined as the product of particle's mass and velocity. To simulate fluid flow and velocity in alkali-silica reaction momentum balance was developed based on the principle of Newton's law per Eq. (10).

$$\mathbf{u} \cdot \nabla c_i = R_i \qquad (10)$$

where, left term u •∇ci accounts for convection i.e. fluid flow in the concrete matrix and right term R_i is consumption rate of each species i.

After combining Eq. (9) and Eq. (10), we derived the coupled equation of mass and momentum balance per Eq. (11).

$$\frac{\partial}{\partial t}(c_i) + \nabla \cdot (-D_i \nabla c_i) + \mathbf{u} \cdot \nabla c_i = R_i \qquad (11)$$

where, c_i is the concentration of species i (mole/m^3), D_i denotes the diffusion coefficient of species i (m^2/s), u is the fluid velocity vector (m/s) with components in x, y, and z direction respectively, and R_i is a source term or consumption rate for the species i (mole/(m^3/s)). The dependent variable in this balance equation is the concentration of each species, c_i.

Eq. (11) shows the two primary transport mechanisms of generic chemical species in the porous concrete matrix, i.e., the natural diffusion by the second Fick's law and the carrying migration by fluid (moisture or pore water) in concrete matrix.

Brinkman Equation

The Brinkman equation was used in this study to compute the unknown fluid velocity, u in Eq. (11) as well as pressure fields for the single-phase flow condition in porous media. This equation extends Darcy's law to describe the dissipation of the kinetic energy by viscous shear. The dependent variables in the Brinkman equations are the Darcy velocity and the pressure. The flow in porous media is governed by a combination of the continuity equation and the momentum equation, which together form the Brinkman equations:

$$\frac{\partial}{\partial t}(\varepsilon_p \rho) + \nabla \cdot (\rho \mathbf{u}) = Q_{br} \quad (12)$$

$$\rho/\varepsilon_p \left(\frac{\partial \mathbf{u}}{\partial t} + (\mathbf{u}.\nabla)\,\mathbf{u}\,/\varepsilon_p\right) = \nabla.(-p) + \nabla.\left[1/\varepsilon_p \left\{\mu(\nabla \mathbf{u} + (\nabla \mathbf{u})^T) - \frac{2}{3}\mu(\nabla.\mathbf{u})\mathbf{I}\right\}\right] - (\mu \boldsymbol{\kappa}^{-1} + Q_{br}/\varepsilon_p^2)\mathbf{u} + \mathbf{F} \quad (13)$$

where, μ is the dynamic viscosity of fluid (kg/(m.s)), **u** is the velocity vector (m/s), ρ is the density of the fluid (kg/m^3), p is the pressure (Pa), ε_p is the porosity, $\boldsymbol{\kappa}$ is the permeability tensor of the porous medium (m^2), F is the volume force (kg/(m^2.s^2)), I is the identity tensor, and Q_{br} is a mass source or mass sink of fluid (kg/(m^3.s)). The mass source, Q_{br}, accounts for mass deposit and mass creation within the domains. The mass exchange is assumed to occur at zero velocity.

The first equation, Eq. (12) of the Brinkman equations (12 & 13), is the equation of Darcy's law which combines the continuity equation and equation of state for the pore fluid and is suitable for porous media. In this study, this concept was used to simulate low-velocity flow in the porous media. Moreover, it was assumed in this study that reaction occurs with sufficient moisture content and reactive silica. That's why Darcy's law was applied to analyze a fully saturated concrete.

To simplify the Brinkman equations several assumptions were made based on this study context. The inertial term in the free flow (Stokes-Brinkman) was neglected and thus the term $(u \bullet \nabla)(u/\varepsilon_p)$ on the left-hand side of Eq. (13) was taken as zero. Influence of volume forces were neglected here because there was no influence of gravity or other volume forces (i.e. due to movement or external forces on the concrete body) considered, and thus F was taken as zero. The model was simulated considering incompressible flow where the density stays constant in any fluid particle, which can be expressed as

$$\frac{\partial}{\partial t}(\varepsilon_p \rho) + \mathbf{u} \cdot \nabla \rho = 0 \qquad (14)$$

and the continuity equation, Eq. (12) was reduced to:

$$\rho \nabla \cdot \mathbf{u} = Q_{br} \qquad (15)$$

Thus, according to this study context simplified Brinkman equations become:

$$\rho/\varepsilon_p \left(\frac{\partial \mathbf{u}}{\partial t}\right) - \nabla.(-p) - \nabla \cdot [1/\varepsilon_p \{\mu(\nabla \mathbf{u} + (\nabla \mathbf{u})^T) - \frac{2}{3}\mu(\nabla \cdot \mathbf{u})\mathbf{I}\}] + (\mu \boldsymbol{\kappa}^{-1} + Q_{br}/\varepsilon_p^2)\mathbf{u} = 0 \qquad (16)$$

$$\rho \nabla \cdot \mathbf{u} = Q_{br} \qquad (17)$$

Note that the physics expressed in Eqs. (11), (16) and (17) were applied together (as a multiphysics phenomenon) in the equation based finite element model to simulate chemical reactions of all six species, their diffusion and convection, fluid flow in porous media concurrently. Eq. (11) solves for the concentration of each species based on the concept of mass & momentum balance in chemical kinetics discussed previously. Eqs. (16, 17) solve for the unknown fluid velocity and pressure field of each species based on the continuity and momentum equation, which is applicable to simulate flow in porous media. To avoid the complexity in simulating ASR mechanisms it was assumed that: 1) reaction occurs with sufficient moisture content and reactive silica *(9)*, 2) no mass change occurs during chemical reaction, i.e. always having a constant concrete mass *(16)*, and 3) no termination of ASR in terms of the (very slow) ionic exchange by mutual diffusion between alkalis in ASR gel and calcium in cement paste *(15)*.

3.2. Mechanical Model

Concrete used in roadway is subjected to traffic loading. Concrete experiences change in shape or size when stresses are applied to it which in turn develop volumetric strain. To analyze the concrete behavior and predict service life, a mechanical model was

developed that accounts for time dependent traffic throughout the simulation period. In this study, traffic loads from vehicles were characterized based on tire loads. To facilitate the model simulation over a period of 30 years, ESAL data was collected from Idaho Transportation Manual (ITD) for highway I084, for years 2018 to 2048 considering one way rigid pavement condition *(22)*. A time-dependent function was developed per Eq. (18) based on ESAR data.

$$q = 0.007t^2 + 0.85t + 17.75 \qquad (18)$$

where q is single axle load (kN), t is time (years). Load exerted by each wheel is q/2 (kN). To make the simulation process simple, a constant tire pressure of 344.5 (kPa) was considered for a single wheel.

The radius of the tire contact area can be determined per Eq. (19) based on study *(23)*.

$$R = \sqrt{\frac{q/2}{\pi.p}} \qquad (19)$$

where R is the radius of tire contact (m), p tire inflation pressure (kPa).

In this study, considered concrete block was assumed to be the middle of a roadway slab. This is a small concrete block and whole concrete surface is in contact with the traffic loads. In the simulation it was assumed that concrete block takes full load from a single wheel when the wheel passes over the slab. Thus, single wheel load (q/2 kN) was divided among the nodes of the top surface of the concrete block. To make a realistic simulation, half of the single wheel load (q/4 kN) was applied to the edge of the concrete block. At the corner of the slab load acts with a radius of R. To simulate the roadway geometry of a pavement slab, subgrade soil below the concrete block was considered as an elastic foundation. Elastic foundation was set based on Winkler foundation which consists of

springs with a spring constant of 0.25 MPa/mm *(23)*. The loss factor due to damping was set to zero. Four side faces were assigned to symmetric boundaries assuming symmetry in geometry and loads, since considered concrete block is in the middle of a roadway slab and surrounded by other portions of the slab.

3.3. Thermo-Hygro Model

Variable heat and moisture distribution develop mechanical stress and strain in concrete blocks. External temperature changes the internal temperature distribution in concrete. Moisture transport is more complex compared to temperature variation. Thermal and moisture-induced strain were calculated based on ambient change of temperature and moisture, and then combined with ASR expansion-induced volumetric strain to analyze coupled hygro-thermo-chemo effect of the concrete block.

Heat transfer governing equation

Internal temperature distribution in solid concrete can be expressed based on the principle of energy conservation. Eq. (20) shows the heat transfer equation which is governed by Fourier's law *(24)*.

$$\rho c_p \frac{\partial T}{\partial t} + \nabla \cdot (k \nabla T) = Q_s \qquad (20)$$

where ρ is the density of the fluid (kg/m^3), c_p denotes specific heat capacity at constant stress (J/(kg-K)), T is temperature (K) (i.e. 0°C = 273 K), k is the thermal conductivity of concrete (W/(m-K)), and Q_s is heat source or sink (W/m^3).

In this study heat source Q_s was ignored for hardened concrete. The density, specific heat capacity, and thermal conductivity of concrete were assumed as constant according to study *(24)*.

The thermal strain induced from temperature variation can be determined using Eq. (21) according to study *(24)*.

$$\varepsilon_{th} = \alpha \cdot \Delta T \quad (21)$$

where, ε_{th} is the thermal strain; α is the thermal expansion coefficient (1/K), and ΔT denotes temperature gradient (K). Temperature gradient is the difference of absolute temperature (T) with a reference temperature (T_{ref}). In this study reference temperature was kept equal to room temperature.

To simulate external temperature variation, Eq. (22) was used as a boundary condition for concrete block, where annual variation of ambient temperature follows a sinusoidal function *(24)*.

$$T_{ambient} = 15 + 10 \cdot \sin(2л \, . \, t) \quad (22)$$

where $T_{ambient}$ represents ambient temperature (K) and t is time elapsed (years).

Moisture transport governing equation

Moisture transport in concrete was simulated using Richards' equation as the governing equation. Eq. (23) shows the Richards' equation which was used to analyze flow in variably saturated porous media. Here, water head or pressure is the dependent variable.

$$\rho(C_m/\rho g + S_e S) \frac{\partial p}{\partial t} + \nabla \cdot \rho(-K_s k_r (\nabla p + \rho g \nabla D)) = Q_m \quad (23)$$

where, ρ is the density of the fluid (kg/m^3), C_m represents specific moisture capacity (1/m), g is the acceleration due to gravity (m/s^2), S_e denotes effective saturation (1), S denotes storage coefficient (1/Pa), p is the pressure (Pa), K_s represents hydraulic conductivity (m/s), k_r represents relative permeability (1), D is the elevation (m), and Q_m is the fluid source ($kg/(m^3.s)$). In this study, elevation, D and fluid source, Q_m were assumed to be zero.

According to study *(23)*, moisture transport in concrete can be determined by liquid volume fraction as per Eq. (24). Liquid volume fraction of concrete in porous medium is related to the pressure or water head in the medium.

$$\theta = \theta_r + \frac{\theta_s - \theta_r}{[1+(\alpha|p|)^n]^m} \quad (24)$$

where θ is the liquid volume fraction in concrete (1), θ_s represents saturated water content (1) and θ_r represents residual water content (1). Here, α, m, and n are constants. Values of θ_s, θ_r, α, m, and n were set based on water retention curves according to study *(23)* (Table 2-1). The constitutive parameter m is equal to 1-1/n *(23)*.

The Richards' equation represents the movement of water in unsaturated condition. 'Specific moisture capacity', C_m is a function describing the rate of change of saturation with respect to the matric head. C_m can be expressed as:

$$C_m = \frac{\partial \theta}{\partial p} \quad (25)$$

The moisture strain induced from moisture variation can be determined per Eq. (26) according to study *(23)*.

$$\varepsilon_{mo} = \beta \cdot (\theta - \theta_{ref}) \quad (26)$$

where, ε_{mo} is the moisture induced strain; β is the hygroscopic swelling/shrinkage coefficient (1), θ is the liquid volume fraction in concrete obtained from Eq. (24), and θ_{ref} denotes a reference moisture content (1).

To simulate external moisture variation liquid volume fraction can be related to the relative humidity in atmosphere per Eq. (27) *(23)* and used as a boundary condition for the concrete block.

$$\theta = \theta_s \cdot (1 - \frac{\ln RH}{B})^{1/C} \quad (27)$$

where θ and θ_s are same as aforementioned, RH denotes relative humidity, B and C are constants. The values of B and C are 0.57 and 0.64, respectively *(23)*. Like ambient temperature annual variation of ambient relative humidity follows a sinusoidal function *(24)* as follows:

$$RH = 0.65 + 0.25 \cdot \sin(2л. t) \quad (28)$$

where t is time elapsed (years).

4 Concrete Damage Model

In an ASR model, damage progresses with the gel diffusion in the concrete block. The density in the damaged state is not the same as that of initial density in a non-damaged state. Volumetric strain is the ratio of volumetric variation to total volume of concrete and can be expressed in terms of a relationship between concrete density in damaged and non-damaged state *(16)* as following:

$$\varepsilon_{gel} = 1 - \frac{\rho_c}{\rho'} = 1 - \frac{\rho_c}{\rho_c + \rho_{gel}} \quad (29)$$

where ε_{gel} is the volumetric strain due ASR expansion, ρ_c is concrete density in non-damaged state, ρ' is density in damaged state and ρ_{gel} is the density i.e. mass concentration of expansive ASR gel. In chemistry, the mass concentration is defined as the mass of a constituent divided by the volume of the mixture *(25)*. Due to ASR expansion and volume increase, density is also increased and thus $\rho' > \rho_c$.

According to study *(25)* conversion to mass concentration, ρ_{gel} from molar concentration, C_{gel} can be calculated per Eq. (30).

$$\rho_{gel} = C_{gel} \times M_{gel} \quad (30)$$

where C_{gel} denotes concentration of expansive ASR gel which is obtained from Eq. (11) and M_{gel} denotes the molar mass of expanded ASR gel.

Stress induced in ASR mechanisms due to volumetric variation can be expressed using Hooke's Law per Eq. (31).

$$\sigma = \mathbf{E}\varepsilon, \tag{31}$$

where σ denotes stress tensor, E is the modulus of elasticity, ε is strain tensor from volumetric variation, E is Young's modulus and ν is the Poisson's ratio.

Strain tensor can be expressed as,

$$\varepsilon = \begin{bmatrix} \varepsilon_{11} & \varepsilon_{12} & \varepsilon_{13} \\ \varepsilon_{21} & \varepsilon_{22} & \varepsilon_{23} \\ \varepsilon_{31} & \varepsilon_{32} & \varepsilon_{33} \end{bmatrix} \tag{32}$$

According to study *(16)*, a chemical damage criteria can be formulated in terms of damage function as following:

$$D = \begin{cases} 0 & \text{when, } \boldsymbol{\varepsilon}_{gel} \leq 0.1\% \\ w & \text{when, } \boldsymbol{\varepsilon}_{gel} > 0.1\% \end{cases} \tag{33}$$

where, $w = 2.021 \times \varepsilon_{gel} - 0.195$, where ε_{gel} represents volumetric strain generated from ASR mechanisms.

5 Finite Element Analysis

To solve the governing equation set, a mesoscale geometry of a concrete block (200mm × 200mm × 40mm) was generated in this work. For finite element analysis, a concrete geometry was created in the virtual cement concrete testing lab following the volume fraction of cement paste and aggregate particles (Table 2-1). We assumed elliptical aggregates to represent aggregates for simulating ASR gel expansion (Figure 2-1).

Ellipsoid of different sizes were created to consider irregular morphology of aggregate particles.

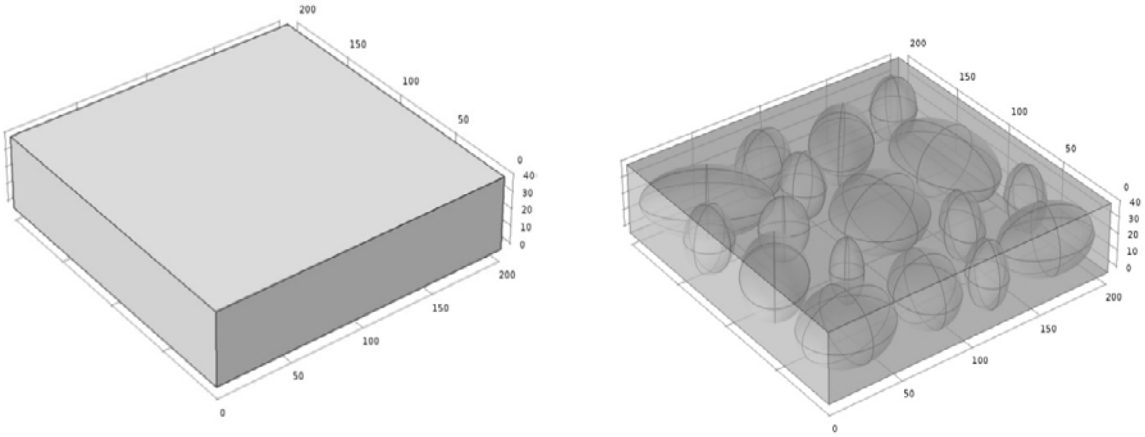

(a) (b)

Figure 2-1 Meso-structure model of concrete block (a) Solid view (b) Transparent view.

The concrete domain was divided into two phases: hardened cement paste and aggregate. Mesh details and material properties vary in cement paste and aggregate domain (Table 2-1).

Table 2-1 Mesh Details and Material properties used in FEM modeling

	Cement Paste	**Aggregate**	**Source**
Type of Mesh	Tetrahedron	Tetrahedron	Calibrated
Maximum element size (mm)	20.8	20.8	
Minimum element size (mm)	3.74	3.74	
No. of elements	50314	38935	
Volume fraction	0.4	0.6	
Diffusion Coefficient of ASR gel (m^2/s)	1×10^{-10}	1×10^{-12}	(*16*)
Young's Modulus (Pa)	5×10^{6}	60×10^{6}	(*23*)
Poisson's Ratio (1)	0.2	0.25	
Density (kg/m^3)	3150	2600	
Viscosity of water (Pa.s)	8.9×10^{-4}	NA	(*26*)
Permeability (m^2)	7.5×10^{-6}	NA	Calibrated
Heat Capacity (J/(kg-K))	1548	850	(*23*)
Thermal conductivity (W/(m-K))	1.73	2.9	
Thermal expansion coefficient (1/K)	7×10^{-6}	10×10^{-6}	
Hygroscopic swelling/shrinkage coefficient (1)	9.93×10^{-3}	NA	
Saturated moisture content (1)	0.185	0.308	
Residual moisture content (1)	0	0.08	
Hydraulic conductivity [m/s]	6×10^{-13}	5.35×10^{-11}	
Constant, α (1/m)	3.23×10^{-4}	15.3	(*23*)
Constant, n	1.217	1.406	
Constant, m	0.178	0.289	

Based on mathematical models and concrete damage models discussed in section 3 and 4, respectively, a comprehensive governing equations set was developed for finite element analysis of coupled multiphysics per Eq. (34-40) to predict damage of concrete pavement slab in terms of volume change.

$$D = 2.021\times \varepsilon_{vol} - 0.195 \tag{34}$$

$$\varepsilon_{vol} = \varepsilon_{gel} + \varepsilon_{traffic} + \varepsilon_{thermo} + \varepsilon_{hygro} \tag{35}$$

$$\varepsilon_{gel} = \frac{[\text{Expanded ASR gel}] \times 0.119}{\rho_c + [\text{Expanded ASR gel}] \times 0.119} \tag{36}$$

$$\frac{\partial}{\partial t}(u) + \nabla \cdot (-D_{gel}\nabla[\text{ASR gel}]) + \mathbf{u} \cdot \nabla u = f(u) \tag{37}$$

$u = [[\text{Siloxane}], [\text{ROH}], [\text{ASR gel}], [\text{Silanol}], [\text{H2O}], [\text{Expanded ASR gel}]]^T$

$f_{[Siloxane]} = -k_1[Siloxane][ROH]$

$f_{[ROH]} = -k_1[Siloxane][ROH] – k_2[Silanol][ROH]$

$f_{[ASR\ gel]} = k_1[Siloxane][ROH] + k_2[Silanol][ROH] – k_3[ASR\ gel][H2O]$

$f_{[Silanol]} = k_1[Siloxane][ROH] – k_2[Silanol][ROH]$

$f_{[H2O]} = k_2[Silanol][ROH] – k_3[ASR\ gel][H2O]$

$f_{[Expanded\ ASR\ gel]} = k_3[ASR\ gel][H2O]$

$$\rho/\varepsilon_p\left(\frac{\partial \mathbf{u}}{\partial t}\right) - \nabla.(-p) - \nabla \cdot [1/\varepsilon_p \{\mu(\nabla \mathbf{u} + (\nabla \mathbf{u})^T) - \frac{2}{3}\mu(\nabla \cdot \mathbf{u})\mathbf{I}\}] + (\mu \boldsymbol{\kappa}^{-1} + Q_{br}/\varepsilon_p^2)\mathbf{u} = 0 \quad (38)$$

$$\rho \nabla \cdot \mathbf{u} = Q_{br} \quad (39)$$

$$Q_{br} = 0.018 \times f_{[H2O]} \quad (40)$$

Percentage of damage can be calculated from Eq. (34) when volume change is greater than 0.1%. Damage is expressed as a function of total volume change.

To determine total volume change an equation was developed in this study per Eq. (35). This equation determines the total volumetric strain, ε_{vol} in terms of resultant volume change induced from expansive gel, traffic loads, temperature and moisture content change. Here, ε_{gel} is the volume change due to ASR expansion, $\varepsilon_{traffic}$ denotes the traffic induced volumetric strain, ε_{thermo} denotes thermal induced volumetric strain and ε_{hygro} denotes moisture induced volumetric strain.

Volumetric strain from expansive gel can be determined from Eq. (36). Here, definitions of all symbols are the same as mentioned previously in this work. Density of concrete was set to 2400 (kg/m^3). Based on the atomic mass of chemical elements that form expanded ASR gel, Si-O-R. $(H2O)_n$ per Eq. (3), molar mass of gel was calculated and set to 119 gm/mole (0.119 kg/mole). It is noteworthy that ASR gel does not have a unique stochiometry. However, this study considered a unique density for the ASR gel for simplification, which is a limitation to the model.

Concentration of expanded ASR gel can be determined from Eq. (37). This equation accounts for the diffusion of ASR gel as per diffusion coefficient, D_{gel} (Table 2-1). Here, u is the dependent variable which is a concentration tensor of all six species involved in chemical kinetics. f(u) is the source term as a function of u. Note that in this study, source term, was defined as a reaction term, which depends on rate change of concentration for each individual chemical species based on Eq. (6). For numerical solution reaction rate k_1, k_2, k_3 were kept constants according to study *(15)* and assigned to a value of 6.34×10^{-9} mole/(m^3.sec), 3.17×10^{-8} mole/(m^3.sec), and 1.6×10^{-7} mole/(m^3.sec), respectively.

The unknown fluid velocity in Eq. (37) can be calculated from Eq. (38). The mass source Q_{br} comes from water/moisture content and was assumed to be $M_w \times f_{[H2O]}$, where $[H_2O]$ stands for water concentration as mentioned previously. M_w is the molar mass of water which is 18 gm/mole (0.018 kg/mole).

Initial and reference values of different parameters used in finite element analysis vary for cement paste and aggregate domain (Table 2-2). Initial concentration of chemical species were set based on temporal variation of reactants and products according to study *(15)*. Initial concentration of siloxane species is zero in cement paste as it comes from aggregate particles only. Initial concentration of hydroxyl ions, ROH and water is zero in aggregate particles as those species come from cement paste only. Initial concentration of Siloxane and ROH must be greater than zero for an ASR reaction to happen *(15)*. In study *(15)* assumptions of initial concentrations were taken considering two cases. In case 1, $B_0 > 2A_0$ and in case 2, $B_0 < 2A_0$; where, A_0 means initial concentration of Siloxane and B_0 means initial concentration of ROH. Since in this present study initial concentration of

Siloxane was taken as 1 (mole/m^3), to simulate both of the cases initial concentration of ROH was taken as 0.7 (mole/m^3) and 2.5 (mole/m^3) respectively. Initially there was no pressure gradient in the concrete block as reference pressure and internal initial pressure both were considered with equal values.

Reference temperature was taken considering room temperature of 20°C or 293.15K. Value of reference moisture content was taken from study *(23)*. The cement paste/mortar phase of the model was considered as a typical saturation of 90% in field conditions, which is equal to a moisture content of 16.5% based on the total volume of the concrete block.

Table 2-2 Initial and reference values used in numerical analysis

Model	**Details**	**Cement Paste**	**Aggregate**	**Source**
ASR model	Initial concentration of Siloxane (mol/m^3)	0	1	Calibrated
	Initial concentration of ROH (mol/m^3)	0.7,2.5	0	
	Initial concentration of H_2O (mol/m^3)	2	0	
	Initial concentration of Silanol (mol/m^3)	0	0	
	Initial concentration of ASR gel (mol/m^3)	0	0	
	Initial concentration of expanded ASR gel (mol/m^3)	0	0	
	Velocity field at X direction (m/s)	0	0	
	Velocity field at Y direction (m/s)	0	0	
	Velocity field at Z direction (m/s)	0	0	
	Initial pressure (atm)	1	1	
	Reference pressure (atm)	1	1	
Thermo-Hygro model	Initial temperature (K)	293.15	293.15	
	Reference temperature (K)	293.15	293.15	
	Initial liquid volume fraction (1)	0	0	
	Reference moisture content (1)	16.5%	NA	(*23*)
	Initial pressure head (m)	-1	NA	
	Displacement at X direction (m)	0	0	
	Displacement at Y direction (m)	0	0	
	Displacement at Z direction (m)	0	0	

It is noteworthy that ASR expansion does not become visible immediately after the beginning of ASR mechanisms. A certain time is required for the reaction to happen depending on the reacting environment of the domain. This phenomenon is defined as a latency period which was analyzed in study *(6)*. However, according to study *(15)*, there is no latency period in the expansion curves when initial concentration of water/moisture is zero (i.e. unsaturated condition). Since this study deals with fully saturated conditions (present of excess water in concrete), the reaction starts from the beginning of the time interval and expansion curves do not show any latency period.

Initially ASR gel continues to fill up free pores in cement paste and during that time there is no obvious volumetric change. When cement pores are completely filled up with ASR gel, continuous gel diffusion initiate volumetric change and expansion becomes visible. The initial time period during which there is no obvious volumetric change is termed as the latency period. Latency period was justified by study *(6)*.

6 Model Validation

To ensure the accuracy of the developed finite element model, predicted ASR expansions were validated by established experimental data which follows a standard C 1293 test method. This is a concrete prism test (CPT) that determines the length change of concrete due to alkali silica reaction. For the validation of the ASR model, experimental data were collected from study *(27)*. According to study *(27)*, experimental data was considered for concrete A which is composed of aggregate type A. Aggregate A is chlorite schist in terms of rock type and amount of silicate is >95 and percent by number is 100. For each type of aggregate, two samples with a combined surface area of approximately 40 cm^2 were prepared. They calibrated heat without stirring for 2 weeks at 38°C. The

impacts on the kinetics order of the reaction was studied for different alkali levels, 0.4%, 0.8% and 1.2 % Na_2O_{eq} for concrete samples. The aggregate sections were observed by Scanning electron microscopy (SEM) to identify the disorder induced by the reaction and to evaluate the reactivity. Based on that result, aggregate A was found as potentially reactive. However, in study *(27)*, a modification of the standard test method was used which consisted essentially of testing concrete incorporating the reactive aggregates at varying alkali contents and temperatures. The concrete samples were immersed in water at 20, 40 and 60°C with alkali contents 0.4, 0.8, and 1.2 (mole/m^3). To match with the chemical, environmental and mechanical conditions of the prism tests conducted in study *(27)*, numerical simulation of ASR model was considered with Alkali concentration of 1.2 (mole/m^3), free expansion of ASR without any applied load, and constant temperature of 20°C (293.15K). Aggregate A was implemented in the model geometry which as a reactive aggregate facilitates alkali-silica reaction. Validation models were simulated over a period of 400 days. Since expansion varies for different points throughout the concrete block, average expansion was calculated based on ASR induced volumetric strain per Eq. (41).

$$E_{avg} = 100 \times \int_V \varepsilon_{gel} \frac{dV}{V} \qquad (41)$$

where E_{avg} is percentage of average expansion.

It is obvious from the comparison that the expansion curve of FEM simulated model is following the trend of experimental curves (Figure 2-2). Thus, simulated outcomes comply with experimental data and the ASR model is validated successfully.

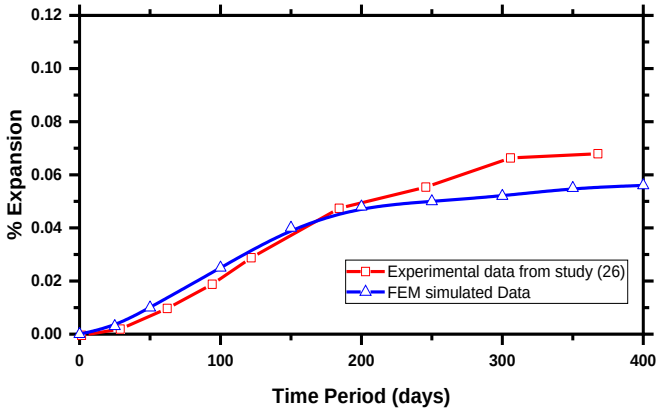

Figure 2-2 Validation of FEM simulated data with experimental data.

7 Results and Discussion

A developed FEM model was simulated for 30 years to assess long term condition of concrete. Results are based on the representative three dimensional FEM model of the reference concrete block. Concentration change and volumetric strain generated in the model were taken as an average value over the volume of the whole domain to avoid variation in results.

To predict how concrete behaves under ASR mechanisms for different concentrations of chemical species, a FEM model was simulated in two cases. In the first case the model was simulated considering low alkali contents in cement matrix (initial concentration of ROH = 0.7 mole/m^3). In the second case the model was simulated considering very high alkali contents in cement matrix (initial concentration of ROH = 2.5 mole/m^3). Initial concentrations of all other species were kept the same for both of the cases. The concentration of expansive gel as well as ASR induced volumetric strain increases with the increase in ROH concentration (Figure 2-3). This is because high ROH concentration accelerates ASR gel production in concrete. In the first case maximum volume change is 6.59×10^{-4} (0.066%) after 30 years (Figure 2-3b), which is less than the

damage limit of 0.1%. However, for the second case maximum volumetric strain of 1.27 × 10^{-3} (0.127%) exceeds the damage limit (Figure 2-3b). Thus, the first case was neglected and concrete damage was predicted based on the second case with high alkali content.

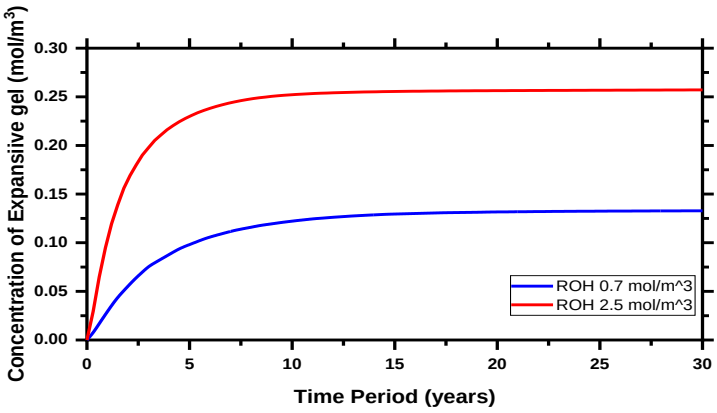

(a)

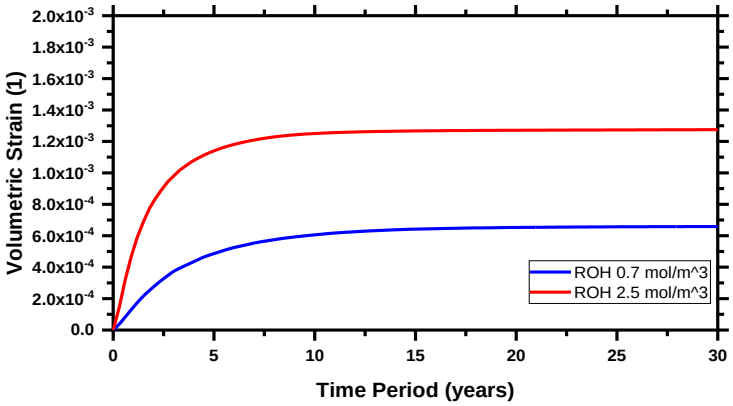

(b)

Figure 2-3 ASR mechanisms for different concentrations of ROH.

Concentration of expansive ASR gel generated due to ASR kinetics increases as time progresses (Figure 2-3a). This simulation result is based on the initial concentration of species considered in this study, no applied loads, and constant temperature of 20°C, model geometry and fully saturated conditions. There is a rapid increase in concentration initially and at 5 years it is 0.23 (mole/m^3). After 5 years the increment continues at a

slower rate than before and concentration becomes 0.255 (mole/m^3) at 15 years. After 15 years there is no significant change in concentration until 30 years when maximum concentration becomes 0.257 (mole/m^3). In the concrete matrix, distribution of expansive gel varies for different time periods, as visualized in Figure 2-4. The concentration of expansive ASR gel is higher in the space between closely positioned aggregate particles. It is also found that the concentration of expansive ASR gel is high around the small sized aggregate particles. This is because more surface area is provided by small particles compared to larger ones. Actually, expansive gel generated inside the reactive aggregates is first followed by aggregate cracking and then cracking in paste. Thus, gel flows along the cracks from the aggregate through the cement paste.

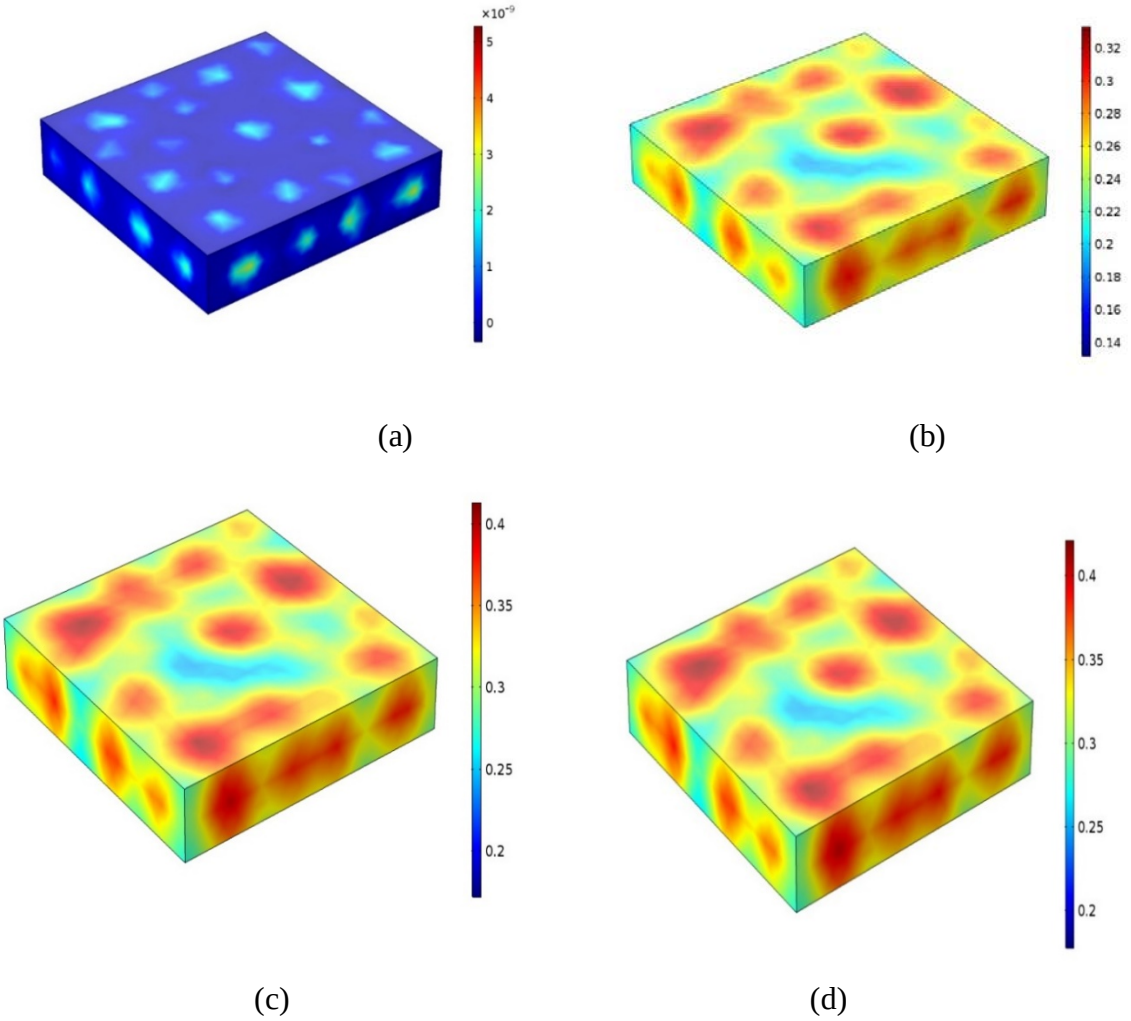

Figure 2-4 Concentration of expansive ASR gel (mole/m^3) in concrete: (a) 0, (b) 5, (c) 15, and (d) 30 years

Average concentrations of all six species involved in ASR kinetics change with the progression of time (Figure 2-5). ROH concentration decreases at a faster rate from the very beginning of alkali silica reaction and continues up to 5 years. The reduction in concentration starts with the reaction between alkali hydroxides and siloxane, and further continues when byproduct silanol reacts with alkali hydroxides. After a certain number of years (15 years) the reduction rate of alkali hydroxides does not change significantly and reaches a more or less stabilized concentration of 1.35 (mole/m^3). Concentration of

expansive ASR changes inversely with that of alkali ions. Thus expansive gel formation speeds up after the latency period and increases at a decreasing rate. According to Eq. (1), (2), and (3) expansive gel formation continues with the chemical reaction and depletion of all other species involved in the kinetics. For this reason, concentrations of siloxane, silanol, water and ASR gel tend to decrease as time progresses. Silanol is a byproduct of the chemical reaction which increases at first and then decreases later with the formation of ASR gel. Concentration of ASR gel also increases initially and then decreases when it starts to convert into expansive gel by absorbing water.

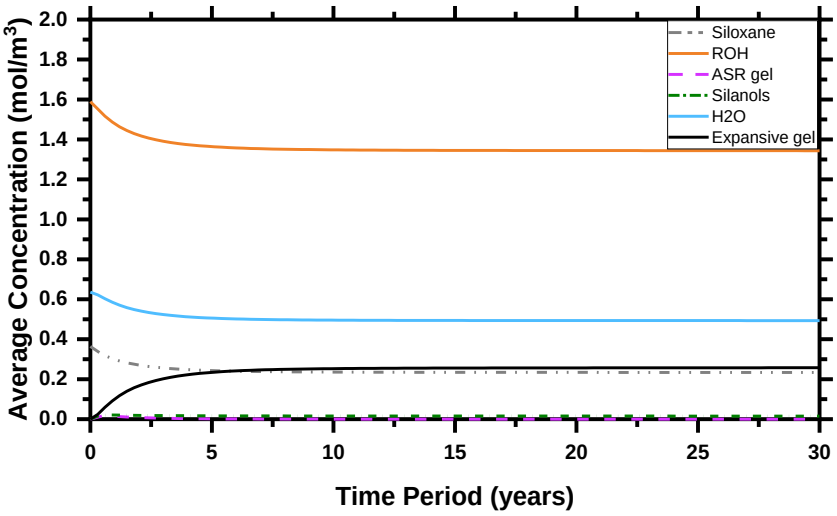

Figure 2-5 Comparison between concentrations of all six species (mole/m^3) in concrete.

Volumetric strain was calculated from the developed comprehensive governing equations set discussed in section 5 (Figure 2-6). ASR expansion is a slow process and maximum volumetric strain due to ASR expansion is 1.27×10^{-3} after 30 years. In addition to the traffic loads volume change becomes higher than that of gel expansion. Volumetric change from coupled temperature and moisture variation is very low compared to traffic loads. Thus, traffic loads govern the damage model in terms of volumetric variation in the

concrete block. However, in a certain roadway condition, ASR expansion accelerates the volume expansion. With the combined effect of ASR expansion, traffic loads, temperature and moisture variation volumetric strain reaches up to a maximum value of around 0.1 after 30 years.

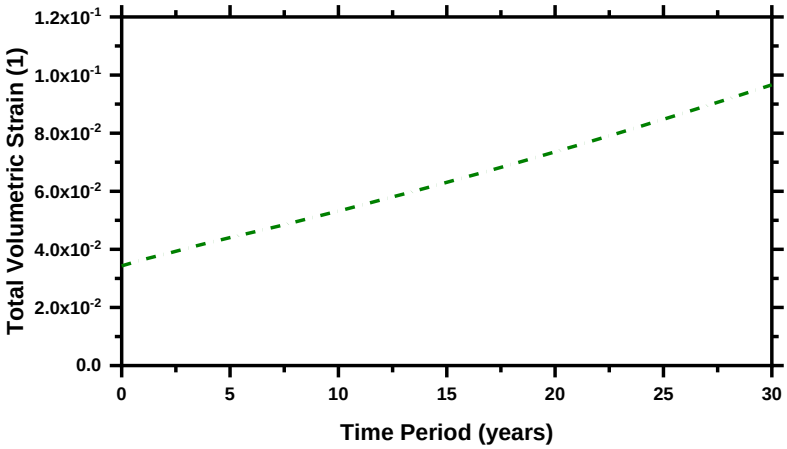

Figure 2-6 Total volumetric strain developed in the concrete block.

Damage function was calculated based on total volumetric strain to predict percentage of damage with time progression. From the damage evolution it is clear that the percentage of damage increases linearly since applied ESAL loads are a linear function that govern the damage model (Figure 2-7). Initially at the year of 2018, damage is just above 5% which increases over time, and after 30 years at 2048, damage reaches around 20%. Hence, with the coupled FEM model it can be predicted that considered concrete block of roadway pavement slab will degrade gradually and effective measure should be taken accordingly.

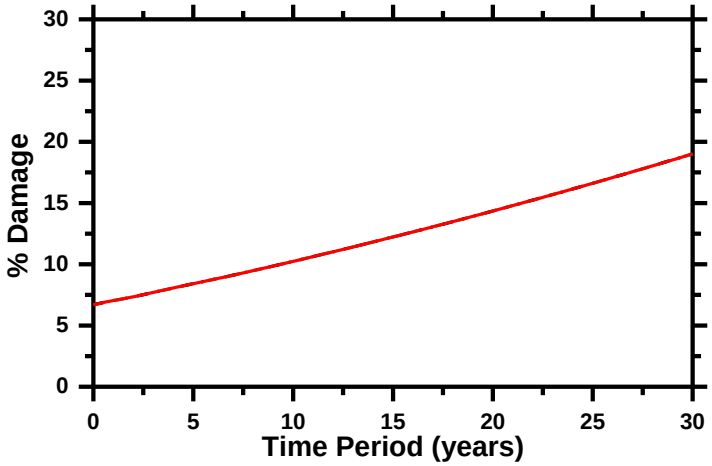

Figure 2-7 Damage progress in concrete block over time.

The results shown on Figure 2-6 and Figure 2-7 are based on total volumetric strain (i.e. expansive gel, traffic load, thermal expansion and hygroscopic swelling). This is a totally new idea to combine all of these effects and no experimental results are available on this context. Hence, these figures cannot be validated.

8 Conclusions

This work proposes a three-dimensional multiphysics model for studying concrete degradation at meso-scale subject to ASR degradation. A developed comprehensive set of governing equations is the major contribution of this work to accurately predict the ASR damage that integrated coupled THM, material mesoscale details and damage modes. A 30 year simulation period provides an in depth view of concrete degradation with the progression of time. The findings of this paper confirmed that average expansion in concrete starts after the latency period and then continues to increase with a decreasing rate. For the first few years, alkali-silica reaction is amplified and then tends to stabilize with the depletion of alkali-hydroxides concentration. Concentration of expansive alkali-silica gel is higher in cement paste than aggregate and thus cement paste have larger

expansion and displacement than aggregate particles during ASR kinetics. This may happen as expanded gel passes through the fine crack of aggregate and enters into the cement matrix. Thus, ultimately high concentration of ASR gel remains in the cement paste. However, traffic loads remain as the driving force to propagate damage in concrete. ASR damage can be minimized by effectively following three strategies: using non-reactive aggregates, limiting the maximum alkali content of concrete and limiting the moisture availability in the field structures. Damage induced from temperature and moisture variation can be avoided by limiting direct contact of concrete surface to the field environments. Implementing thermo-hygro proof coatings on the concrete surface could be one solution to this problem. Damage generated from traffic loads can be controlled by future oriented roadway design and effective traffic control.

The developed governing equation set can be calibrated further for any pavement slab by changing initial concentrations of chemical species and concrete density according to roadway condition. The percentage of damage will propagate with time based on the damage model discussed in this study. Thus, this physics-based model can be used to accurately determine damage level and predict the service life of concrete. There is great potential for this model to be used for future study and evaluation purposes.

Author Contribution Statement

The authors confirm contribution to the paper as follows: study conception and design: Md. Asif Rahman, Dr. Yang Lu; data collection: Md Asif Rahman, Dr. Yang Lu; analysis and interpretation of results: Md. Asif Rahman; draft manuscript preparation: Md. Asif Rahman; approval of the final version of manuscript: Dr. Yang Lu.

References

1. Alexander, M. and S. Mindess. Aggregates in Concrete: Modern Concrete Technology 13. Taylor & Francis, London and New York, 2010.
2. Prezzi, M., P. J. M. Monteiro, and G. Sposito. The Alkali-Silica Reaction, Part I: Use of The Double-Layer. ACI Materials Journal, 1997. January-February: 10-16.
3. Chatterji, S. Chemistry of Alkali–Silica Reaction and Testing of Aggregates. Cement & Concrete Composites, 2005. 27: 788–795.
4. Mukhopadhyay, A. K. An Effective Approach to Utilize Recycled Aggregates (RAs) From Alkali-Silica Reaction (ASR) Affected Portland Cement Concrete. In Handbook of Recycled Concrete and Demolition Waste (F. Pacheco-Torgal, V. W. Y. Tam, J. A. Labrincha, Y. Ding, and J. de Brito), Woodhead Publishing Limited, Cambridge, UK, 2013. pp. 555-568.
5. Taylor, H. F. W. Cement chemistry. Thomas Telford Services Ltd., London, 1997.
6. Ulm, F.J., O. Coussy, L. Kefei, and C. Larive. Thermo-Chemo-Mechanics of ASR Expansion in Concrete Structures. Journal of Engineering Mechanics, 2000. 126: 233-242.
7. Ferraris, C. F., E. J. Garboczi, F. L. Davis, and J. R. Clifton. The Effect of Stress Relaxation, Self-Desiccation, and Water Absorption on Alkali-Silica Reaction in Low Water/Cement Ratio Mortars. Cement and Concrete Research, 1997. 27: 1153-1560.
8. Touma, W. E., D. F. Fowler, and R. L. Carrasquillo. Alkali-Silica Reaction in Portland Cement Concrete: Testing Methods and Mitigation Alternatives. Research Report ICAR 301-1F. International Center for Aggregates Research (ICAR), The University of Texas at Austin, 2001.
9. Poyet, S., A. Sellier, B. Capra, G. Thèvenin-Foray, J. M. Torrenti, H. Tournier-Cognon, and E. Bourdarot. Influence of Water on Alkali-Silica Reaction: Experimental Study and Numerical Simulations. Journal of Materials in Civil Engineering, 2006. 18: 588-596.

10. Thomas, M. D. A., B. Fournier, and K. J. Folliard. Alkali-Aggregate Reactivity (AAR) Facts Book. Publication FHWA-HIF-13-019. FHWA, U.S. Department of Transportation, 2013.

11. Leger, P., P. Cote, and R. Tinawi. Finite Element Analysis of Concrete Swelling Due to Alkali-Aggregate Reactions in Dams. Computers & Structures, 1996. 60: 601-611.

12. Hobbs, D. W. The Alkali-Silica Reaction - A Model For Predicting Expansion in Mortar. Magazine of Concrete Research, 1981. 33 (117): 208 - 220.

13. Steffens, A., and Z. P. Bazant. Mathematical Model For Kinetics of Alkali-Silica Reaction in Concrete. Cemente and Concrete Research, 2000. 30: 419-428.

14. Bournazel, J. P., and B. Capra. Modeling of Induced Mechanical Effects of Alkali-Aggregate Reactions. Cement and Concrete Research, 1998. 28: 251-260.

15. Saouma, V. E., R.A. Martin, M. A. Hariri-Ardebili, and T. Katayama. A Mathematical Model For The Kinetics of The Alkali–Silica Chemical Reaction. Cement and Concrete Research, 2015. 68:184-195.

16. Balbo, F. A. N., G. A. Pianezzer, L. M. Gramani, E. Kaviski, and M. R. Teixeira. An Application to the Diffusion Equation in a Model For The Damage in Concrete Due to Alkali-Silica Reaction. Applied Mathematical Sciences, 2015. 9: 4135-4147.

17. Ichikawa, T., and M. Miura. Modified Model of Alkali-Silica Reaction. Cement and Concrete Research, 2007. 37: 1291-1297.

18. Kim, T., J. Olek. Influence of Alkali Silica Reaction on The Chemistry of Pore Solutions in Mortars With and Without Lithium Ions. Brittle Matrix Composites, 2012. 10: 11-20.

19. Poole, A.B. Proceedings of The Third International Symposium on The Effect of Alkalis on The Properties of Concrete. Cement and Concrete Association, Wexham Springs, Slough, UK, 1976.

20. Peterson, Marcus G. A Chemoplastic Model for Alkali-Silica Expansion: Effect of Stress-Induced Anisotropy, MS Thesis, Massachusetts Institute of Technology, June 2000.

21. Gradoń, L. Principles Of Momentum, Mass And Energy Balances, Chemical Engineeering And Chemical Process Technology, Vol. I, Warsaw University of Technology, Warsaw, Poland.

22. Pavement Design, ITD Manual, Section 500, http://apps.itd.idaho.gov/apps/manuals/Materials/Sec%20500.pdf

23. Pan, T., C. Chen, and Q. Yu. Three-Dimensional Micromechanical Modeling of Concrete Degradation Under Multiphysics Fields. Composite Structures, 2017. 175: 7-18.

24. Chen, D., S. Mahadevan. Cracking Analysis of Plain Concrete Under Coupled Heat Transfer and Moisture Transport Processes. Journal of Structural Engineering, ASCE, 2007. 133(3): 400-410.

25. IUPAC, Compendium of Chemical Terminology, 2nd ed. (the "Gold Book") (1997). DOI: http://goldbook.iupac.org/html/A/A00295.html

26. Korson, L. Drost-Hansen, W. and J. Millero, F. Viscosity of Water at Various Temperatures, Contribution No. 980 from the Institute of Marine Sciences, University of Miami, Miami, Florida 88149 (Received April 12, 1968).

27. Ben Haha, M. Mechanical Effects of Alkali Silica Reaction in Concrete Studied by SEM-Image Analysis. Doctoral dissertation, École Polytechnique Fédérale de Lausanne. À La Faculté Sciences Et Techniques De L'ingénieur, France, 2006.

CHAPTER 3: A TIME-DEPENDENT CHEMO-MECHANICAL ANALYSIS OF ALKALI-SILICA REACTION FOR THE DISPARATE GEOMETRY OF CONCRETE MESO-STRUCTURE[2]

Abstract

Complex chemophysics of alkali-silica reaction (ASR) in Portland cement concrete deteriorates concrete service life and requires quantitative assessment. Within this context, the developed model provides a new perspective from mesoscale chemo-mechanical scheme for a better understanding of ASR kinetics. The simulated results shows how ASR expansion as well as ASR-induced damage progresses in concrete structure based on different composition of reactive aggregate and alkali hydroxide concentrations. This model can be used as an effective tool in the field of concrete materials to predict the service life, as well as on time maintenance decisions of concrete structure.

Keywords: ASR Chemophysics, ASR model, Mechanical model, Concrete Meso-structure, Anm model, Concrete damage model

[2] This chapter includes results already published in the following publication. Contribution of the coauthor is sincerely acknowledged: Rahman, M. A., and Lu, Y. "A Time-Dependent Chemo-Mechanical Analysis of Alkali-Silica Reaction for the Disparate Geometry of Concrete Meso-Structure", *Journal of Construction and Building Materials*, 2019. Volume 211, 847-857.

1. Introduction

Portland cement concrete is a common construction material that is frequently used due to its durability, long service life and great economy. Chemical composition of cement, aggregate particles, water and other binding agents forms the hard skeleton of concrete structure which is the most popular load carrying component for construction. However, chemical reactions between reactive aggregate particles & cement paste lead to concrete degradation over time. Alkali-aggregate reaction is one of those undesirable chemical reactions. The two major types of alkali-aggregate reaction are alkali-carbonate reaction (ACR) and alkali-silica reaction (ASR). Though incidences of ACR are hardly seen and generally formed with dolomitic or ACR-susceptible aggregates, ASR is the most common source of concrete deterioration worldwide and is of more significance in the United States. The chemophysical mechanisms governing ASR are also quite complex [1]. It is a slow process and takes several years to manifest. Moreover, variable environmental conditions and structural loading significantly influence ASR expansion.

Though aggregates are chemically inert to a certain extent, in ASR, reactive aggregate particles make chemical contact with the highly alkaline pore solution present in the cement paste. Reactive aggregates contain silica which reacts with alkali hydroxide in concrete and forms solid alkali silica gel [2]. This gel further swells when it absorbs water from surrounding cement paste or the environment and induce increasing internal pressure in the cementitious matrix of concrete structure [3]. This pressure initiates expansion which is capable of breaking down the concrete skeleton and developing cracks in concrete structure with the progression of time.

ASR kinetics depends on three variables: (1) sufficient pH and alkalies from cement clinker; (2) reactive silica from aggregates and (3) sufficient moisture/water [4]. Each of these criteria must be met for the reaction to occur [5]. The alkali-silica reaction takes place between silica and hydroxides. Alkalies (namely K^+ and Na^+) coming from cement clinker ultimately reside in the concrete pore solution [6]. Hydration in concrete pore solution are associated with hydroxyl ions (OH^-) which produce high pH in the pore solution [7]. Reactive silica in aggregate tends to breakdown due to the high alkalinity of pore solution in concrete and subsequently react with alkali-hydroxides to form ASR gel. There may be two forms of silica in natural aggregates: crystalline or non-crystalline. In a crystalline silicate structure like quartz (SiO_2) there are no complete tetrahedron formed on the surface and structural impermeability of such structures allow it to react only on the surface, and thus, they are less reactive [8]. Unlike crystalline silicate, non-crystalline silicate structures are formed by irregular tetrahedral arrangements which make it more porous with greater surface area and thus, they are more susceptible to reaction [8]. Hence, aggregate's reactivity to alkalis are greatly influenced by its irregular crystallinity. Sufficient moisture is important for potential ASR reactions [4]. Moisture facilitates the flow of ions in the porous media and allows hygroscopic gel to swell when it absorbs water. Expansion is directly related to the percentage of relative humidity in concrete. Many researchers have reported increasing ASR expansions as the relative humidity tends to increase [9]. A minimum relative humidity of 80 percent is required to set out alkali-silica reaction and cause significant expansion [10]. Moreover, increased temperature accelerates the alkali-silica reactions in some extent [11].

Since the 1940s, several research studies have been conducted to identify this expansive characteristic of the alkali-silica reaction. Previous studies [6, 12-16] attempted to clarify ASR mechanisms and develop expansion models to figure out the problems related to ASR damage in concrete.

Despite decades of phenomenological observation study, the chemophysical mechanism of ASR from the mesoscale perspectives remains to be fully understood for clearly capturing the ASR induced damage processes. The proposed model attempts to predict ASR- induced damage in concrete meso-structure on a case by case basis.

In this work, a time-dependent chemo-mechanical model was developed that quantifies ASR kinetics and analyzes mechanical behavior under mesoscale characteristics of ASR concrete for different geometric proportions of cement and aggregate particles. Modeling was done considering four key steps: mesoscale geometry, concrete chemistry, solid mechanics, and concrete damage model to predict the service life of concrete. Firstly, a 2D geometry was defined based on the representative concrete meso-structure. Five sets of geometry were introduced to simulate variable cement-aggregate proportions in concrete. Secondly, finite-element method (FEM) was employed to model the ingress of multiple chemical species into a variably saturated concrete matrix. For chemical kinetics it was assumed that there was enough moisture to stimulate chemical reaction. Several sets of governing equations were established to implement ASR kinetics into the model. Two different concentrations of alkali hydroxide content were considered to simulate variance in concentration of chemical species. Thirdly, mechanical deterioration due to ASR was analyzed and mechanical properties like volumetric change, strain, stress were determined on a case by case basis. A fixed load was applied and coupled with ASR expansion to

simulate structures under loading conditions. Finally, a damage model was developed in terms of the changing density of concrete block to predict damage in concrete structure. In the analysis, representative 2D concrete block was considered as a middle portion of a concrete structure.

Based on the simulation results, this proposed model has potential to predict ASR damage in concrete up to 30 years. The flexibility to change cement-aggregate ratio per concrete mix, and alkali hydroxide and siloxane concentrations per cement-aggregate mineralogy add broader applicability to this model. Based on the analysis, concrete expects to expand under alkali-silica reaction, and undergoes damage, large enough to form crack on concrete structure. However, external loads or any confinement tend to mitigate ASR expansion as well as damage to some extent.

2 ASR Chemophysics

The alkali-silica reaction in Portland cement concrete is a multi-stage process [17]. The process starts with the dissolution of siliceous components on the surface of the aggregate particles. Though numerous research studies have been conducted since the mid-1900s, to identify the mechanisms governing alkali-silica reaction, the exact chemistry of ASR expansion is still unclear. In general, alkali-silica reaction can be treated as acid-base reaction where silica in aggregate is acid reactant, hydroxides (K^+ or Na^+) remaining in the pore solution are basic reactants, water is the transport medium for reaction and calcium potassium (or sodium) silicate hydrate are the reaction product [18]. The pore water facilitates mass transport of hydroxyl and alkali ions required for the reaction to occur. ASR mechanism can be divided into three stages: (1) Hydration, (2) Neutralization and (3) Osmosis. Equations (1), (2), and (3) were considered to depict chemical reactions that

represent three stages, respectively [17]. In the first stage hydrolysis of the reactive silica (siloxane) by hydroxyl ions (OH^-) takes place. The siloxanes on reactive aggregate are attacked by the hydroxyl ions that remain dissolved in the pore solution with high pH. With this attack on silicate core structure, siloxane bonds (≡Si–O–Si≡) are broken and replaced by silanol bonds (≡Si–O–H) as illustrated by Eq. (1). This is a slow process due to sluggish participation of aggregate compared to cement paste. In the second stage, weak silanol groups further react with hydroxyl ions to generate alkali-silicate gel. This is a charge balance stage. Readily available positive alkaline cations (K^+ or Na^+) are attracted by the negatively charged species and diffuse in the gel to initiate charge balance in the basic pore solution [3]. Na^+ and K^+ are supposed to have the same effect, they are interchangeable in the model. At the last stage hydrophilic alkali-silicate gel formed in the earlier stages imbibes water or moisture from hydrated cement paste or the surrounding environment due to osmotic pressure and increases in volume. According to osmotic cell pressure theory, the difference in chemical potentials between the inside and outside layer of the gel, relates moisture absorption and expansion of the alkali-silica [19]. This expansive gel induces damage in the concrete structure. Concrete structures subject to alkali-silica reaction typically show at least one of the following degradations: cracking, expansion of concrete block, misalignments of structural components, or gel 'pop-outs' [20]. It is noteworthy that ionic exchange between alkalis in ASR gel and calcium in cement paste converts ASR gel into non expansive calcium silicate gel (CSH) and thus limits the ASR mechanisms. Alkalis (K^+ or Na^+) in ASR gel are replaced by abundant calcium ions (Ca^{2+}) in concrete per Eq. (4) to form stable calcium silicate bond (C–S–H) [15]. However, C–S–H mechanism was not considered in the chemical model of this study.

$$\equiv \underbrace{Si-O-Si}_{\text{Siloxane}} \equiv + \underbrace{R^{+} + OH^{-}}_{\text{ROH}} \rightarrow \equiv \underbrace{Si-O-R}_{\text{ASR gel}} + \underbrace{H-O-Si}_{\text{Silanol}} \equiv \qquad (1)$$

$$\underbrace{H-O-Si}_{\text{Silanol}} \equiv + \underbrace{R^{+} + OH^{-}}_{\text{ROH}} \rightarrow \equiv \underbrace{Si-O^{-}R^{+}}_{\text{ASR gel}} + \underbrace{H_2O}_{\text{Water}} \qquad (2)$$

$$\equiv \underbrace{Si-O-R}_{\text{ASR gel}} + \underbrace{nH_2O}_{\text{Water}} \rightarrow \equiv \underbrace{Si-O^{-} + \left(H_2O\right)_n + R^{+}}_{\text{Expanded ASR gel}} \qquad (3)$$

$$\equiv \underbrace{Si-O^{-} + \left(H_2O\right)_n + R^{+}}_{\text{Expanded ASR gel}} + \underbrace{\frac{1}{2}Ca^{2+}}_{\text{Calcium Ions}} \rightarrow \equiv \underbrace{Si-O^{-} + \frac{1}{2}Ca + \left(H_2O\right)_n}_{\text{C-S-H gel}} + \underbrace{R^{+}}_{\text{Excluded Alkali}}$$

(4)

where, R^{+} denotes an alkali ion (K^{+} or Na^{+}).

ASR kinetics is the study of reaction rates related to ASR mechanisms. Reaction rate is different for each stage [15]. Reaction rates, k_1, k_2, and k_3 were assigned to first, second and third stages respectively. The reaction rates are dependent on temperature through the Arrhenius equation [21] given as Eq. (5).

$$k = Ae^{(-E_a/R_gT)} \qquad (5)$$

where k is reaction rate, A is the frequency factor, E_a is activation energy, R_g is the gas constant and T represents temperature.

The rate of change of concentration for each of the six species can be expressed in the group Eq. (6) according to study [15]. All chemical species participating in the chemical kinetics of ASR were considered in this study to include their ionic exchange and thus,

change in their concentrations. This will quantify the total concentration of ASR gel in concrete after a certain time period based on all steps involved in the chemical kinetics.

$$\begin{aligned}
\frac{d[Siloxane]}{dt} &= -k_1[Siloxane][ROH] \\
\frac{d[ROH]}{dt} &= -k_1[Siloxane][ROH] - k_2[Silanol][ROH] \\
\frac{d[ASR\ gel]}{dt} &= k_1[Siloxane][ROH] + k_2[Silanol][ROH] - k_3[ASR\ gel][H_2O] \\
\frac{d[Silanol]}{dt} &= k_1[Siloxane][ROH] - k_2[Silanol][ROH] \\
\frac{d[H_2O]}{dt} &= k_2[Silanol][ROH] - k_3[ASR\ gel][H_2O] \\
\frac{d[Expanded\ ASR\ gel]}{dt} &= k_3[ASR\ gel][H_2O]
\end{aligned} \tag{6}$$

where, $[Siloxane], [ROH], [ASR\ gel], [Silanol], [H_2O]$, and $[Expanded\ ASR\ gel]$ represent concentration of each species, respectively.

3 Mathematical Models

3.1. ASR Model

ASR mechanisms progress with the change in concentration of chemical species, gel formation and penetration of gel into the pores in the cement matrix. It is noteworthy that less viscous Na-K rich gel generated inside the reactive aggregates first followed by aggregate cracking and then cracking in paste. Thus, gel flows along the cracks from the aggregate through the cement paste. In this study, finite-element method (FEM) was used to compute numerical approximation of PDEs and predict ASR-induced expansion. There are six reacting species that participate in the ASR mechanisms according to chemical kinetics discussed previously in section 2. Therefore, to solve ASR kinetics a system of six coupled governing equations is required that will account for gel diffusion and

concentration of each species. In this work, relevant physics of the ASR model were coupled together based on the principles of mass balance and momentum balance. Mass balance theory and Darcy's Law were used here to simulate transport of diluted properties and gel diffusion in the concrete porous media.

Mass Balance and Momentum Balance

Eq. (7) shows the coupled mass balance and momentum balance equation which models chemical species transport through diffusion and convection of each chemical species. The full derivation of this coupled equation was provided in author's previous paper per study [22]. This balance equation considers the two primary transport mechanisms, i.e., diffusion transport and diluted species transport, for the chemical species remaining in the porous concrete matrix. Fick's law governs the diffusion of chemical species and fluid (moisture/water) governs the migration of diluted species. The dependent variable in this equation is the concentration of species.

$$\frac{\partial}{\partial t}(c_i) + \nabla \cdot (-D_i \nabla c_i) + \mathbf{u} \cdot \nabla c_i = R_i \qquad (7)$$

where, c_i is the concentration of species i (mole/m^3), D_i denotes the diffusion coefficient of species i (m^2/s), **u** is the fluid velocity vector (m/s) with components in x, y, and z direction respectively, and R_i is a source term for the species i (mole/(m^3/s)).

Darcy's Law

Eq. set (8) shows the equations of Darcy's law. Darcy's law provides a complete mathematical model suitable for a variety of applications involving porous media flows. It is used here to model low-velocity flows in the porous media where the pressure gradient is the major driving force. Considering the gel to be a viscous fluid Darcy's law is used to

describe the gel permeation into the cement paste by generating pressure within the aggregate. The dependent variable in the Darcy's law is pressure.

$$\frac{\partial}{\partial t}(\varepsilon_p \rho) + \nabla \cdot (\rho \mathbf{u}) = Q_m$$
$$\mathbf{u} = -\frac{\kappa}{\mu}\nabla p \qquad (8)$$

where, ε_p is the porosity, ρ is the density of the fluid (kg/m^3), **u** is the velocity vector (m/s), Q_m is a mass source or mass sink of fluid (kg/(m^3.s)), κ is the permeability of the porous medium (m^2), μ is the fluid viscosity (Pa.s), and p is the pressure (Pa). The value of the permeability was kept constant for the whole simulation period as this model considered fully saturated condition only.

Note that equations set (7) and (8) are coupled equations where chemistry and flow in porous media of all six species, their diffusion and convection progress simultaneously.

To avoid the complexity in simulating ASR mechanisms it was assumed that: 1) reaction occurs with sufficient moisture content and reactive silica [9], 2) no mass change occurs during chemical reaction, i.e. always having a constant concrete mass [16], 3) no presence of calcium substances and hence, no reaction between ASR gel and calcium ions [15], 4) Na^+ & K^+ are supposed to have the same effect, i.e. they are interchangeable in the model, and 5) the attack is uniform on the surface of the aggregate.

3.2. Mechanical Model

Due to ASR mechanisms damage progresses with the gel diffusion in the concrete block. Expansion of ASR gel results in volume change of the concrete domain with time. Volumetric strain is the ratio of volumetric variation to total volume of concrete and can be calculated per Eq. (9).

1. $$\varepsilon = \frac{\Delta V}{V} \qquad \textbf{(9)}$$

where, ΔV is the volume change and V is total volume of concrete.

It is noteworthy that, volumetric strain is not visible immediately after the beginning of ASR mechanisms. Initially ASR gel continues to fill up free pores in cement paste and during that time there is no obvious volumetric change. When cement pores are completely filled up with ASR gel, continuous gel diffusion initiate volumetric change and expansion becomes visible. The initial time period during which there is no obvious volumetric change is termed as a latency period. Latency period was justified by study [23].

Concrete used in construction is subjected to loading conditions. Concrete experiences change in shape or size when stresses or loads are applied to it which in turn develop volumetric strain. To visualize concrete behavior under loading condition a small vertical stress of -1kPa (1 Pa=1N/m^2) was applied on the top portion of the considered 2D concrete block in modelling. A negative sign means that it was a downward loading. The bottom portion was considered as a fixed constraint assuming concrete block was lying on a fixed component of any structure. The other two portions at the left and right side were assigned to symmetric boundaries assuming symmetry in geometry and loads, since the considered block is in the middle of a concrete structure. Thus, due to this mechanical boundary condition, the concrete block is experiencing compressive stresses under vertical loading.

According to study [24], ASR damage is anisotropic under the loading conditions. ASR expansion and progression of damage may not be isotropic under the real world

scenario. However, the model was developed based on isotropy of concrete under the applied load and ASR expansion for simplicity and to reduce computational cost.

Stress induced in concrete structure due to volumetric variation can be expressed using Hooke's Law per Eq. (10).

$$\sigma = \mathbf{E}\varepsilon \tag{10}$$

where, σ denotes stress tensor, E is the modulus of elasticity, and ε is strain tensor from volumetric variation.

Strain tensor can be expressed as,

$$\varepsilon = \begin{pmatrix} \varepsilon_{11} & 1 & 1 \\ 1 & \varepsilon_{22} & 1 \\ 1 & 1 & \varepsilon_{33} \end{pmatrix} \tag{11}$$

According to study [16], a chemical damage criteria can be formulated in terms of damage function as following:

$$D = \begin{cases} 0 & when, \varepsilon_{gel} \leq 0.1\% \\ w & when, \varepsilon_{gel} > 0.1\% \end{cases} \tag{12}$$

where, $w = 2.021 \times \varepsilon_{gel} - 0.195$; where, ε_{gel} represents volumetric strain generated from ASR mechanisms.

Chemical damage is the deterioration of concrete structure due to alkali-silica reaction. The considered damage in this work is based on the change in density of concrete after ASR expansion. Increased volume and thus, increased density puts the concrete surface on tension. When developed stress surpasses the tensile capacity of concrete, crack forms in the concrete structure. The density in the damaged state is not same as that of initial density in non-damaged state.

ASR induced volumetric strain (ε_{gel}) can be expressed in terms of a relationship between concrete density in damaged and non-damaged states [16] as following:

$$\varepsilon_{gel} = 1 - \frac{\rho_c}{\rho'} = 1 - \frac{\rho_c}{\rho_c + \rho_{gel}} \qquad (13)$$

where, ρ_c is concrete density in non-damaged state, ρ' is density in damaged state and ρ_{gel} is the density of expansive ASR gel.

4 Finite Element Analysis

To solve the governing equation set, a two dimensional mesoscale geometry of concrete block (200mm × 200mm) was generated in this work. A mesoscopic approach was introduced to this work for visualizing concrete material at larger scale comparing to microstructures. For finite element analysis, concrete geometry was constructed in the virtual cement concrete testing lab with the X-ray CT image processing captured from actual concrete structure. X-ray computed tomography (CT) was initially used in the field of non-destructive medical anatomy for recovering internal structure of a subject [25]. CT images were further analyzed to justify the accuracy of it as a tool of finite element modeling [26]. Note that a 3D material meso-structure model, entitled Anm, of mortar and concrete [27-29] was created using the idea of representing actual measured shapes of star-shaped aggregate particles by spherical harmonic series [30, 31] . A further development of the Anm model is the ability to place a uniform-thickness shell around each aggregate particle in cement paste or concrete models to simulate the ITZ regions [29]. This technique makes use of an algorithm that has been developed for star-shaped particles to coat a particle with a uniform-thickness shell [32]. In this work, 3D virtual concrete block was created using the Anm model first. To save the computing cost, several 2D slices were

generated from the 3D virtual block of concrete structure. For simplification, the domain of concrete meso-structure was divided into two phases: cement paste and aggregate particles, while ITZ and voids were not considered in the simulation process.

Five cases of geometry were created based on the ratio of cement and aggregate particles (Table 3-1). The basic mechanism was considered as the same for all aggregate sizes. Different cement-aggregate ratios were introduced to simulate ASR expansion for irregular morphology of aggregate particles and their compositions in concrete (Figure 3-1). Using a developed meshing code [33], relevant physics controlled meshing was done for each set of the geometry to facilitate finite element analysis.

Table 3-1 Geometric properties and Mesh details used in FEM modeling

Geometry Sets	Cement to Aggregate Ratio (C/A)	Cement Proportion	Aggregate Proportion	Type of Mesh	No. of element in cement paste	No. of element in aggregate particles
Case 1	1.13	0.53	0.47	Triangular	11792	15746
Case 2	1.61	0.617	0.383	Triangular	22589	16793
Case 3	2	0.67	0.33	Triangular	18269	13540
Case 4	0.5	0.33	0.67	Triangular	23639	25287
Case 5	1	0.5	0.5	Triangular	23450	19916

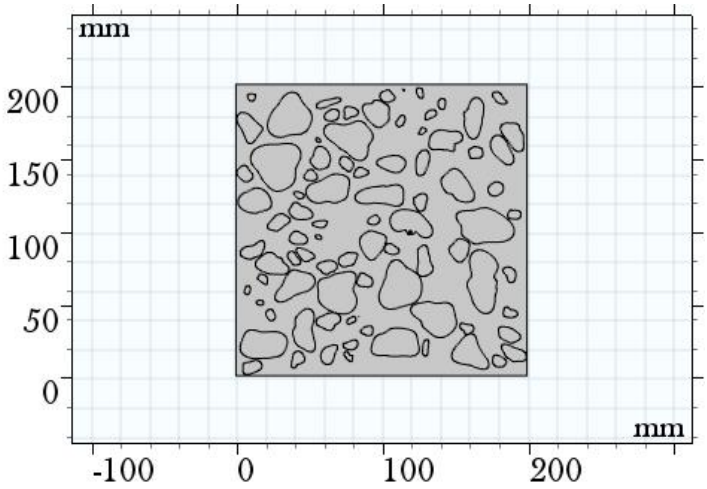

Figure 3-1 Meso-structure domain of concrete block for case 1.

Material properties are different for cement paste and aggregate domain (Table 3-2).

Table 3-2 Material properties used in FEM modeling

	Cement Paste	**Aggregate**	**Source**
Diffusion Coefficient of ASR gel (m^2/s)	1×10^{-10}	1×10^{-12}	[16]
Young's Modulus (Pa)	5×10^{6}	60×10^{6}	[34]
Poisson's Ratio (1)	0.2	0.25	
Density (kg/m^3)	3150	2600	
Viscosity of water (Pa.s)	8.9×10^{-4}	NA	[35]
Permeability (m^2)	7.5×10^{-6}	NA	Calibrated

Based on mathematical models discussed in section 3, a comprehensive governing equations set were developed for finite element analysis of chemo-mechanical analysis per Eqs. (14-20) to predict damage of concrete structure in terms of volume change.

$$D = 2.021\times\varepsilon_{vol} - 0.195 \tag{14}$$

$$\varepsilon_{vol} = \varepsilon_{gel} + \varepsilon_{stress} \tag{15}$$

$$\varepsilon_{gel} = \frac{\rho_{gel}}{\rho_c + \rho_{gel}} \tag{16}$$

$$\rho_{gel} = [Expanded\ ASR\ gel]\times M_{gel} \tag{17}$$

$$\frac{\partial}{\partial t}(u) + \nabla\cdot(-D_{gel}\nabla[ASR\ gel]) + \mathbf{u}\cdot\nabla u = f(u) \tag{18}$$

$$u = [[Siloxane],[ROH],[ASR\ gel],[Silanol],[H2O],[Expanded\ ASR\ gel]]^T$$

$$f_{[Siloxane]} = -k_1[Siloxane][ROH]$$

$$f_{[ROH]} = -k_1[Siloxane][ROH] - k_2[Silanol][ROH]$$

$$f_{[ASR\ gel]} = k_1[Siloxane][ROH] + k_2[Silanol][ROH] - k_3[ASR\ gel][H_2O]$$

$$f_{[Silanol]} = k_1[Siloxane][ROH] - k_2[Silanol][ROH]$$

$$f_{[H_2O]} = k_2[Silanol][ROH] - k_3[ASR\ gel][H_2O]$$

$$f_{[Expanded\ ASR\ gel]} = k_3[ASR\ gel][H_2O]$$

$$\frac{\partial}{\partial t}(\varepsilon_p \rho) + \nabla \cdot (\rho \mathbf{u}) = Q_m$$

$$\mathbf{u} = -\frac{\kappa}{\mu}\nabla p \tag{19}$$

$$Q_m = 0.018 \times f_{[H2O]}$$

$$\varepsilon_{stress} = \varepsilon_{11} + \varepsilon_{22} + \varepsilon_{33} \tag{20}$$

Percentage of damage can be calculated from Eq. (14) when volume change is greater than 0.1%. Damage is expressed as a function of total volume change.

To determine total volume change an equation was developed in this study per Eq. (15). This equation determines the total volumetric strain, ε_{vol} in terms of resultant volume change induced from expansive gel and applied external stress. Here, ε_{gel} is the volume change due to ASR expansion, and ε_{stress} denotes external stress induced volumetric strain.

Volumetric strain from expansive gel can be determined from Eq. (16). Here, definitions of all symbols are same as mentioned previously in this work. Density of concrete was set to 2400 (kg/m^3).

Density of ASR gel can be calculated per Eq. (17). Here, [*Expanded ASR gel*] denotes concentration of expansive ASR gel which is obtained from Eq. (7) and M_{gel} denotes the molar mass of expanded ASR gel. Based on the atomic mass of chemical elements that form expanded ASR gel, $Si-O-R.\ (H_2O)_n$ per Eq. (3), molar mass of gel was calculated and set to 119 gm/mole (0.119 kg/mole).

Concentration of expanded ASR gel can be determined from Eq. (18). This equation accounts for the diffusion of ASR gel as per diffusion coefficient, D_{gel} (Table 3-2). Here, u is the dependent variable which is a concentration tensor of all six species involved in chemical kinetics. $f(u)$ is the source term as a function of u. Note that in this

study, source term, was defined as a reaction term, which depends on rate change of concentration for each individual chemical species based on Eq. (6). For numerical solution reaction rate k_1, k_2, k_3 were kept constants throughout the simulation period and assigned to a value of 6.34×10^{-9} mole/(m^3.sec), 3.17×10^{-8} mole/(m^3.sec), and 1.6×10^{-7} mole/(m^3.sec), respectively. k_3 impacts final expansion.

The unknown fluid velocity in Eq. (18) can be calculated from Eq. (19). The mass source Q_m comes from water/moisture content and was assumed to be $M_w \times f_{[H_2O]}$, where $[H_2O]$ stands for water concentration as mentioned previously. M_w is the molar mass of water which is 18 gm/mole (0.018 kg/mole).

Volumetric strain induced from external loading/stress, can be calculated from Eq. (20) according to mechanical model. Here, ε_{11}, ε_{22}, ε_{33} are strain tensor in XX, YY and ZZ component, respectively.

Initial and reference values of different parameters used in finite element analysis vary for cement paste and aggregate domain (Table 3-3). Initial concentration of chemical species were set based on temporal variation of reactants and products according to study [15]. Initial concentration of siloxane species is zero in cement paste as it comes from aggregate particles only. Initial concentration of hydroxyl ions and water is zero in aggregate particles as those species come from cement paste only. Initially there was no pressure gradient in the concrete block as reference pressure and internal initial pressure both were considered with equal values. ASR model was simulated considering constant room temperature of 20°C (293K).

Table 3-3 Initial and reference values used in numerical analysis

Details	Cement Paste	Aggregate	Source
Initial concentration of Siloxane (mole/m^3)	0	1	Calibrated
Initial concentration of ROH (mole/m^3)	1.2; 2.5	0	
Initial concentration of H_2O (mole/m^3)	2	0	
Initial concentration of Silanol (mole/m^3)	0	0	
Initial concentration of ASR gel (mole/m^3)	0	0	
Initial concentration of expanded ASR gel (mole/m^3)	0	0	
Velocity field at X direction (m/s)	0	0	
Velocity field at Y direction (m/s)	0	0	
Velocity field at Z direction (m/s)	0	0	
Initial pressure (atm)	1	1	
Reference pressure (atm)	1	1	

5 Model Validation

To ensure the accuracy of the chemo-mechanical model, predicted ASR expansions were validated by established experimental data. Standard test method ASTM C 1293 was introduced for validation purposes. This is a concrete prism test (CPT) that determines the length change of concrete due to alkali silica reaction. For the validation of ASR model experimental data were collected from study [36]. Data was considered for concrete prism with reactive aggregate type A [36]. To match with the chemical, environmental and mechanical conditions of the prism tests conducted in study [36], numerical simulation of ASR model was considered with Alkali concentration of 0.8 (mole/m^3) and 1.2 (mole/m^3), free expansion of ASR without any applied load, and constant temperature of 20°C (293.15K). Validation model was simulated over a period of 400 days. Expansion varies for different points throughout the concrete block. That's why average expansion was calculated for the cement matrix inside the concrete block. Unit thickness was assumed for 2d concrete block.

$$E_{avg} = 100 \times \int_{A} \varepsilon_{gel} \frac{dA}{A} \qquad (21)$$

where, E_{avg} is the percentage of average expansion. 'A' means area of the domain.

It is obvious from the comparison that the expansion curve of expansive gel simulated in FEM model is following the trend of experimental curves (Figure 3-2). However, the ASR expansion curve does not show any latency period at the very beginning of the ASR mechanisms. This is because, since this study deals with fully saturated condition (presence of excess water in concrete), the reaction starts from the beginning of time interval. This phenomenon is also valid according to study [15], where there is no latency period in the expansion curves when initial concentration of water/moisture is zero (i.e. unsaturated condition).

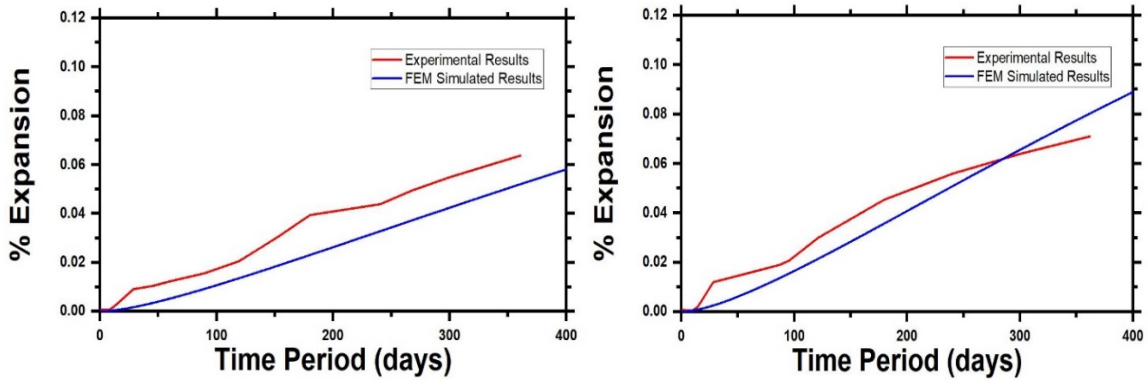

(a) (b)

Figure 3-2 Comparison of FEM simulated data with the experimental data as per case 4 (C/A: 0.5): (a) 20°C ROH 0.8 mole/m^3, (b) 20°C ROH 1.2 mole/m^3

In Figure 3-2(a), comparison is given for ROH concentration of 0.8 (mole/m^3) and in Figure 3-2(b), comparison is given for ROH concentration of 1.2 (mole/m^3). Though, simulated curves are not a perfect match compared to the experimental curves, they more or less comply with the experimental data. The variation could be because of the

assumptions and parameters considered in this model simulation. Thus, it can be said that, proposed ASR model is validated successfully according to the assumptions and considerations made in this proposed model.

6 Result and Discussion

Developed FEM model was simulated for 30 years to assess long term condition of concrete. Results are based on the representative two dimensional FEM model of the reference concrete block. All values including concentration, volumetric strain, stress and damage of each species were calculated as an average value over the whole concrete domain of FEM model to avoid variation in results.

To predict how concrete behaves under ASR mechanisms for different concentrations of chemical species, FEM model for each of the five cases of geometry discussed before was divided into two sub-cases. In the first the sub-case model was simulated considering low alkali contents in cement matrix (initial concentration of ROH = 1.2 mole/m^3). In the second the sub-case model was simulated considering very high alkali contents in cement matrix (initial concentration of ROH = 2.5 mole/m^3). Initial concentrations of all other species were kept same for both of the sub-cases.

Concentration of expansive ASR gel generated due to ASR kinetics increases as time progresses for all of the cases and shows the highest value at 30 years (Figure 3-3). Concentration is maximum for case 4 with ROH of 2.5 mole/m^3 (0.18 mole/m^3) and minimum for case 3 with ROH of 1.2 mole/m^3 (0.07 mole/m^3). If we focus on the trend of the graphs (Figure 3-3), it is obvious that concentration of expansive gel increases with the decrease of cement to aggregate ratio (C/A). That means when concrete domain contains more aggregate particles than the cement paste concentration increases. The more

aggregate particles in amount, the higher expansive gel gets in concentration. This is because a higher aggregate proportion supplies more reactive particles that come in contact with alkali hydroxide dissolved in the pore solution of the cement paste and accelerate chemical reaction to produce more expansive gel. However, if all ROH concentration is consumed by the reaction for the lowest aggregate proportion, additional aggregate proportion would not have any effect on the expansion mechanisms. Like aggregate particles concentration of expansive gel increases with the increase in ROH content. In all of the cases concentration is maximum for ROH of 2.5 mole/m^3 and minimum for ROH of 1.2 mole/m^3. For example, in case 1 expansive gel concentration at ROH of 1.2 mole/m^3 is 0.092 mole/m^3 and at ROH of 2.5 mole/m^3 is 0.137 mole/m^3. This is because high ROH concentration in pore solution attacks more reactive aggregate particles and accelerates ASR gel production in concrete.

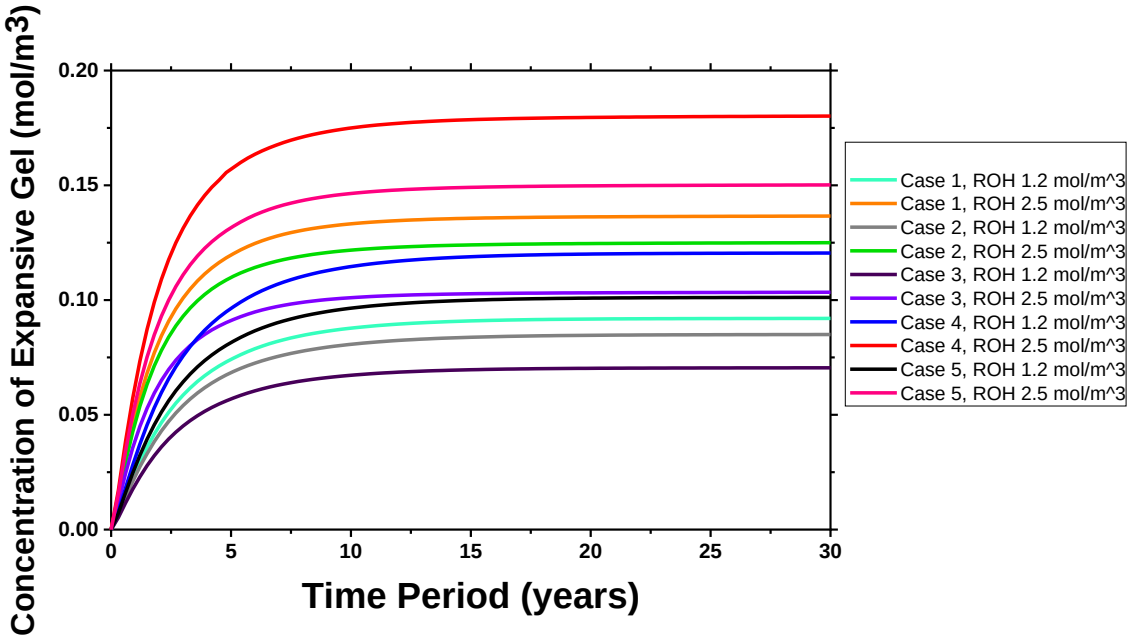

Figure 3-3 Concentration of expansive ASR gel (mole/m^3) in concrete for different cases.

The change in concentration varies for different time intervals of the simulation period. There is a rapid increase in concentration initially and then tends to increase with a decreasing rate (Figure 3-3). If we consider the maximum one i.e. case 4 with ROH 2.5 mole/m^3, the rate change of concentration of the expansive gel is higher after time 0 and at 5 years it becomes 0.157 (mole/m^3). After 5 years the increment continues at a slower rate than before and concentration becomes 0.179 (mole/m^3) at 15 years. After 15 years there is no significant change in concentration until 30 years when maximum concentration becomes 0.18 (mole/m^3).

The distribution of expansive gel can be visualized for different time periods (Figure 3-4). The concentration of expansive ASR gel is higher in the space between closely positioned aggregate particles. The reason could be, closely positioned aggregates limit the space for ASR gel to flow. It is also found that the concentration of expansive ASR gel is high around the small sized aggregate particles. This is because of the more surface area provided by small particles comparing to larger ones. Moisture movement through pores and cracks in concrete can transport the ASR gel to the surface, where it can exude. However, this phenomenon is not so common.

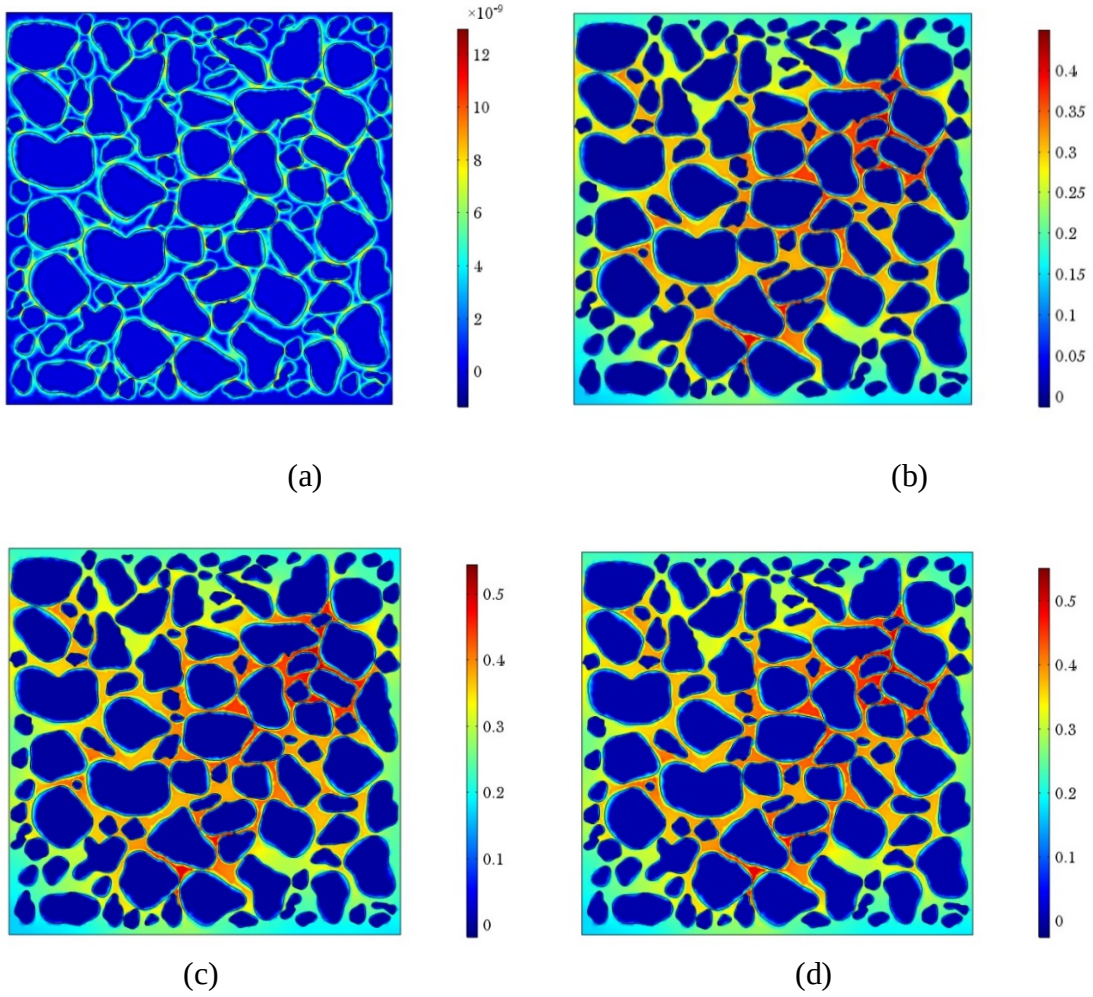

Figure 3-4 Concentration of expansive ASR gel (mole/m^3) in concrete for case 4 with ROH of 1.2 mole/m^3: (a) 0, (b) 5, (c) 15, and (d) 30 years

Average concentrations of all six species involved in ASR kinetics change with the progression of time (Figure 3-5). ROH concentration decreases at a faster rate from the very beginning of alkali silica reaction and continues up to 5 years. The reduction in concentration starts with the reaction between alkali hydroxides and siloxane, and further continues when byproduct silanol reacts with alkali hydroxides. After certain years (15 years) reduction rate of alkali hydroxides does not change significantly and reach a more or less stabilized concentration of 0.714 mole/m^3. At 30 years the concentration becomes 0.713 mole/m^3. Concentration of expansive ASR changes inversely with that of alkali ions.

Thus expansive gel formation speeds up after the latency period and increases at a decreasing rate. According to Eq. (1), (2), and (3) expansive gel formation continues with the chemical reaction and depletion of all other species involved in the kinetics. For this reason, concentrations of siloxane, silanol, water and ASR gel tend to decrease as time progresses. Silanol is a byproduct of the chemical reaction which increases at first and then decreases later with the formation of ASR gel. Concentration of ASR gel also increases initially and then decreases when it starts to convert into expansive gel by absorbing water. It is noteworthy that, after 10-15 years reactions tend to stabilize though there is high alkali concentration in the solution. This is because, after certain time there are not sufficient H_2O and silica content in the solution to react with ROH.

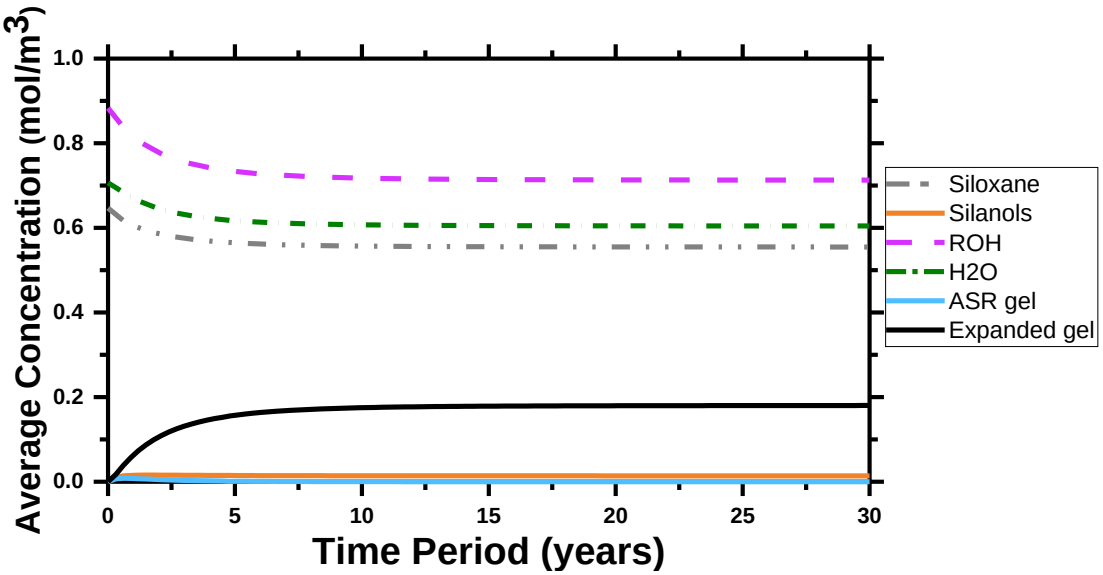

Figure 3-5 Comparison between concentrations of all six species (mole/m^3) in concrete for case 4 with ROH of 2.5 mole/m^3.

Volumetric strain was calculated from developed comprehensive governing equations set discussed in section 4. Volumetric strain induced from ASR gel expansion follows the changing trend of the concentration of expansive gel (Figure 3-6). Thus, ASR

induced volumetric strain is maximum for case 4 with ROH of 2.5 mole/m^3 (8.93×10^{-4}) and minimum for case 3 with ROH of 1.2 mole/m^3 (3.49×10^{-4}) at 30 years. Volumetric strain is also higher for cases with more aggregate particles and more ROH concentration. This is because volumetric strain is a function of the concentration of expansive gel and change in the volume gets higher when more expansive gel is in the domain of concrete block.

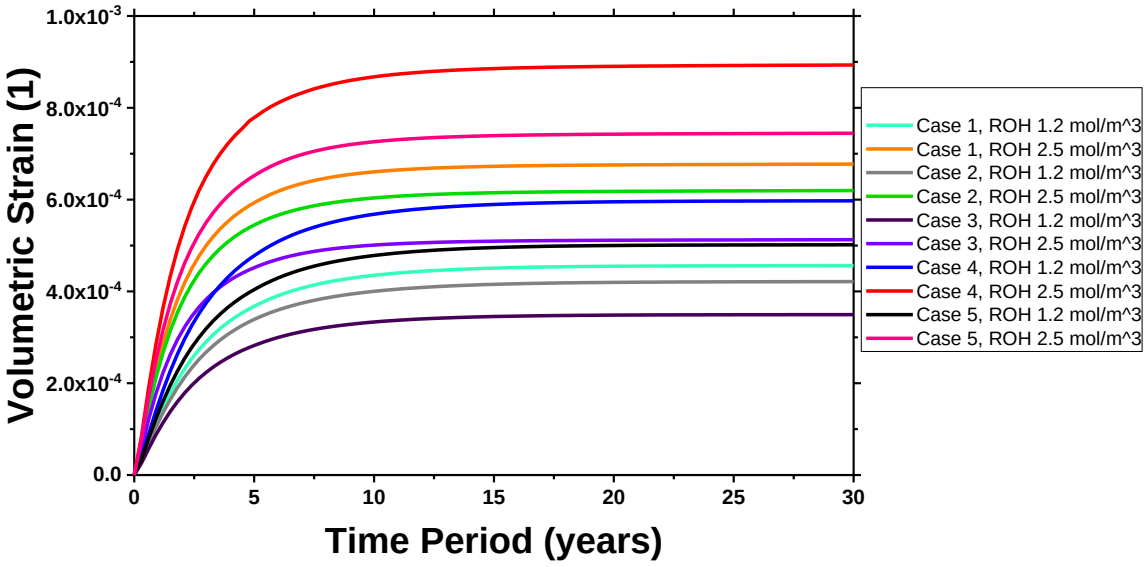

Figure 3-6 ASR gel induced volumetric strain in concrete domain for different cases.

Stress was calculated from the Mechanical model discussed in section 3.2. To minimize computational cost a mechanical model was developed in a more simplified form and the material was considered as isotropic in the simulation. Tensile stress induced from ASR gel expansion was taken in terms of global stress, which was obtained by integrating the local stresses through the concrete block thickness. In this case concrete was allowed to expand freely, i.e. no external load/stress on concrete block. This follows the changing

trend of the volumetric strain (Figure 3-7). Thus, maximum stress was generated for case 4 with ROH of 2.5 mole/m^3 (1.92 × 107 Pa) and minimum for case 3 with ROH of 1.2 mole/m^3 (7.53 × 106 Pa) at 30 years. Hence, stress is also higher for cases with more aggregate particles and more ROH concentration. This is because stress is proportional to the volumetric strain and more stress generates for cases with larger volume change in the concrete domain.

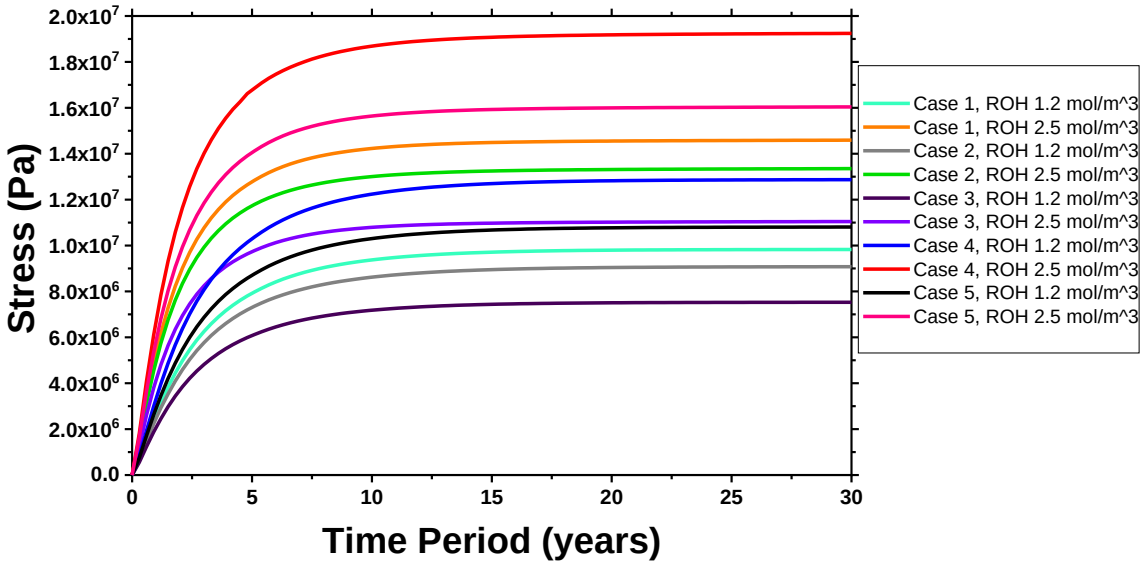

Figure 3-7 Stress developed from ASR gel expansion in concrete domain for different cases.

In addition to the external loads/stress on concrete block, ASR induced volumetric strain tends to decrease (Figure 3-8). ***This is a significant finding of this work***. Though, ASR expansion accelerates the volume change, applied loading decreases the rate by which volumetric strain changes. This is because applied vertical loading initiates compressive loads by acting downward, which in turn mitigates the upward expansion of concrete block since the bottom side of the block is at a fixed boundary. For case 4 with ROH of 2.5

mole/m^3, maximum volumetric strain developed in the concrete domain is 8.93 × 10^{-4} without external load and 8.39 × 10^{-4} with external load at 30 years. However, at initial time period, there is no visible expansion due to ASR and volumetric strain generated from downward load surpasses the ASR induced volumetric strain. Thus, total volumetric strain tends to be negative at that time interval.

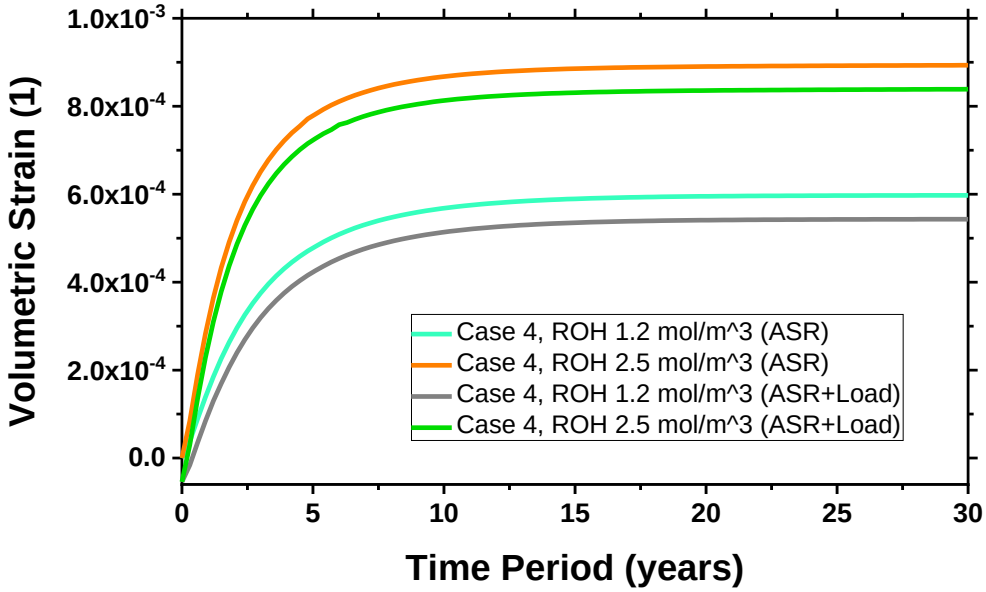

Figure 3-8 Total volumetric strain (ASR gel + external load) in concrete domain for case 4.

Stress developed from ASR expansion in concrete also tends to decrease in addition to external loadings (Figure 3-9). Due to downward loading stress generated from it also acts downward which mitigates ASR induced stress and thus total stress is less than ASR induced stress. Here, compressive stress is applied in a vertical direction only, and thus, stress decrease also occurs in vertical direction only. For case 4 with ROH of 2.5 mole/m^3, maximum stress developed in the concrete domain is 1.92 × 107 Pa without external load and 1.81 × 107 Pa with external load at 30 years. At initial time period, total stress also

tends to be negative. This is because stress is a function of volumetric strain and proportional to it as discussed before.

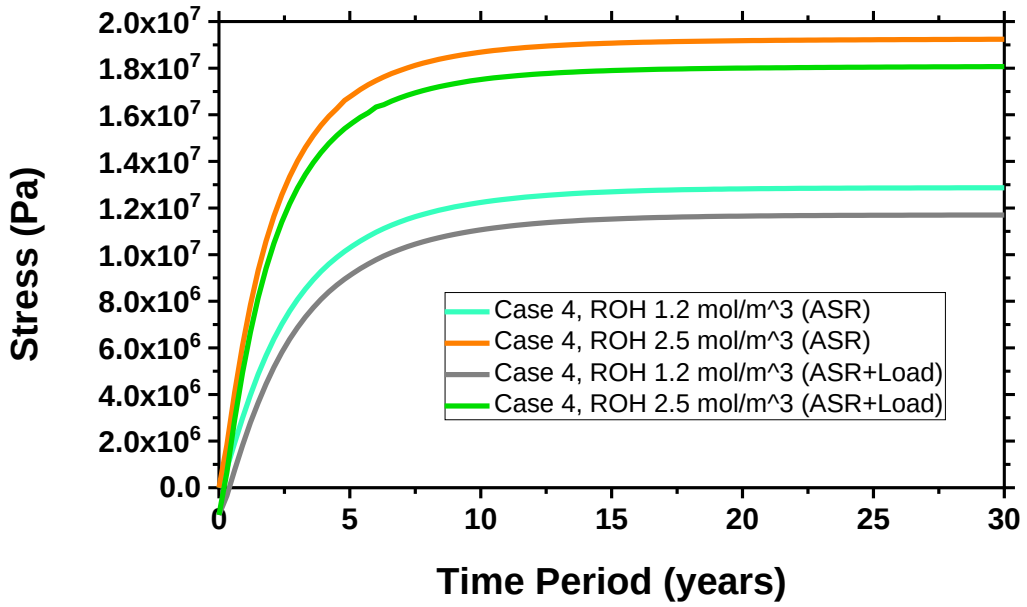

Figure 3-9 Total stress (ASR gel + external load) in concrete domain for case 4.

Damage function was calculated based on volumetric strain following the equation sets discussed in section 4, to predict percentage of damage with time progression. ***Developing a tool to visualize the damage propagation in concrete structure with time is one of the major contributions of this work***. The percentage of damage follows the trend of volume change (Figure 3-10). It is obvious from the figure that for a few initial years damage is zero. At initial time periods, volume change in concrete is less than 0.1% and damage was neglected. This is because, initially, there is no significant expansion or volume change in the concrete block. Thus, damage propagation complies with the damage criteria formulated in study [16]. Percentage of damage is larger in cases where there is more aggregate particles and more concentration of ROH in the concrete domain. For example in case 4, maximum damage is 3.74% with ROH of 1.2 mole/m^3 and 9.16% with

ROH of 2.5 mole/m^3 at 30 years. External loadings also tends to mitigate damage developed from ASR expansion. However, in concrete there could be cracking or other damages due to loading conditions which were not considered in this study. Damage values founded in this work are based on the assumptions and other compositions considered in the model. ***Thus, developing the damage model per damage function and showing the trend of damage propagation in concrete are the first time findings from this work***.

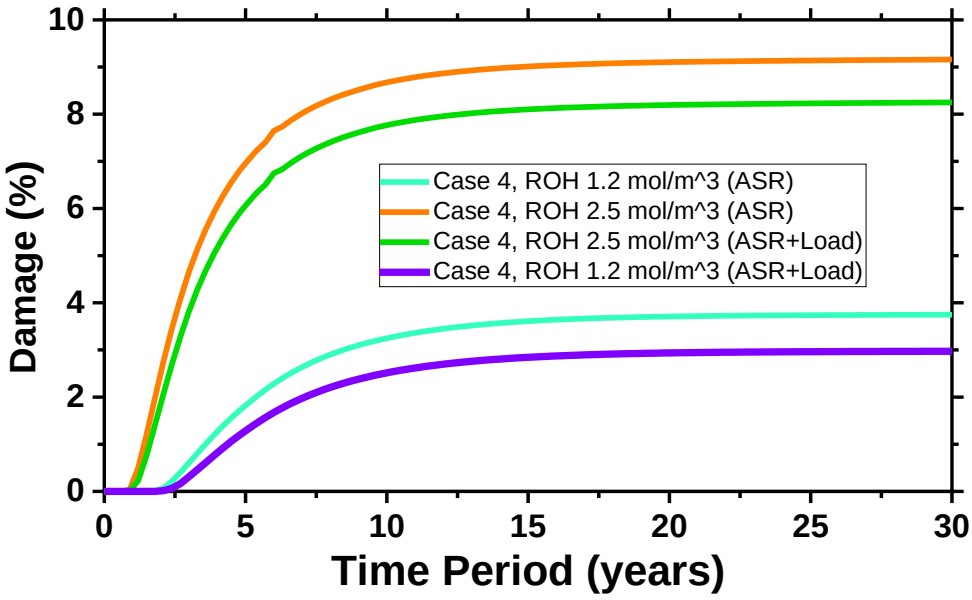

Figure 3-10 Percentage of damage in concrete domain for case 4.

Damage in 2d concrete block can be visualized for case 4 at different time intervals (Figure 3-11). Hence, with the FEM model it can be predicted that considered concrete block subjected to ASR mechanisms will degrade gradually and effective measure should be taken accordingly.

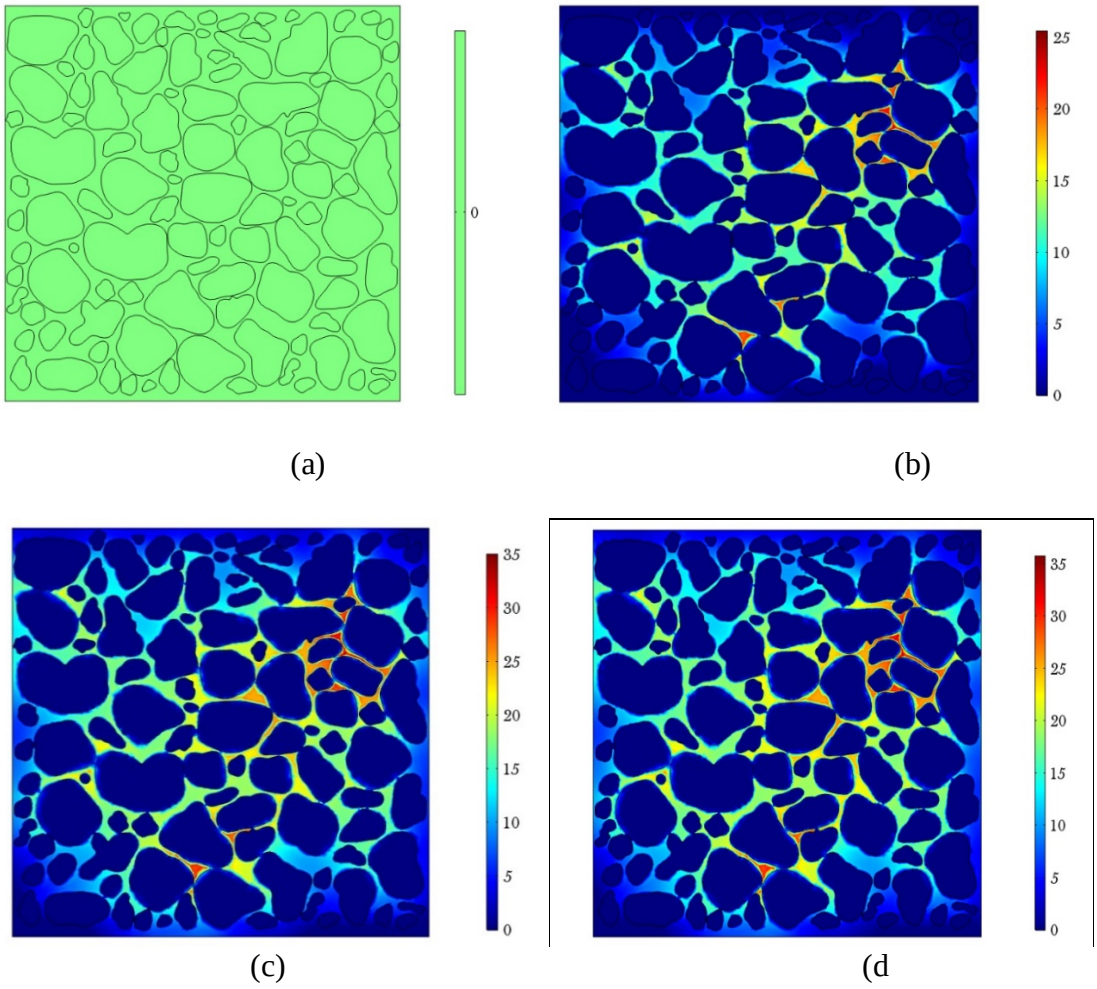

Figure 3-11 Damage in concrete domain due to ASR gel case 4 with ROH of 1.2 mole/m^3: (a) 0, (b) 5, (c) 15, and (d) 30 years

7 Conclusions

This work proposes a three-dimensional coupled chemo-mechanical model for analyzing ASR chemophysics and mechanical properties of concrete at meso-scale. Virtual cement concrete meso-structures considering various geometric proportions of cement and aggregate particles were generated based on our novel model, Anm. Developing coupled mass balance-momentum balance equations and their numerical implementation as per chemical kinetics are the major contributions of this work to accurately predict the ASR damage that integrated ASR expansion in addition to external loadings, material mesoscale

details and damage modes. A 30 year simulation period as well as 10 case studies corresponding to concrete domain and ROH concentration, provide an in depth view of concrete degradation with the progression of time. The findings of this paper confirmed that average expansion in concrete starts after the latency period and then continues to increase with a decreasing rate. For the first few years, alkali-silica reaction is amplified and then tends to stabilize with the depletion of alkali-hydroxides concentration. ASR expansion continues as long as there are enough reactive silica, alkali hydroxide and water content in concrete structure. Depletion of any one of these contents may limit the ASR production and gel diffusion. ASR damage is not that significant initially, but, after certain years damage surpasses the accepted limit based on the damage function, which can deteriorate service life of concrete. External load or constraint has the potential to mitigate ASR damage in concrete. Thus, ASR damage can be minimized by effectively following three strategies: using non-reactive aggregates, limiting the maximum alkali content of concrete and limiting the moisture availability in the field structures.

The developed model is based on the specific environmental conditions, initial concentrations of the species involved and their compositions, and, the reaction rates considered in this paper. In real cases, ASR expansion can continue for more than 30 years as well as a latency period that may last for several years. Pressure of crystallization was not included in this developed model. The effect of crystallization and subsequent expansion is a mechanism of alkali-carbonate reaction (ACR). Thus, this model is valid for alkali-silica reaction (ASR) only. This developed model is only valid for fully saturated conditions with constant room temperature. The damage model is for isotropic concrete block only.

The developed governing equation set can be calibrated further for any concrete structure by changing initial concentrations of chemical species, concrete density, and loading conditions according to the purpose, proportion or properties of concrete domain. Thus, this physics-based model can be used to accurately determine damage level and predict the service life of concrete. There is great potential for this model to be used for future study and evaluation purposes.

Author Contribution Statement

The authors confirm contribution to the paper as follows: study conception and design: Md. Asif Rahman, Yang Lu; data collection: Md Asif Rahman, Yang Lu; analysis and interpretation of results: Md. Asif Rahman; draft manuscript preparation: Md. Asif Rahman; approval of the final version of manuscript: Yang Lu.

Acknowledgements

Declarations of interest

None.

Funding

This research did not receive any specific grant from funding agencies in the public, commercial, or not-for-profit sectors.

References

[1]. Chatterji, S. Chemistry of Alkali–Silica Reaction and Testing of Aggregates. Cement & Concrete Composites, 2005. 27: 788–795.

[2]. Alexander, M. and S. Mindess. Aggregates in Concrete: Modern Concrete Technology 13. Taylor & Francis, London and New York, 2010.

[3]. Prezzi, M., P. J. M. Monteiro, and G. Sposito. The Alkali-Silica Reaction, Part I: Use of the Double-Layer. ACI Materials Journal, 1997. January-February: 10-16.

[4]. Mukhopadhyay, A. K. An Effective Approach to Utilize Recycled Aggregates (RAs) from Alkali-Silica Reaction (ASR) Affected Portland Cement Concrete. In Handbook of Recycled Concrete and Demolition Waste (F. Pacheco-Torgal, V. W. Y. Tam, J. A. Labrincha, Y. Ding, and J. de Brito), Woodhead Publishing Limited, Cambridge, UK, 2013. pp. 555-568.

[5]. Taylor, H. F. W. Cement chemistry. Thomas Telford Services Ltd., London, 1997.

[6]. Ulm, F.J., O. Coussy, L. Kefei, and C. Larive. Thermo-Chemo-Mechanics of ASR Expansion in Concrete Structures. Journal of Engineering Mechanics, 2000. 126: 233-242.

[7]. Ferraris, C. F., E. J. Garboczi, F. L. Davis, and J. R. Clifton. The Effect of Stress Relaxation, Self-Desiccation, and Water Absorption on Alkali-Silica Reaction in Low Water/Cement Ratio Mortars. Cement and Concrete Research, 1997. 27: 1153-1560.

[8]. Touma, W. E., D. F. Fowler, and R. L. Carrasquillo. Alkali-Silica Reaction in Portland Cement Concrete: Testing Methods and Mitigation Alternatives. Research Report ICAR 301-1F. International Center for Aggregates Research (ICAR), The University of Texas at Austin, 2001.

[9]. Poyet, S., A. Sellier, B. Capra, G. Thèvenin-Foray, J. M. Torrenti, H. Tournier-Cognon, and E. Bourdarot. Influence of Water on Alkali-Silica Reaction: Experimental Study and Numerical Simulations. Journal of Materials in Civil Engineering, 2006. 18: 588-596.

[10]. Thomas, M. D. A., B. Fournier, and K. J. Folliard. Alkali-Aggregate Reactivity (AAR) Facts Book. Publication FHWA-HIF-13-019. FHWA, U.S. Department of Transportation, 2013.

[11]. Leger, P., P. Cote, and R. Tinawi. Finite Element Analysis of Concrete Swelling Due to Alkali-Aggregate Reactions in Dams. Computers & Structures, 1996. 60: 601-611.

[12]. Hobbs, D. W. The Alkali-Silica Reaction - A Model for Predicting Expansion in Mortar. Magazine of Concrete Research, 1981. 33 (117): 208 - 220.

[13]. Steffens, A., and Z. P. Bazant. Mathematical Model for Kinetics of Alkali-Silica Reaction in Concrete. Cement and Concrete Research, 2000. 30: 419-428.

[14]. Bournazel, J. P., and B. Capra. Modeling of Induced Mechanical Effects of Alkali-Aggregate Reactions. Cement and Concrete Research, 1998. 28: 251-260.

[15]. Saouma, V. E., R.A. Martin, M. A. Hariri-Ardebili, and T. Katayama. A Mathematical Model for the Kinetics of the Alkali–Silica Chemical Reaction. Cement and Concrete Research, 2015. 68:184-195.

[16]. Balbo, F. A. N., G. A. Pianezzer, L. M. Gramani, E. Kaviski, and M. R. Teixeira. An Application to the Diffusion Equation in a Model for the Damage in Concrete Due to Alkali-Silica Reaction. Applied Mathematical Sciences, 2015. 9: 4135-4147.

[17]. Ichikawa, T., and M. Miura. Modified Model of Alkali-Silica Reaction. Cement and Concrete Research, 2007. 37: 1291-1297.

[18]. Kim, T., J. Olek. Influence of Alkali Silica Reaction on the Chemistry of Pore Solutions in Mortars With and Without Lithium Ions. Brittle Matrix Composites, 2012. 10: 11-20.

[19]. Diamond, S. Alkali Silica Reactions – Some Paradoxes. Cement and Concrete Composites, 1997. 19: 391-401.

[20]. Poole, A.B. Proceedings of the Third International Symposium on The Effect of Alkalis on The Properties of Concrete. Cement and Concrete Association, Wexham Springs, Slough, UK, 1976.

[21]. Furusawa, Y., H. Ohga, and T. Uomoto. An Analytical Study Concerning Prediction of Concrete Expansion Due to Alkali-Silica Reaction. Durability of Concrete: Third International Conference, 1994. ACI SP: 145-40, 757-778.

[22]. Rahman, Md. Asif, and Y. Lu. A Meso-Scale Multiphysics Model for Predicting Concrete Pavement Performance Subject to ASR Degradation. TRB Annual Meeting Paper, 2019. 19-03839R1.

[23]. Saouma, V. E., and L. Perotti. Constitutive Model for Alkali-Aggregate Reactions. ACI materials journal, 2006. 103: 194-202.

[24]. Grimal et al, Creep, shrinkage, and anisotropic damage in alkali-aggregate reaction swelling Mechanism-Part I: A constitutive model, ACI Materials Journal, 2008. 105(3):227-235.

[25]. Deng, J. Parallel Computing Techniques for Computed Tomography. IA: University of Iowa, 2011.

[26]. Guldberg, R.E., S.J. Hollister, and G. Charras. The Accuracy of Digital Image-Based Finite Element Models. Ann Arbor, 1998. 1050: 48109.

[27] Qian, Z. Multiscale Modeling of Fracture Processes in Cementitious Materials. Delft University of Technology, Netherlands, 2012.

[28] Qian, Z., E.J. Garboczi, G. Ye, and E. Schlangen. Anm: A Geometrical Model for the Composite Structure of Mortar and Concrete Using Real-Shape Particles. Materials and Structures, 2016. 49: 149-158.

[29] Thomas, S., Y. Lu, and E.J. Garboczi. Improved Model for Three-Dimensional Virtual Concrete: Anm Model. Journal of computing in civil engineering, 2016. 30: 04015027-04015027.

[30] Garboczi, E.J. Three-Dimensional Mathematical Analysis of Particle Shape Using X-ray Tomography and Spherical Harmonics: Application to Aggregates Used in Concrete. Cement and Concrete Research, 2002. 32: 1621-1638.

[31] Erdogan S.T., P.N. Quiroga, D.W. Fowler, H.A. Aleh, R.A. Livingston, E.J. Garboczi, P.M. Ketcham, J.G. Hagedorn, and S.G. Satterfield. Three-Dimensional Shape Analysis of Coarse Aggregates: New Techniques for and Preliminary Results on Several Different Coarse Aggregates and Reference Rocks. Cement and Concrete Research, 2006. 36: 1619-1627.

[32] Garboczi, E.J., and J.W. Bullard. Contact Function, Uniform-Thickness Shell Volume, and Convexity Measure for 3D Star-Shaped Random Particles. Powder Technology, 2013. 237: 191-201.

[33]. Lu, Y., and E.J. Garboczi. Bridging the Gap between Random Microstructure and 3D Meshing. Journal of Computing in Civil Engineering, 2014. 28(3): 04014007.

[34]. Pan, T., C. Chen, and Q. Yu. Three-Dimensional Micromechanical Modeling of Concrete Degradation Under Multiphysics Fields. Composite Structures, 2017. 175: 7-18.

[35]. Korson, L. Drost-Hansen, W. and J. Millero, F. Viscosity of Water at Various Temperatures, Contribution No. 980 from the Institute of Marine Sciences, University of Miami, Miami, Florida 88149 (Received April 12, 1968).

[36]. Ben Haha, M. Mechanical Effects of Alkali Silica Reaction in Concrete Studied by SEM-Image Analysis. Doctoral dissertation, École Polytechnique Fédérale de Lausanne. À La Faculté Sciences Et Techniques De L'ingénieur, France, 2006.

CHAPTER 4: A STOCHASTIC MODEL TO EVALUATE ALKALI-SILICA REACTION (ASR) IN CONCRETE SUBJECT TO GLOBAL WARMING AND CLIMATE CHANGE IMPACTS[3]

Abstract

Alkali-silica reaction (ASR) is a most common source of concrete deterioration worldwide. Global warming (GW) has anticipated frequent climate change and caused global extreme weather events in recent years. These events convey potential threats to infrastructure made by concrete due to ASR. That's why complex mechanisms of ASR under seasonal change and dynamic global warming impacts require a precise quantitative assessment to guide durable infrastructure materials design practices. Given the set of facts, this work captures the concrete meso-structure and develops a simplified ASR model that integrates chemo-physio-mechanical damage under stochastic weather impact. The results from the validated model elucidate that ASR kinetics and evolution of ASR expansion can be more destructive under the influence of global warming and stochastic weather change. Thus, this proposed model can support precise long-term degradation forecasts of concrete infrastructure damage subject to alkali-silica reaction due to global warming and climate change impacts.

Keywords: Chemical model, Seasonal change, Global Warming, Stochastic weather, parametric study

[3] This chapter includes results already reported in the following publication. Contribution of the coauthor is sincerely acknowledged: Rahman, M. A., and Lu, Y. "A Stochastic Model to Evaluate Alkali-Silica Reaction (ASR) in Concrete Subject to Global Warming and Climate Change Impacts", Submitted to the Journal of Cement and Concrete Composites, 2020 (Under Review).

1. Introduction

Aging of concrete infrastructure, e.g. pavements, bridges, buildings, and hydraulic dams, is a worldwide problem. Alkali-silica reaction (ASR) is one of many undesirable chemical reactions that initiate concrete infrastructure deterioration over time. Alkali-silica reaction have attracted significant research efforts to understand fundamental mechanisms of damage growth [1-5]. The driving effect of ambient temperature and humidity on ASR expansion have already been explained previously [6, 7]. The trajectory is clear – higher temperature, higher humidity, and more severe ASR damage. Alkali silica reaction becomes favorable to the right direction, and therefore, product generation tends to accelerate, with the increased temperature and relative humidity (RH). However, the evolution of ASR expansion under the impact of extreme weather condition is yet to be justified.

Extreme weather can be defined as a sudden increase/decrease in temperature or humidity. This is an emerging problem to the entire world. Frequent climate change along with the global warming can elevate extreme weather condition. Climate change describes overall change in the mean temperature and humidity or the moisture condition. Researchers have found that climate change gives a boost to the frequency or intensity of extreme events like heat waves, rainfall, humidity or air vapor, as well as snowfall during the winter. Human-induced climate change has increased the chances of heat waves recently [8-9]. Even a small change in global warming can boost the frequency of extreme weather events, especially heat waves and rainfall [10]. These events have warmed the United States faster than the global rate since the late 1970s [11]. Warmer air produced through heat waves may contain more water vapor than cooler air. It is also evident that

the human-induced warming has increased the amount of available water vapor in the atmosphere [12-13]. There is also an increase in the heavy snowfall in some regions during the winter season. Researchers have found that the intensity of snowstorms have increased since the 1950s [14], and become more frequent across the northern part of the United States [15-16].

Thus, climate change and global warming have initiated extreme weather events with an increase in prolonged periods of extreme temperature and humidity. These events supply extra moisture and temperature to the infrastructure. It may also be found in many cases that maximum temperature gets maximized and minimum temperature gets minimized. This intrinsic uncertainty of extreme events can alter the environmental conditions and adversely effects our infrastructures, especially, their chemical processes that rely on the surrounding environments. Particularly, the uncertain changes of the environmental conditions can create an anomaly in the chemical kinetics of ASR, gel production, and subsequent accelerated expansion. Favorable weather (i.e. high temperature or humidity) initiates the ASR expansion, whereas, unfavorable weather (i.e. low temperature or humidity) minimizes the further expansion. This frequent expansion and shrinkage generate greater stress levels in concrete and can potentially lead to much faster crack development in the concrete structure. Thus, extreme weather conditions may create an even worse scenario and can cause more degradation to ASR damaged structures. Extreme weather has also triggered sharp changes to the degree of saturation in the porous media. Aggregates containing amorphous silica are more porous, provide a large surface area, and thus, are more susceptible to deleterious alkali-silica reactions [17]. The moisture absorption-induced volume expansion depends on the saturation status of this porous

material. Moisture effects on the ASR mechanism and relevant drying shrinkage of the unsaturated or variably saturated porous media have already been justified [18-20]. With the immediate change in temperature and random evaporation of the moisture content, the tiny pores inside the porous concrete may feel an increase or decrease in the internal vapor. This situation may generate a pressure gap inside the pores. This pressure drop between unsaturated and saturated media may pose internal shrinkage stress and can cause further damage.

Existing saturated porous media and highest alkali-silica reaction assumption (high temperature or humidity) might lead to over conservative design, which is not cost effective. Nevertheless, counting the influence of global warming and climate change on the extreme weather events and its impact on concrete infrastructures have been frequently underestimated. Present lab practice with constant temperature and humidity, also disregard the random weather change and thus, can't capture ASR damage accurately. From an engineering point of view, the effects of uncertain environmental and extreme weather conditions on the performance of concrete structure should be evaluated accurately. Moreover, researchers have been struggling to develop numerical models that can assess constitutive properties accurately and quantify the chemo-physical damage induced by alkali silica reactions [21-26]. Within this context, a simplified alkali silica reaction model is proposed in this work as an attempt to identify ASR properties and bridge the existing research gap in the field of numerical modeling. A two-dimensional (2-D) concrete meso-structure was generated as a representative of ASTM prism test. The aim was to replicate environmental and material properties stated in ASTM C1293 standard [27], to validate the model in first place. The model relies on several partial differential

equation (PDE)-based governing equation sets, which represent relevant chemophysics of ASR expansion. Richards' equation was adopted to capture the unsaturated or partially saturated porous media of concrete. Uncertainties involved in the transport of the chemical species in the porous media were assessed through the regression analysis based on the relevant unknown parameters. The effects of variable moisture conditions (i.e. ambient humidity) and temperature were incorporated into the validated model by modifying the rate constants involved in the ASR kinetics. Analysis was done on a case by case basis. Stochastic processes were adopted to address extreme weather conditions in the model. All the analyses were done on the same reactive media, to extrapolate the data in a meaningful way. Finite element method (FEM) was applied to solve partial differential equation (PDE) based governing equation sets. In sum, this work adopted the following framework for ASR damage analysis:

- Partially or variably saturated porous media to match with uncertain moisture access
- Weather-dependent rate constants for the ASR kinetics
- Seasonal variation addressing four equal-length seasons in a year: winter, spring, summer, and fall
- Extreme weather impact and its stochastic distribution
- Long-term damage assessment of concrete meso-structure

Damage in the concrete structure is considered when it passes the pre-defined threshold. The simulated results from this work identified that ASR expansion is maximized with the constant high temperature and humidity. However, seasonal change and random weather manipulate the conventional rhythm of gel production and produces

highly non-linear expansion. Hence, stochastic distribution of extreme weather damages the concrete structure faster and in severe manners.

Thus, the proposed model integrates global warming impact-induced weather data and its stochastic representation as input, and provides a new perspective from meso-scale chemo-physio-mechanical scheme for a better understanding of ASR kinetics and the ultimate consequences.

2 Governing Equation Sets

2.1. Chemical Model

The coupling between the hydroxyl ions in the pore solution of concrete and siliceous components of the reactive aggregates produces ASR gel. This gel, in itself, does not initiate any damage to concrete. Rather, hydrophilic ASR gel imbibes available water or moisture from the surroundings, and thus, gets converted to expansive gel with a noticeable increase in the percent volume expansion. As the gel continues to absorb more water from the surroundings, it develops internal stress in the concrete domain. The cumulative stress can surpass the tensile capacity of concrete and may result into visual or internal cracking of the concrete domain. The basic chemical reactions involved in the ASR mechanism can be found in study [28].

There are six chemical species involved in the gel production as presented in Table 4-1[28, 29]. Their evolutions were addressed through several PDE based equation sets. This was done based on the principles of mass balance and momentum balance [30]. Mass balance theory and Richards' equation are used here to simulate chemical species transport and diffusion in the partially or variably saturated concrete porous media.

Table 4-1 Chemical species involved in the alkali-silica reaction

Species	Comments
Siloxane	Available in the reactive aggregates
ROH	Hydroxyl ions, available in the cement paste
Silanol	A byproduct of the chemical reaction
ASR gel	Hydrophilic gel
H_2O	Water or moisture
Expanded ASR gel	Final product when ASR gel absorbs water and swells

Mass & Momentum Balance Equation

Due to chemical reaction there is continuous migration and diffusion of chemical species through the moisture or pore water available in the concrete matrix. Thus, along with the mass transfer there is fluid flow in the matrix. These mass transfers and flow velocities need to be counted on time to capture the transport mechanism and production of the chemical process. Eq. (1) represents the mass & momentum balance equation for chemical species transport in the porous media [25]. Instead of individual masses, the concentration of each species was considered as a dependent variable in the equation, while balancing the mass transport in the cement-aggregate interactive media. The rate change of concentration is proportional to the diffusivity and instantaneous rate of change of the concentration of each species.

$$\frac{\partial}{\partial t}(c_i) + \nabla . (-D_i \nabla c_i) + \mathbf{u}. \nabla c_i = R_i \qquad (1)$$

where c_i is the concentration of each species i (mole/m^3), D_i denotes the diffusion coefficient of species i (m^2/s), **u** is the fluid velocity vector (m/s) with components in x, y, and z direction, respectively, and R_i is a source term, which is defined as the rate change of concentrations of species i (mole/(m^3/s)).

Diffusion Coefficients of ASR gel (m^2/s) were taken as 1×10^{-10} and 1×10^{-12} for Mortar and aggregate phases, respectively [26]. Diffusion Coefficient of H_2O was considered as 5×10^{-10} m^2/s in mortar [31]. It was assumed there was no moisture diffusion through aggregate. Diffusion coefficient of ROH was calculated through parameter estimation as discussed in section 3.2. Initial concentration of ROH was taken based on the validation standards and discussed on section 3.1. Initial concentration of H_2O can be found in the case studies presented in Table 4-4. Initial concentration of silanol and ASR gel were assumed as zero based on the explanation presented in study [29]. Initial concentration of siloxane for aggregate sample can be found in Table 4-3. The rate of change of concentration for the species involved in the ASR can be found in author's previous work [29].

Rate Constants

The relationship between the rate constants and temperature is defined through the Arrhenius equation as given by Eq. (2).

$$k = \mathrm{A}\exp\left(-\frac{\mathrm{E_a}}{\mathrm{R_g}T}\right) \qquad (2)$$

where k is the rate constant, A is the pre-exponential factor (also known as frequency factor), $\mathrm{E_a}$ is activation energy, $\mathrm{R_g}$ is the universal gas constant and T represents absolute temperature.

To calculate the rate constants Eq. (2) was modified further as Eq. (3) to capture the combined effects of temperature and relative humidity (RH) in the porous media.

$$k = \mathrm{A}\exp\left(-\frac{\mathrm{E_a}}{\mathrm{R_g}T}\right) \mathrm{f_{RH}} \qquad (3)$$

where f_{RH} is a factor to the relative humidity. This work assigned a factor to the relative humidity to count their effects on the ASR expansion. Further details can be found in section 2.2.

Rate constants as identified by the three stages of chemical reaction [29] were correlated through Eq. (3), and assigned as $k_1 = k$, $k_2 = 50k_1$, and $k_3 = 100k_1$, respectively [25].

Richards' Equation

Richards' equation can capture the fluid flow in partially or variably saturated porous media. This is an improvement over the Darcy's law which is limited to fully saturated conditions only. Richards' equation was first published by the English mathematician and physicist Lewis Fry Richardson to develop empirical methods for weather forecasting [32]. Later, the equation was attributed to Richards that describes the fluid as capillary conduction through porous mediums [33]. Many attempts have been made to simplify Richards' equation while simulating fluid flow in porous media. A very general form of Richards' equation was used in this work as of Eq. (4) [34, 35]. Unsaturated or fully saturated porous media can't account for the variable moisture supply generated from the extreme weather condition. This situation misestimates the ASR expansion, which is a waste of designed materials. On the other hand, Richards' equation provides an added benefit to incorporate the variable moisture transport into the model. It's a nonlinear partial differential equation where pressure is considered as the dependent variable.

$$\rho\left(\frac{C_m}{\rho g} + S_e S\right)\frac{\partial p}{\partial t} + \nabla.(\rho \mathbf{u}) = Q_m \qquad (4)$$

where ρ is the fluid density (kg/m^3), C_m denotes the specific moisture capacity (1/m), g is the acceleration due to gravity (m/s^2), S_e represents the effective saturation (1),

S represents storage coefficient (1/Pa), p is the pressure (Pa), **u** is the fluid velocity vector (m/s), and Q_m is the fluid source (kg/(m^3.s)).

The fluid velocity vector across the faces of an infinitesimally small surface can be defined as Eq. (5).

$$\mathbf{u} = -\frac{\kappa_s}{\mu} k_r(\nabla p + \rho g \nabla D) \qquad (5)$$

where κ_s defines the hydraulic permeability (m^2), μ is the fluid dynamic viscosity (Pa.s), k_r represents the relative permeability (1), and D is the elevation (m).

In this work, effect of elevation, D was not considered and assumed as zero. Initial pressure level and reference pressure level were kept the same to avoid any pressure gradient at the initial stage. Hydraulic conductivity was considered as the permeability model which combines the fluid permeability and dynamic viscosity. Hence, fluid dynamic viscosity, μ was ignored in this work. Thus, final Richards' equation used in this study was formulated as Eq. (6).

$$\rho\left(\frac{C_m}{\rho g} + S_e S\right)\frac{\partial p}{\partial t} + \nabla.\rho(-K_s\, k_r \nabla p) = Q_m \qquad (6)$$

where K_s is the hydraulic conductivity (m/s). Value of K_s is presented in Table 4-2.

The compressibility of fluid or cement-concrete matrix was not considered in this work and thus, the value of storage coefficient, S was simply defined as 1 (1/Pa). Fluid source term was calculated as, $Q_m = R_{H_2O} * 0.018$ [kg/mole] [29].

Retention model

Richards' equation provides a platform under variably saturated media to input weather randomness in the ASR model. However, a mathematical process is needed to add these inputs in the model. Retention models can do this job by capturing the moisture

content of the partially saturated media. In this work, the van Genuchten retention model was used to calculate the unsaturated hydraulic properties of the flow medium, i.e., liquid volume fraction, θ, effective saturation, S_e, specific moisture capacity, C_m, and relative permeability, k_r [36]. Variably saturated media works through the liquid volume fraction, which may range from a residual value, θ_r to a saturated value, θ_s or total porosity depending on the available moisture content in the media [36]. According to the van Genuchten model, unsaturated condition occurs when pressure head in the media becomes negative and it reaches saturation level when pressure head is equal to or greater than zero [36]. Eq. set (7) describes the van Genuchten equations.

Unsaturated Condition ($H_p < 0$):

$$\theta = \theta_r + \frac{\theta_s - \theta_r}{[1+(\alpha|H_p|)^n]^m} = \theta_r + S_e(\theta_s - \theta_r)$$

$$S_e = \frac{1}{[1+(\alpha|H_p|)^n]^m}$$

$$C_m = \frac{\alpha m}{1-m}(\theta_s - \theta_r) S_e^{\frac{1}{m}} \left(1 - S_e^{\frac{1}{m}}\right)^m$$

$$k_r = S_e^{\frac{1}{2}} \left(1 - \left(1 - S_e^{\frac{1}{m}}\right)^m\right)^2$$

Saturated Condition ($H_p \geq 0$):

$$\theta = \theta_s$$

$$S_e = 1$$

$$C_m = 0$$

$$k_r = S_e^{\frac{1}{2}} \left(1 - \left(1 - S_e^{\frac{1}{m}}\right)^m\right)^2$$

(7)

where pressure head, $H_p = \frac{p}{\rho g}$, $m = 1 - \frac{1}{n}$, and α, m, n are the van Genuchten coefficients. Material properties along with other values of θ_s, θ_r, α, and, n are presented in Table 4-2, based on the water retention curve for mortar and aggregate phases (weathered granite) [37, 38].

Note that, Eq. (1) and Eq. (6) were simulated concurrently to quantify concentration of expansive alkali-silica gel in the variably saturated porous media of concrete. Richards'

equation took care of the Darcy's velocity field of moisture flow, involved in the mass balance equation.

2.2. Weather Impact Model

Environmental conditions greatly affect the frequency of ASR expansion and induced damage in concrete structures. High humidity supplies more moisture to concrete which creates a pressure difference inside concrete. This facilitates micro-structural flow of moisture in concrete and induces hygroscopic swelling of alkali silica gel. Researchers suggested a critical value of 80% for relative humidity to produce significant expansion of the gel [39]. Moreover, global warming can influence the ASR expansion and carries a potential threat to the existing concrete structures. Increasing temperature and seasonal variations propel the reaction rate constants, involved in the ASR kinetics, and thus, concrete structures are more susceptible to ASR damage in warmer region. It is noteworthy that global mean temperature can potentially increase by 5°C within the year 2100, based on the projection of climate models [40]. For these reasons, a comprehensive model is highly desired to assess in depth effects of the weather parameters, i.e. temperature and relative humidity, on the concrete structures subjected to ASR expansion.

Temperature:

Heat transfer in porous media of concrete was simulated using the following equation which corresponds to the differential form of the Fourier's law.

$$\rho C_p \frac{\partial T}{\partial t} + \nabla \cdot (\mathbf{q}) = Q_s$$
$$\mathbf{q} = -k\nabla T \qquad (8)$$

where ρ is the density of the solid (kg/m^3), C_p denotes specific heat capacity at constant pressure (J/ (kg-K)), T is temperature (K), k is the thermal conductivity of concrete (W/ (m-K)), and Q_s is heat source or sink (W/m^3).

In the model, concrete was considered without insulation and all sides were subjected to ambient temperature at the boundary. The heat source, Q_s, usually considered for early-age concrete under cement hydration was ignored for hardened concrete. Initial and reference temperature were kept same to avoid any temperature gradient at the initial stage. The values of specific heat capacity and thermal conductivity can be found in Table 4-2.

Relative Humidity

Percentage of ambient relative humidity was considered and fed into the model through Eq. (3) as discussed in section 2.1, to account for its effects on ASR expansion. From 2 years ASR expansion vs relative humidity relationship for Rhyolitic Tuff [41], an empirical equation in terms of a RH factor was developed as Eq. (9). This factor was addressed to easily connect the effects of ambient humidity to the ASR expansion. It has been adopted in such a way that it becomes 1 when RH reaches 100%, and can vary in between 0 to 1 depending on different humidity levels. For the lower values of RH, the ASR expansion is minimal, and thus, associated factor is also very less in numbers. However, after 80% RH, there is a sharp increase in the ASR expansion, and same is true for the factor. Figure 4-1 depicts the plot of this equation and justifies the trend of change.

$$\begin{aligned} f_{RH} &= 0.0006\exp(0.0717RH); RH < 85 \\ &= 0.0485RH - 3.85; 85 \leq RH \leq 100 \end{aligned} \quad (9)$$

where RH is relative humidity expressed in %.

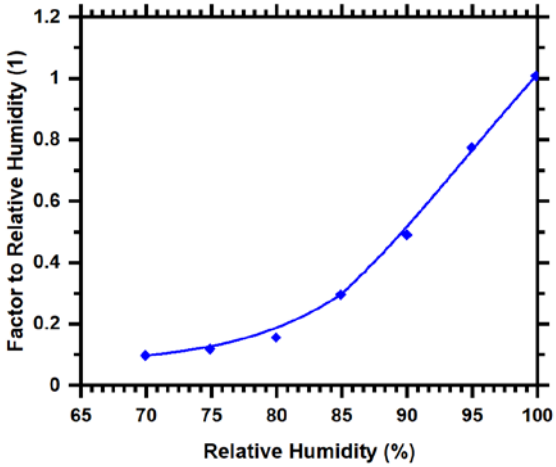

Figure 4-1 Effect of RH on the expansion of prisms Concrete [41]

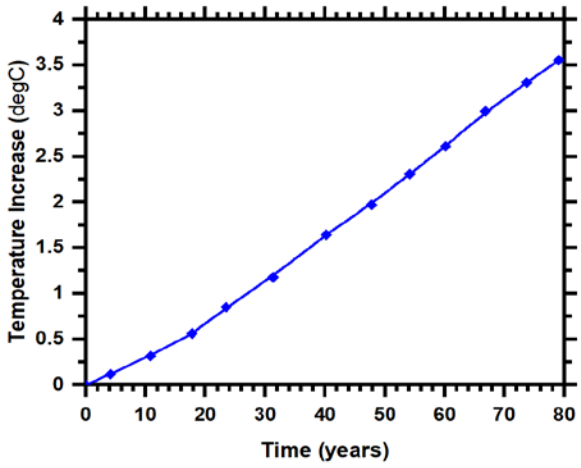

Figure 4-2 Projected future global surface temperature increase [40]

Global Warming

Global warming comes up with a temperature increase, which can boost the ASR kinetics through Eq. (3). The effect of global warming was adopted based on the projection of climate model under Representative Concentration pathway (RCP) 8.5 [40]. According to this model, the global surface warming can increase by 3.6℃ within the next 80 years (2020-2100). The effect of global warming was modeled assuming a polynomial variation of temperature with time as Eq. (10).

$$\Delta T = -3\exp(-6)t^3 + 0.0005t^2 + 0.0257t - 0.003;\ 0 \le t \le 80 \qquad (10)$$

where ΔT is the temperature increase (°C), and t is the time (years). Figure 4-2 illustrates the polynomial relationship developed in this equation.

Table 4-2 Material properties used in the Chemical and Weather Model

	Mortar	**Aggregate**	**Source**
Activation Energy, E_a (J/mole) for ASR	43000	43000	[42]
Universal gas constant, R_g (J/(mole.K))	8.3144598	8.3144598	
Initial Pressure (atm)	1	1	
Reference Pressure (atm)	1	1	
Residual water content, θ_r	0	0.08	[37, 38]
Saturated water content, θ_s	0.185	0.308	
van Genuchten coefficient, α (1/m)	3.23×10^{-4}	15.3	
van Genuchten coefficient, n	1.217	1.406	
Hydraulic Conductivity, K_s (m/s)	6×10^{-13}	5.35×10^{-11}	[43]
Heat Capacity (J/(kg-K))	1548	850	
Thermal conductivity (W/(m-K))	1.73	2.9	
Initial Temperature (K)	293.15	293.15	
Reference Temperature (K)	293.15	293.15	

2.3. Stochastic Model

Chemical kinetics of alkali-silica reaction and possible expansion are highly sensitive to the surrounding temperature and relative humidity. Moreover, climate change, global warming and seasonal variations add uncertainty to the complex ASR mechanisms. Thus, to conduct realistic simulation of concrete damage under variable environmental conditions, extreme weather should be addressed properly. This can be done by incorporating associated randomness or stochasticity of extreme weather in the model. Hence, this work utilizes a stochastic approach to synthesize the random nature of weather and associated uncertainty in the ASR-induced damage of heterogeneous concrete meso-structure. The stochastic process was coupled with the Weather Model in reproducing the temperature and humidity to imitate the real-world weather condition.

The Karhunen–Loève expansion (KL) was implemented to account for the stochastic approach. KL expansion is a popular approach of series expansion, where the stochastic process is represented as a truncated finite series [44]. Thus, it is adopted to explicitly represent the weather anomaly in the predictive model. The Karhunen–Loève expansion of a zero-mean random process $X(t,\theta)$ as shown in Eq. (11) is based on the spectral decomposition of its covariance function [44]. If the covariance function is bounded, symmetric, and defined by the orthogonal Eigen-decomposition, the KL expansion of random process $X(t,\theta)$ over the stochastic domain, $\mathcal{D}$ can be expressed as Eq. (11) [44].

$$X(t,\theta) = \sum_{n=1}^{m} \sqrt{\lambda_n}\varphi_n(t)\xi_n(\theta) \qquad (11)$$

where φ_n and λ_n are the orthogonal deterministic Eigen functions and Eigenvalues of the covariance function, respectively. $\xi_n(\theta)$ is a set of uncorrelated random variables. The series is approximated by a finite number of terms, m for solving practical problems. The deterministic set of Eigen functions is used to represent the stochastic process in weather parameters.

The values of φ_n and λ_n can be determined from the analytical solution for the covariance kernel as Eq. (20) [12].

$$\int_{\mathrm{D}} C_X(t_i,t_j)\,\varphi_n(t_j)\mathrm{d}t_j = \lambda_n\varphi_n(t_i) \qquad (12)$$

where $C_X(t_i,t_j)$ is the covariance function, t_i and t_j are the coordinates of point i and j, respectively.

In this work, we implemented exponential covariance kernel as Eq. (13) in the symmetrical domain, $\mathcal{D}$ = [−1, 1] to solve the integral problem. Exponential function was

considered to simulate the randomness of extreme weather events. This function consists of only two parameters (σ^2 and b).

$$C_X(t_i, t_j) = \sigma^2 \exp\left(\frac{|t_i - t_j|}{b}\right) \qquad (13)$$

where σ^2 is the variance and b is a correlation length parameter. Variance is a scaling factor which determines how far function values can vary from the mean. Length parameter, defines the smoothness of the function, i.e. how frequent the value can change. In this work, we assumed variance, $\sigma^2 = 1$ so that the function stays close to their mean values, and correlation length parameter, $b = 0.1$ so that the function value can change quickly to imitate abrupt change in temperature or humidity due to extreme events.

Thus, for a certain mean, μ for the process, the KL expansion of random process $X(t, \theta)$ was further derived as Eq. (14).

$$X(t, \theta) = \mu + \sum_{n=1}^{m} \sqrt{\lambda_n}\varphi_n(t)\xi_n(\theta) \qquad (14)$$

Random variables set, $\xi_n(\theta)$ was assumed as a Gaussian process. Details derivation for the Eigenvalues and Eigenvectors estimation can be found in study [44].

Stochastic Temperature and Humidity:

The derived KL expansion was used to consider time-dependent stochasticity of both temperature and relative humidity. Eq. (14) was further modified as Eq. (15) to calculate the stochastic temperature of the surrounding environments.

$$T(t, \theta) = (\mathrm{T}_{\mathrm{mean}} + \Delta\mathrm{T}) + \sum_{n=1}^{m} \sqrt{\lambda_n}\varphi_n(t)\xi_n(\theta) \qquad (15)$$

where $T(t, \theta)$ represents the stochastic temperature.

Relative humidity and dew-point temperature indicate the amount of available moisture in the air. Global warming increases the dew-point temperature, and thus, relative humidity also increases with it. To calculate stochastic humidity, Eq. set (16) was derived based on the relation between temperature and humidity [45].

$$\mathrm{T_d} = (\mathrm{T_{mean}} + \Delta\mathrm{T}) - (\frac{100 - \mathrm{RH}_{mean}}{5})$$
$$RH = 100 - 5(T - \mathrm{T}_d) \qquad (16)$$

where $\mathrm{T_{mean}}$ is the mean temperature (°C), $\mathrm{T_d}$ is the dew-point temperature (°C), T is the stochastic temperature (°C), RH_{mean} denotes mean relative humidity (%), and RH is the stochastic humidity (%), at any certain time.

2.4. Damage Model

Volume change happened in the ASR-damaged concrete was calculated through Eq. (17) according to study [29].

$$\varepsilon_{\mathrm{gel}} = \frac{\rho_{\mathrm{gel}}}{\rho_{\mathrm{gel}} + \rho_{\mathrm{c}}} \qquad (17)$$

where $\varepsilon_{\mathrm{gel}}$ is the volumetric strain from ASR expansion, ρ_{gel} and ρ_{c} represent mass density of alkali silica gel and concrete, respectively. Concrete density, ρ_{c} after 90 days was calculated as 2475.5 kg/m^3. The derivation of ρ_{gel} can be found in study [29].

Intensity of ASR damage can be calculated from Eq. (18), following the chemical damage criteria presented in study [26]. Damage is considered when volumetric strain or percent expansion is greater than 0.1%.

$$\mathrm{D_{gel}} = 2.021 \times \varepsilon_{\mathrm{gel}} - 0.195; \qquad \varepsilon_{\mathrm{gel}} > 0.1\% \qquad (18)$$

where $\mathrm{D_{gel}}$ is the damage due to ASR expansion.

3 Numerical Analysis

In this work, a meso-scale model was developed to accommodate for the non-linear evolution of ASR damage in both space and time. Based on the derivation discussed above we came up with the governing equation sets to run the simulation. Mixed mineralogy gravel, C8 [46] was considered for the validation purposes. This model was simulated 1 year for the parameter estimation and validation purposes. It was simulated further for 30 years to extrapolate data from the model and predict service life of concrete.

3.1. Mesoscopic Geometry

This work captured concrete geometry at the meso-scale, to replicate concrete damage propagation subjected to ASR, in a 2D computational framework. A meso-scale concrete prism with square cross section of 75mm was created according to ASTM C 1293 concrete prism test [27]. A 3D Anm geometric model of concrete prism was developed in the virtual cement concrete testing lab according to study [47]. Details of the process and algorithm for Anm model can be found in our previous publication [47, 48]. A uniform-thickness shell as interfacial transition zone (ITZ) region was further added into the cement paste around the aggregate particle to locate the transition area of alkali silica gel. To do the easy meshing and saving simulation time a processed 2D slice of concrete prism describing two basic phases (mortar and aggregate) was created from the 3D Anm model as shown in Figure 4-3(a).

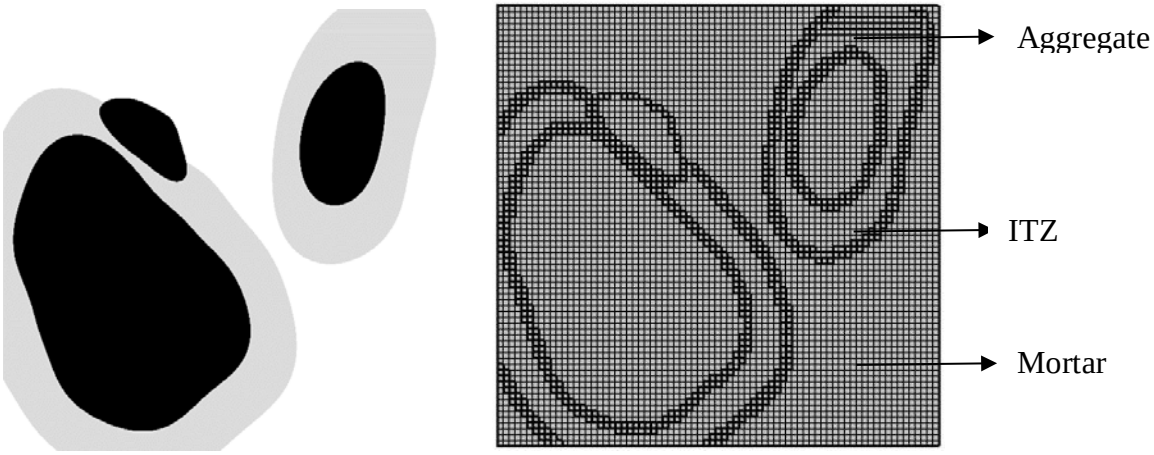

Figure 4-3 Concrete meso-scale geometry: (a) 2D slice, (b) Meshing

A developed 2D slice was meshed using quadrilateral elements. An in-house MATLAB code was developed to convert each pixel of 2D geometry into a quadrilateral element. The meshed geometry was further processed to make it readable in the NASTRAN bulk data format, a common format for importing 3D or 2D meshes into the finite element solver. A total of 158 different faces were generated from the pixel meshing. Figure 4-3(b) depicts the complete 2D mesh geometry of concrete prism block.

Material Properties

To match with the ASTM C 1293 concrete prism test [27], the concrete block was considered with a cement content of 420 (kg/m^3) and an alkali content of 1.25% Na_2O_{eq}. A corresponding initial hydroxyl ion concentration for cement was calculated as 875 (mole/m^3) from the relationship between ROH concentration and % equivalent Alkali [39]. A detail case study of the effects of ROH concentration on ASR gel production can be found in study [29]. Other material properties such as Young's Modulus, Poisson's Ratio, and Density for mortar and aggregate domain can also be found in study [29].

3.2. ASR Kinetics Parameter Estimation

Parameter estimation is the determination of the best values for uncertain parameters in a numerical model. This is a sort of inverse modeling system through data accumulation from any relevant experimental or technical setup. The value of many parameters associated with the ASR kinetics, i.e. diffusion coefficients of ROH, initial siloxane concentration of aggregate, pre-exponential factor etc. is not clear and unspecified. These values depend on the reaction intensity, aggregate reactivity, surrounding environments (temperature or humidity) etc. Variable environmental conditions may also affect the intensity of these parameters. Thus, an effective approach is needed to estimate these uncertain parameters so that the output from the developed model aligns with the experimental observations. This can be done through the calibration of the model by comparing with the available experimental data.

In this work, we developed an in-house MATLAB code to estimate the unknown parameters through the regression analysis and to ensure reliability of them in the Chemical Model. Experimental data of ASR expansion for mixed mineralogy gravel, C8 was considered in this case [46]. The process started with an initial guess for the uncertain parameters. Initial guesses for the diffusion coefficients of ROH in mortar and in aggregate were considered as 7.5×10^{-12} m^2/s [42], and 5×10^{-14} m^2/s [42], respectively. Initial guesses for pre-exponential factor and concentration of siloxane in aggregate were assumed based on the results after first simulation, and were considered as 0.00035 (1/s), and 750 ($mole/m^3$), respectively.

A range of possible values was proposed as uniform random function based on those initial guesses. This work utilized accept and reject methods where a threshold value

of 0.001 was considered to limit the parameter values. Error calculation and estimations were completed through the following algorithm:

$$Error = (T_2 - T_1)^2;$$

$$If\ Error \leq 0.001: Accept\ the\ sample$$

$$Else: Reject\ the\ sample$$

where T_1 and T_2 are the experimental and simulated data, respectively.

Figure 4-4 shows the distribution of the sample values for the unknown parameters. The values associated with the maximum frequency produce less error and thus, simulation results align more accurately with the experimental data.

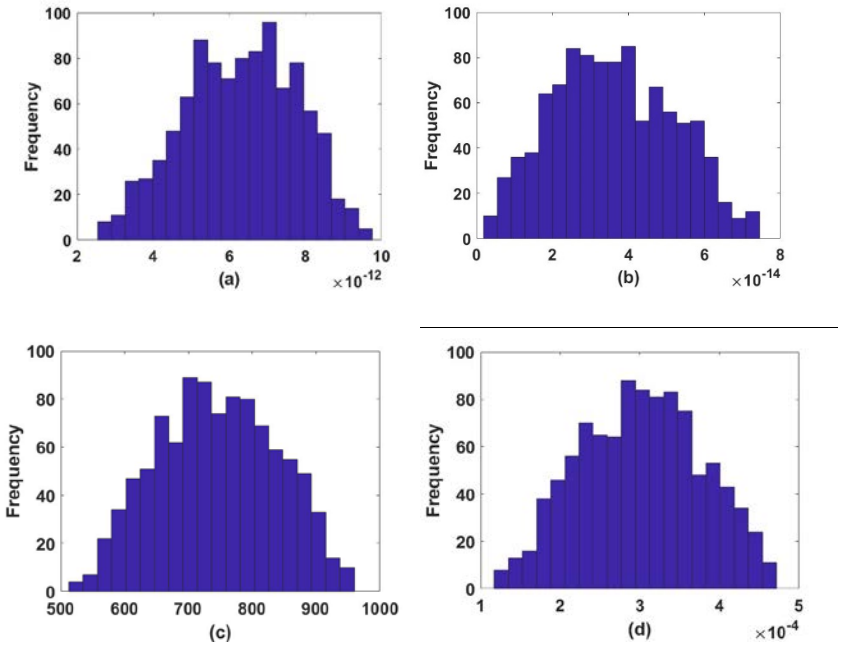

Figure 4-4 Histogram of the estimated parameters: (a) diffusion coefficient of ROH in mortar (m^2/s), (b) diffusion Coefficient of ROH in aggregate (m^2/s), (c) initial concentration of siloxane in aggregate ($mole/m^3$), (d) pre-exponential factor (1/s).

From these histograms, the following values were adopted for the uncertain parameters in the model.

Table 4-3 Parameter estimation

	Mortar	**Aggregate**
Diffusion Coefficient of ROH (m^2/s)	7×10^{-12}	4×10^{-14}
Pre-exponential factor, A (1/s)	0.00029	0.00029
Initial Concentration of siloxane ($mole/m^3$)	0	710

3.3. Parametric Study

There could be a common question: how ASR expansion would evolve under different weather conditions. As an effort to address this question, this work implemented a parametric study of temperature and relative humidity, to assess the weather events in the model. A number of benchmark problems have been proposed in terms of the case study, to account for the ASR evolution under variable weather conditions.

Temperature, relative humidity and boundary water level were fed into the Weather Model as discussed in section 2.2 for a detailed case study. Case 1 was considered as a validation case for weather conditions, which was required by ASTM C 1293 concrete prism test [27].

Seasonal Variations

There exists a correlation between temperature and humidity. In this work, this correlation is taken into account by considering the effect of water-vapor on relative humidity. The water–vapor required to saturate air during cooler seasons is lower, and therefore, the relative humidity is larger for these seasons. On the contrary, the relative humidity has lower values for warmer seasons.

We incorporated seasonal variations of temperature and humidity in the model in terms of the four seasons of equal duration— winter, spring, summer, and fall, which follow one another regularly. Following sinusoidal functions as shown in Eqs. (19-22) were

developed to represent randomness in the daily weather due to seasonal variation. Figure 4-5 and 4-6 show the graphical representations of these functions. We assumed such abrupt changes in the daily temperature and relative humidity to replicate the extreme weather events.

Winter:

$$T\ (^{\circ}C) = 5+10\sin(2\pi t/24) \quad 0 \le t \le 24h\ (1\ day)$$

$$RH\ (\%) = 82.5+12.5\sin(2\pi t/24) \quad 0 \le t \le 24h\ (1\ day) \qquad (19)$$

Spring:

$$T\ (^{\circ}C) = 25+10\sin(2\pi t/24) \quad 0 \le t \le 24h\ (1\ day)$$

$$RH\ (\%) = 70+15\sin(2\pi t/24) \quad 0 \le t \le 24h\ (1\ day) \qquad (20)$$

Summer:

$$T\ (^{\circ}C) = 35+10\sin(2\pi t/24) \quad 0 \le t \le 24h\ (1\ day)$$

$$RH\ (\%) = 65+15\sin(2\pi t/24) \quad 0 \le t \le 24h\ (1\ day) \qquad (21)$$

Fall:

$$T\ (^{\circ}C) = 12.5+12.5\sin(2\pi t/24) \quad 0 \le t \le 24h\ (1\ day)$$

$$RH\ (\%) = 80+15\sin(2\pi t/24) \quad 0 \le t \le 24h\ (1\ day) \qquad (22)$$

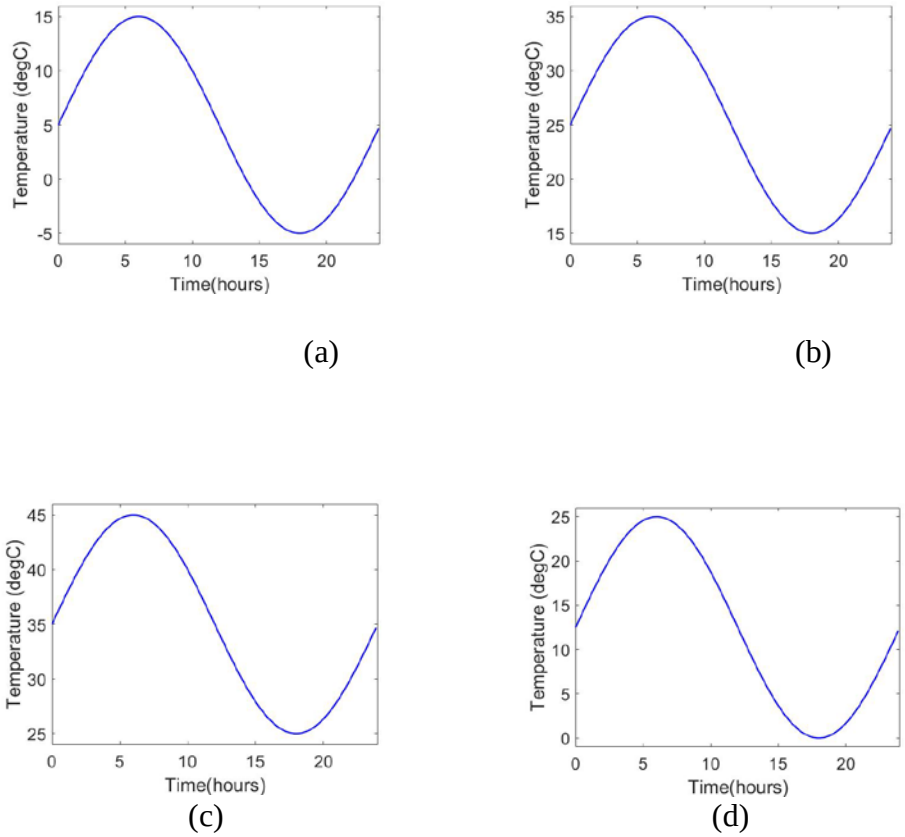

Figure 4-5: Daily temperature variations: (a) winter, (b) spring, (c) summer, (d) fall

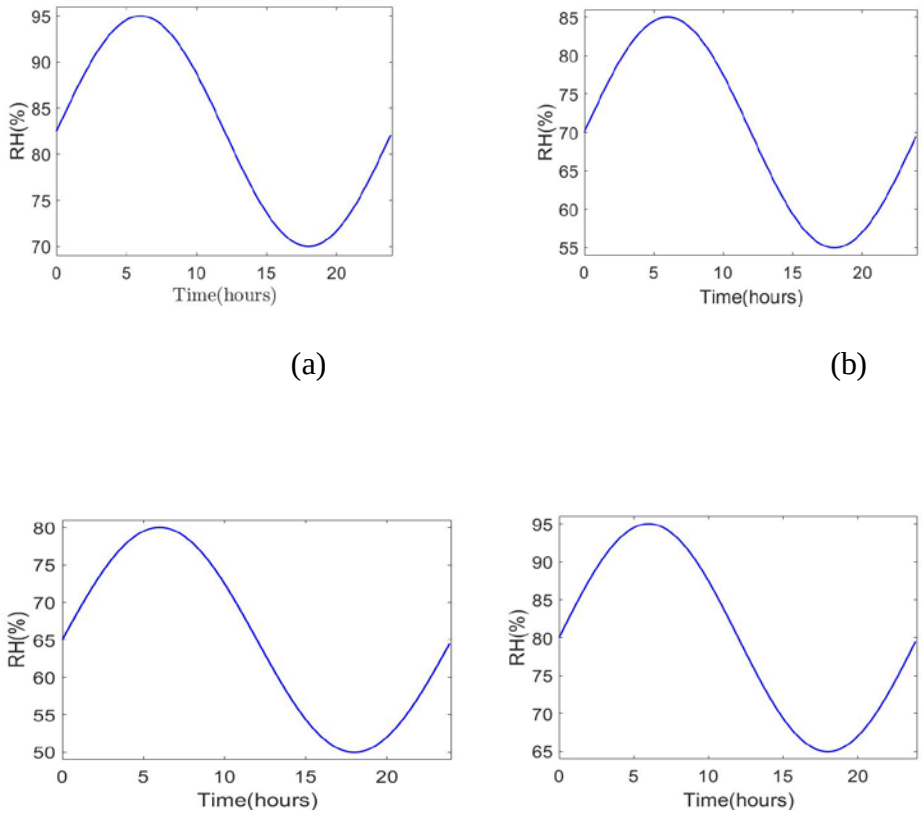

Figure 4-6 Daily relative humidity variations: (a) winter, (b) spring, (c) summer, (d) fall

A piecewise function was generated to capture all the seasons together in a 1 year timeframe. Figure 4-7(a) and Figure 4-7(b) visualizes the piecewise function graphically for temperature and relative humidity anomaly, respectively. Time is presented in months.

It has been found from the past 30 years of climate data that mean daily temperature anomaly follows a half-sine distribution round the year [49]. Keeping that in mind, we assumed daily temperature and humidity in such a way that it also produces a half-sine distribution of these weather parameters at the end of a complete year.

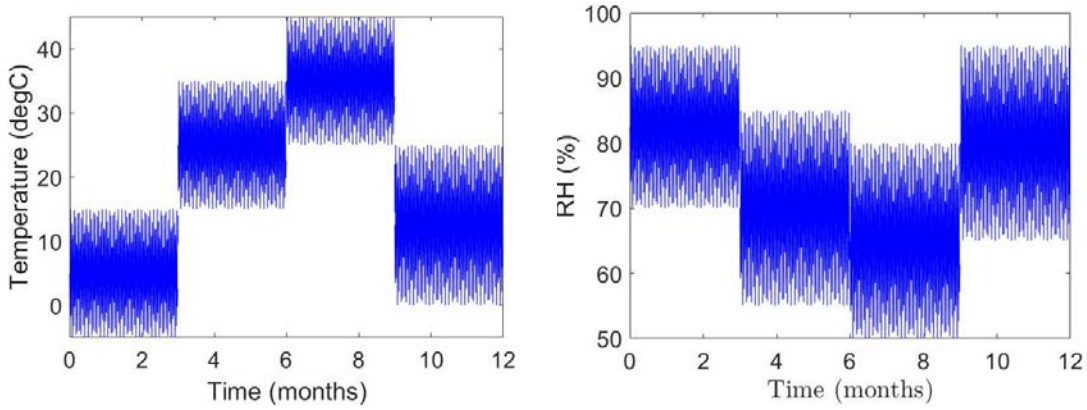

(a) (b)

Figure 4-7 (a) Yearly temperature variations (T_1), (b) Yearly relative humidity variations (RH_1)

Stochastic Distributions

Mean ambient temperature and humidity were added into the Stochastic Model as discussed in section 2.3.

To represent the yearly seasonal temperature and humidity distribution as shown above, we formulated the following half-sine functions as Eqs. (23-24), which periodically repeats each year throughout the simulation period. Figure 4-8 and 4-9 show the distribution of these functions.

$$T\ (\%) = \frac{T_{max} + T_{min}}{2} - \frac{T_{max} - T_{min}}{2} * \sin(2\,\pi\,t\ - f\,\pi) \qquad (23)$$

$$RH\ (\%) = \frac{RH_{max} + RH_{min}}{2} - \frac{RH_{max} - RH_{min}}{2} * \sin(2\,\pi\,t\ - f\,\pi) \qquad (24)$$

where T_{max} and T_{min} are the maximum and minimum temperature in a year which were assumed as 45℃ and -5℃, respectively. RH_{max} and RH_{min} are the maximum and minimum relative humidity in a year which were assumed as 95% and 50%, respectively. The terms t represents the simulation time and f is a frequency factor. A value of 0.5 was assigned to the frequency factor, f to produce half-sine curves that match with the

distribution of Figure 4-7. The temperature or relative humidity considered in this study are for the purpose of a case study, and thus, do not represent any specific location.

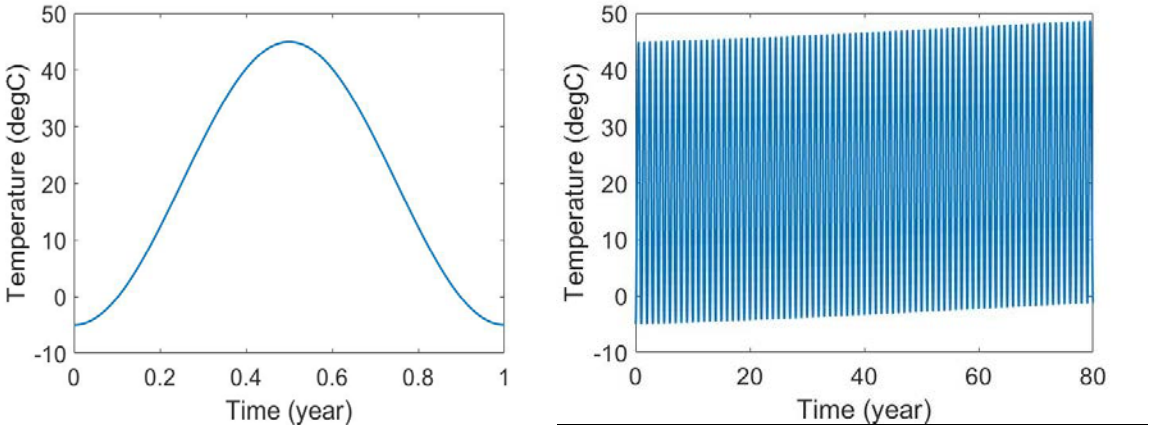

(a) (b)

Figure 4-8 Yearly temperature variations: (a) 1 year. (b) 80 years

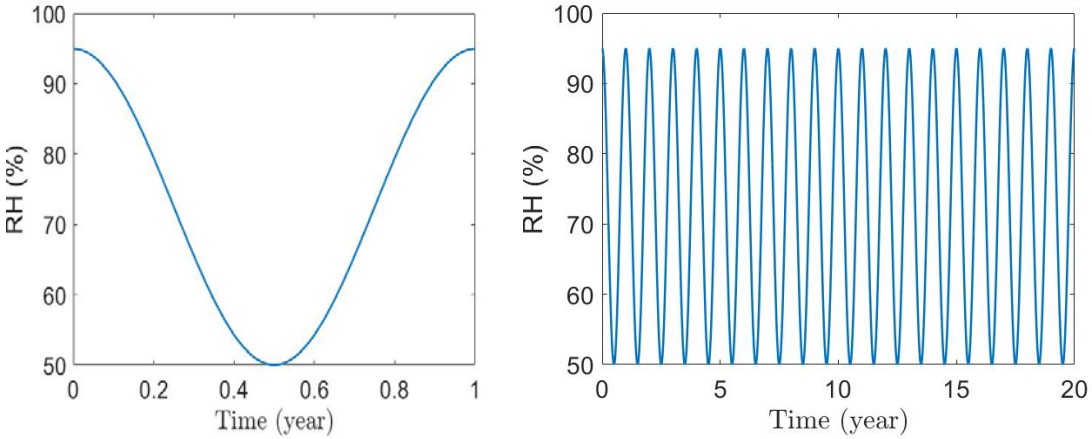

(a) (b)

Figure 4-9 Yearly relative humidity variations: (a) 1 year. (b) 20 years

The temperature from Eq. (23) and relative humidity from Eq. (24) were further imported as mean in the Stochastic Model, to facilitate the stochastic process. Figure 4-10 shows the random field realization of the KL expansion which added the randomness to mean temperature and humidity plot.

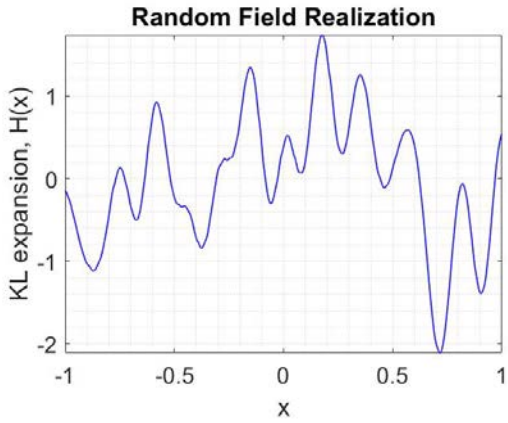

Figure 4-10 Random field of KL expansion

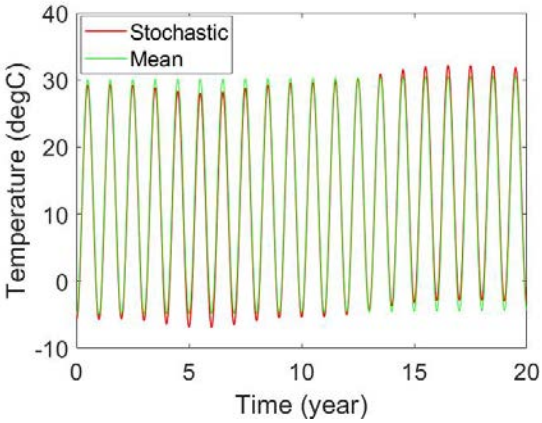

Figure 4-11 Stochastic temperature

Figure 4-11 shows the stochastic distribution of temperature for the next 20 years. It is obvious that temperature keeps increasing gradually due to global warming. Figure 4-12 further shows the temperature and relative humidity for the next 80 years. It is noticeable that the T and RH are decreasing at some points and also increasing sometimes later. Thus, these stochasticity represent the extreme weather events that can happen due to the effects of ongoing global warming and climate change.

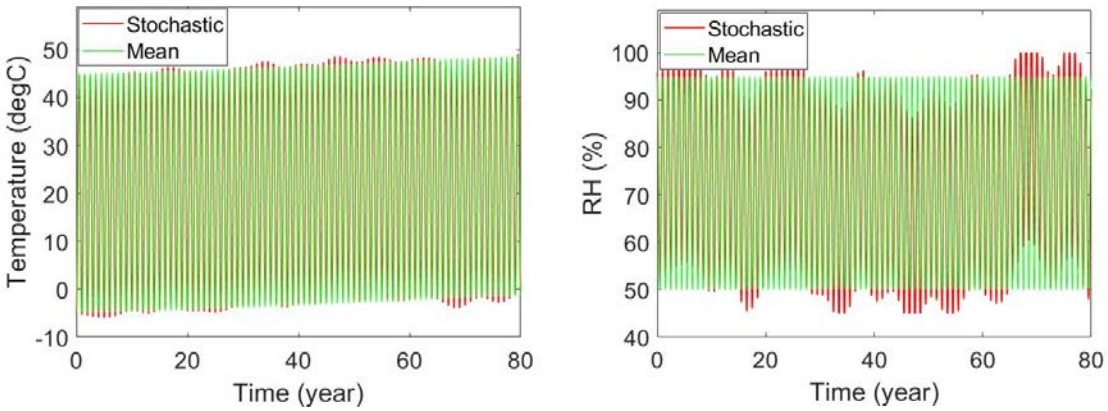

(a) (b)

Figure 4-12 (a) Stochastic temperature (T_2) (2020-2100), (b) Stochastic RH (RH_2) (2020-2100)

Finally, based on these temperature and humidity data, several case studies were conducted to visualize environmental effects on the alkali silica expansion. Table 4-4 depicts the details of all the cases studied in this work.

Table 4-4 Case studies for Weather Model

Case ID	Ambient Humidity (%)	Ambient Temperature (°C)	Initial Water Concentration [mole/m^3]	Representing Conditions
Case 1	100	38	0	Validation [46];
Case 2	0	38	0	Fully coated/insulated;
Case 3	100	38	1000	Uncoated & maximum saturation; A concrete dam submerged in water from the beginning;
Case 4	0	60	0	Fully coated/insulated; High temperature;
Case 5	100	60	0	Uncoated & maximum saturation; High temperature;
Case 6	100	60	1000	Uncoated & maximum saturation; High temperature as Nuclear storage; Nuclear reactor submerged in water;
Case 7	70	25	0	Room temperature and ambient humidity;
Case 8	100, 60	38	0	100% humidity for first half of the year and then drying to 60% over the last half of the year;
Case 9	60, 100	38	0	Drying with 60% humidity for first half of the year and then boosted to 100% over the last half of the year;
Case 10	RH_1	T_1	0	Seasonal variation;
Case 11	RH_2	T_2	0	Stochastic distribution;

Based on the facts discussed so far, a developed model was analyzed in finite element method (FEM) to simulate complex concrete matrix.

4 Results and Analysis

Analysis was done based on the material properties, case studies and input parameters as discussed before. Accumulated results represent the average value over the whole concrete domain, i.e. both mortar and aggregate phases

4.1. Validation of the developed Model

To ensure the accuracy of the extrapolated data, a deterministic analysis is needed to check the compatibility of the simulation results with the governing equation sets and

associated environmental conditions. In such, a developed model was validated comparing with the 1 year experimental data of aggregate type C8 [46], by assuming free expansion and adopting case 1 in the parametric study. Goodness of fit of the model was estimated through Root Mean Square Error (RMSE) method through the following equation.

$$RMSE = \sum_{i=1}^{N} \sqrt{\frac{(Z_i - Z_0)^2}{N}}) \qquad (25)$$

where $(Z_i - Z_0)^2$ is the differences, squared, and N is sample size.

Fig. 4-13 illustrates the validation plot along with the experimental data. Although the model shows a slight discrepancy in the expansion from a certain point at the beginning, simulation results intersect with it eventually at a later stage, which ensures better extrapolation beyond the validation period. This model also shows a latency period at the beginning stage, which is more logical for the ASR kinetics to manifest. Moreover, RMSE values lie close to zero (1×10^{-3} ~ 0.1×10^{-3}), which identify the goodness of fit, and ensure the accuracy of the estimated unknown parameters. Thus, the developed model predicts well the expansion behavior, to guess the potential damage of concrete and decide on-time remedy.

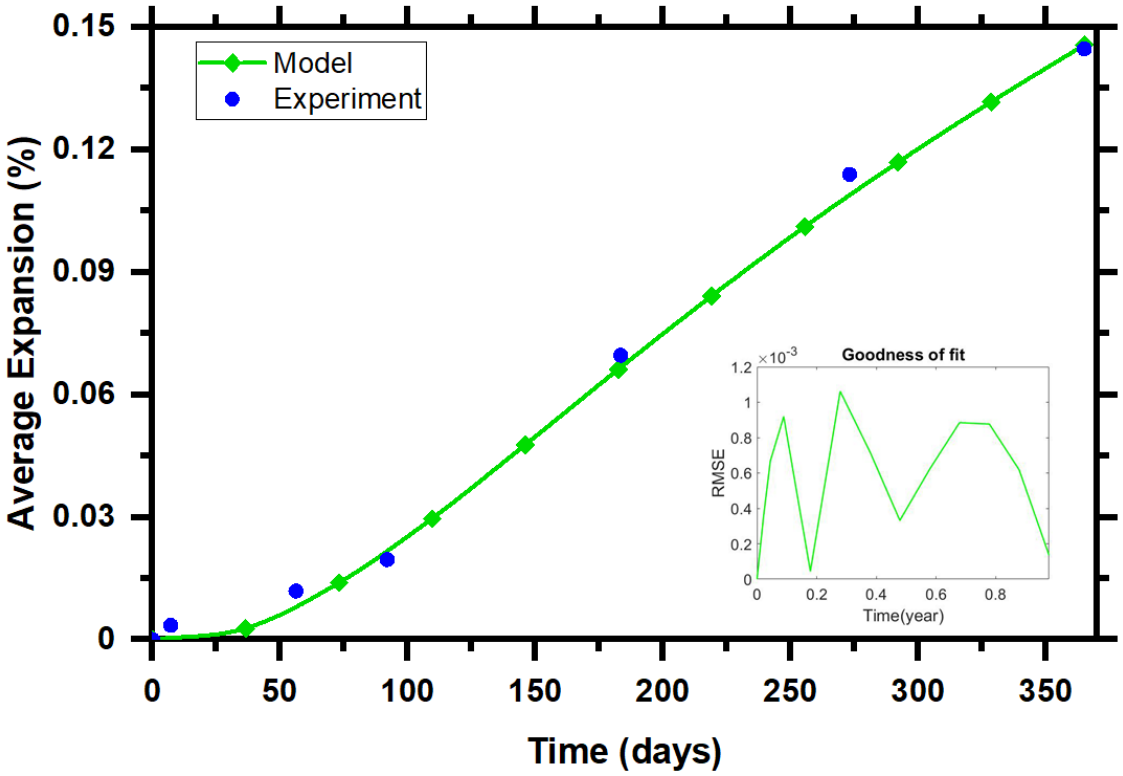

Figure 4-13 Validation of the Developed Model

This validated model will perform in light of the following considerations:

- NaOH and KOH are interchangeable in the model
- This work focused on the ASR gel production and its evolution over time. Thus, the production of non-expansive calcium silicate gel (CSH) which limits the ASR expansion through reaction between available calcium and ASR gel, was kept out of the consideration
- ASR-induced volumetric expansion is not unidirectional, i.e. values may change depending the boundary condition applied on each sides of the concrete block
- This model representation the stationary boundaries, i.e. geometry is not changing with time or expansion

4.2. Sensitivity Analysis

ASR Expansion

Alkali silica reaction in concrete was evaluated in terms of the volume change. Volume change was expressed as percent expansion of the domain. As the ASR progresses the concentration of each species involved in the chemical kinetics as well as the associated expansion changes with time. Analysis was done for 1 year on the type C8 aggregate under case 1 to visualize these relations. Polynomial functions were included to estimate these relations in the future. Figure 4-14 explains how the concentration of expanded gel and percent expansion vary with the concentration of ASR gel. It is obvious that, at the initial stage concentration of the expanded gel doesn't increase with ASR gel production. It takes a while to show the ASR expansion. This happens because ASR gel needs favorable weather condition (moisture) to expand, and there is a latency period to start this process.

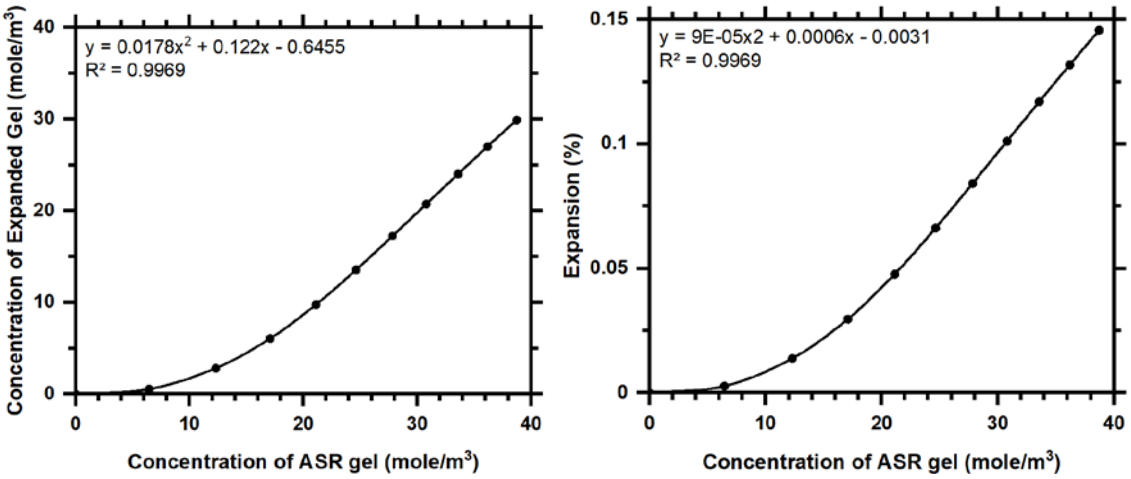

(a) (b)

Figure 4-14 Effects of ASR gel concentration on: (a) expanded gel concentration, (b) 1 year ASR expansion

Figure 4-15 depicts the effects of temperature and humidity on the ASR expansion. High temperature and humidity provide with most favorable condition for ASR kinetics to

happen, and thus, boost the expansion further. Expansion is significant when temperature is above 300K, and RH is above 85%.

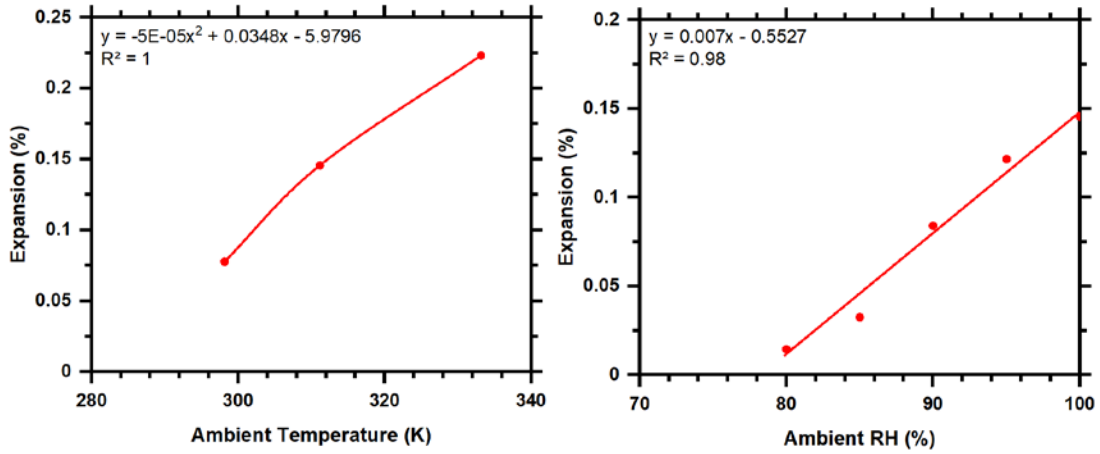

Figure 4-15 Evolution of 1 year ASR expansion with: (a) ambient temperature, (b) ambient RH

Figure 4-16 shows 1-year expansion of type C8 aggregate, for all cases of the Weather Model. Maximum expansion happens for case 6 (0.48%). Case 6 represents a nuclear reactor, which considers the most severe environmental conditions. High temperature and submerged water increase the ASR expansion significantly. Unlike case 6, case 5 represents concrete with zero initial water concentration. Thus, expansion for case 5 is much less than that of case 6 (0.22%). Case 1 is the validation case that represents an ASTM concrete prism test condition, and shows an expansion of 0.145%. Case 3 adds a submerged water condition to those of case 1 and represents a concrete dam under water. Thus, expansion in case 3 is larger than that of case 1 (0.35%). Case 2, 4, and 7 represent some weak or restricted weather conditions and show a little or no visible expansion after 1 year.

Case 8 considers an uncoated state initially, and then it goes through drying during last half of the year. With a high supply of RH, ASR expansion continues to increase

initially, and reaches a value of 0.05%. When a drying stage is applied to concrete after half the year, expansion doesn't go back to zero, rather it continues showing no visible increase in expansion. Finally, after 1 year expansion gets to a value of 0.055%. Case 9 represents a reverse phenomenon of case 8. Here, drying is done for the first half of the year and shows no significant ASR expansion throughout that period. Later, expansion increases significantly with an application of high RH and gets to a value of 0.1% after 1 year.

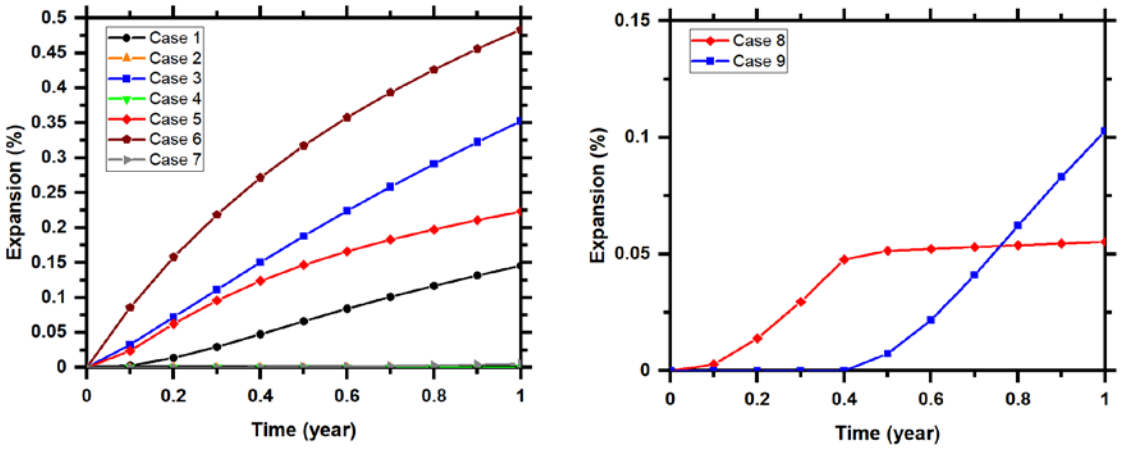

(a) (b)

Figure 4-16 Expansion of ASR gel in concrete for different cases: (a) case 1-7, (b) case 8-9

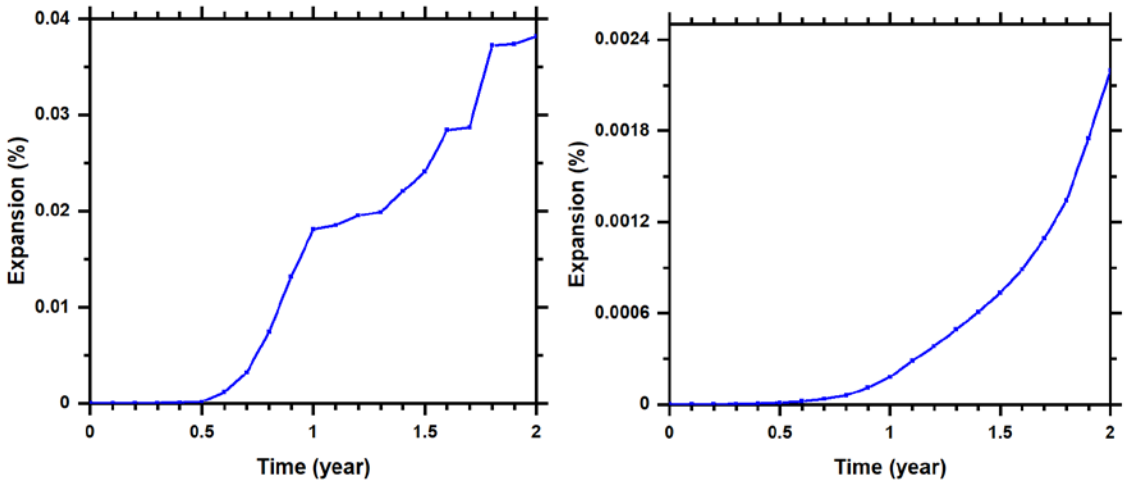

(a) (b)

Figure 4-17 2 years expansion of ASR gel in concrete: (a) case 10, (b) case 11

Moreover, Figure 4-17 portrays the effects of extreme weather events on ASR expansion. Case 10 shows sharp changes in the expansion due to the assumed piecewise function of the seasonal weather change. Expansion takes a while to show up initially due to the latency period needed for ASR gel to absorb available moisture from the surrounding, and then expand. However, as soon as there is expansion it comes up with visible fluctuations after 1 year due to the random change in weather parameters. Low temperature of winter stabilizes the ASR gel production to some extent, whereas, expansion is bumped up again with the available moisture from high humidity. Concentration of ASR gel as well as associated expansion jumps up at the beginning of spring, which further jumps up during the summer due to high temperature. On the other hand, case 11 shows the stochastic weather variations. The change in expansion is more or less flat because of the stochastic weather events which work on a periodic half-sinusoidal mean. However, expansion behavior follows the trend as that of case 10 due to the seasonal variations in temperature and humidity.

4.3. Long-term ASR Forecasts

An extended analysis was done for a 30 years period. Stochastic weather case 11 was considered in type C8 aggregate to represent the real-world scenario of an existing concrete structure.

Figure 4-18 visualizes how ASR evolves at different locations on the concrete prism. Expansion is maximum at a point located on the outer surface close to the reactive aggregate (1.57%). Expansions in the middle and on concrete face located away from the reactive aggregate are very slow and insignificant at the end of 30 years. That means,

locations in the close proximity of reactive aggregate are more likely to show ASR expansion and damage.

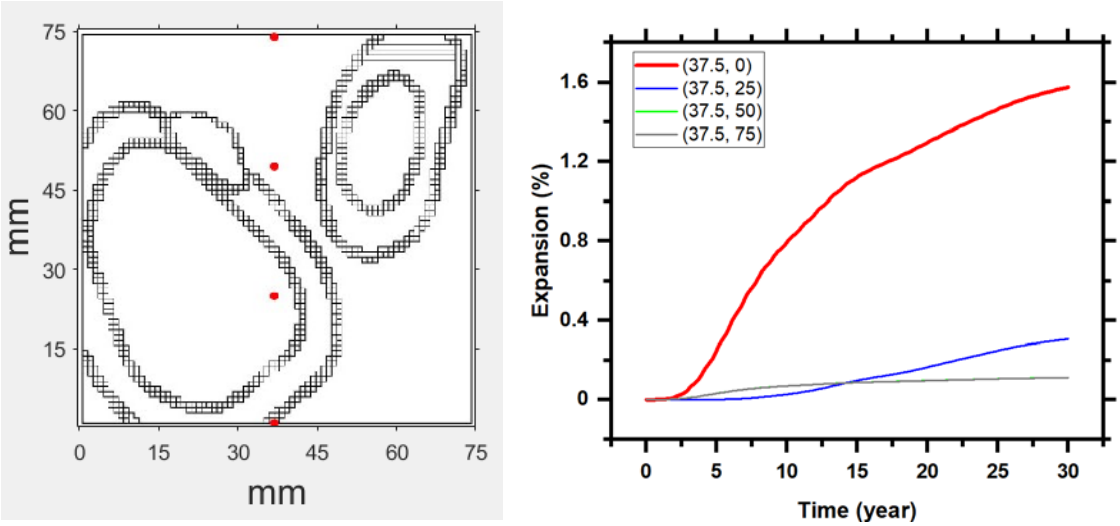

(a) (b)

Figure 4-18 Point graph for 1 year expansion: (a) cut plane 2d, (b) concentration of expanded gel

Figure 4-19 visualizes the contour plots for concentrations of ASR gel and expanded products. ASR gel is distributed on the aggregate surface. Concentration of expanded gel is flowing through the aggregate micro cracks and diffusing into the mortar phase.

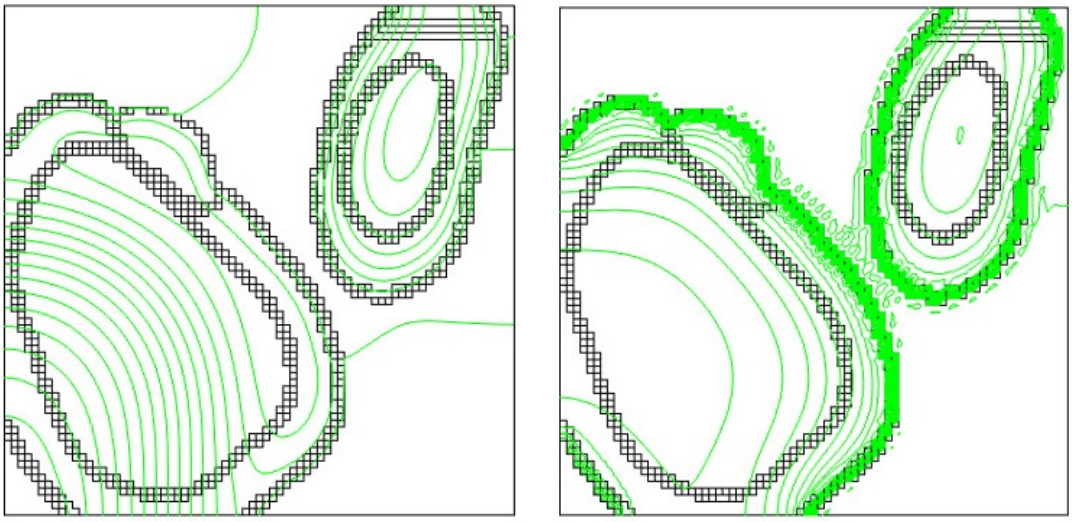

(a) (b)

Figure 4-19 Contour plot for 30 years concentration: (a) ASR gel, (b) expanded gel

Figure 4-20 shows that damage due to ASR expansion is maximum around smaller aggregate than the larger one. Hence, smaller reactive aggregates are more favorable to the ASR process. It also confirms that the damage is visible after 7.5 years and keeps worsening rapidly with the progression of time under the effects of stochastic weather events.

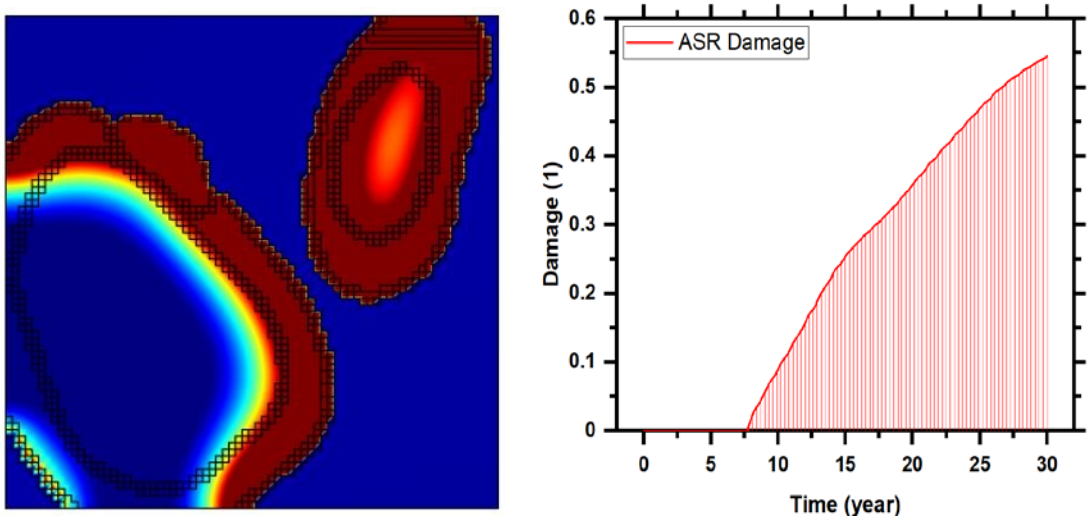

(a) (b)

Figure 4-20 30 years ASR damage in concrete due to stochastic weather condition: (a) 2D plot, (b) 1D plot

Other weather cases were considered further for 30 year simulation periods to compare the ASR expansion and damage propagation in concrete. Figure 4-21 depicts the expansion in concrete after 30 years. Maximum expansion is found for case 5 (0.52%). While 1 year expansion of case 7 is close to zero, it shows a significant expansion at the end of 30 years (0.36%). It is obvious from case 10 that, for each single year, ASR expansion increases significantly at the beginning due to high humidity in winter, which is bumped up further in summer due to high temperature. Case 11 presents randomness of the stochastic weather condition, and shows the sinusoidal rhythm in its changing pattern. This case also shows consistency with the case 10 after boosting the expansion at the end of each year due to high humidity. Moreover case 5 tends to stabilize within a 30 year simulation period, whereas other cases still show potential scope of further damage. Thus, considering constant weather parameters with conventional lab tests can lead to over or under-estimation of ASR expansion as well as associated damage.

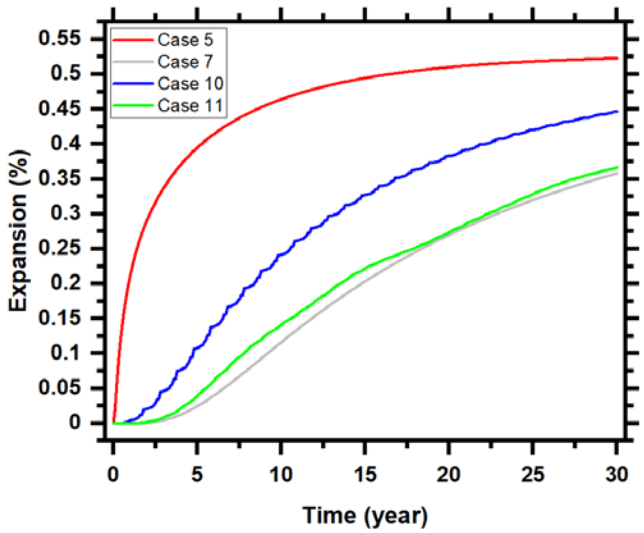

Figure 4-21 Effects of weather cases on 30 years ASR expansion

Figure 4-22 illustrates the 30 year evolution of ASR in concrete under the influence of critical times for different global warming scenarios. Global warming increases the ASR expansion gradually as time progresses. Stochasticity shows a major difference in influencing ASR gel production due to extreme weather events. Thus, under the real weather exposures inherent randomness of the extreme weather events affect the service life condition of concrete. It is obvious that after 30 years the reduction in service life is minimum (50.95%) for mean weather condition which further increased due to added global warming (52.1%), and stochastic weather events (54.5%).

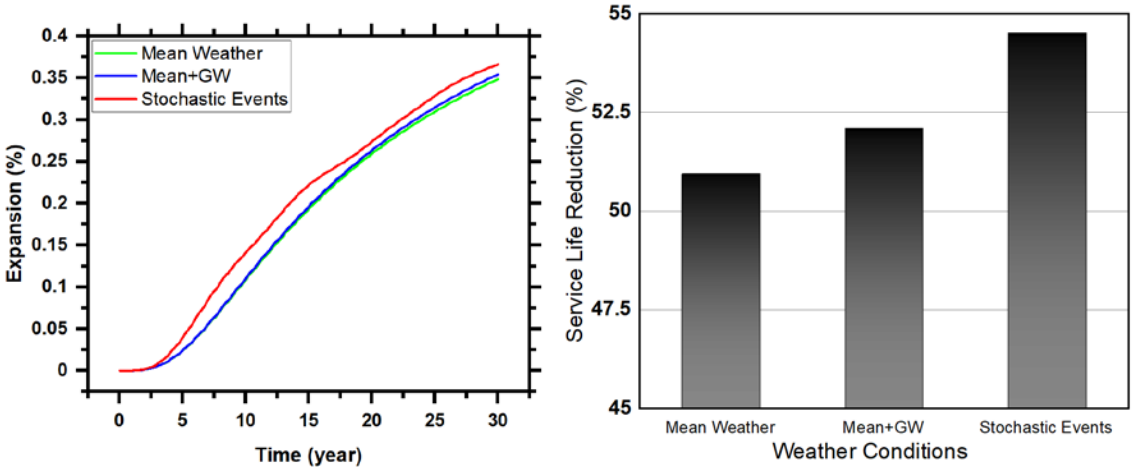

(a) (b)

Figure 4-22 Effects of extreme weathers on 30 years ASR evolution in concrete: (a) ASR Expansion, (b) Lifetime reduction

It is evident that surrounding weather conditions, especially, RH and temperature, greatly influence the ASR expansion, and thus, justify the consideration of extreme weather events in the ASR prediction model. As such, the developed model of this work can potentially predict the ASR damage, and service life of concrete under variable environmental conditions.

5 Conclusions

This work renders the concrete prism at the meso-scale from a two-dimensional perspective, and proposes a stochastic model to predict ASR damage. Stochastic realization adds the extreme values to the time-variant mean, which better represents the real-world values. Construction of the model includes numerical analysis of mortar-aggregate chemistry under the influence of extreme weather events. This is the first ever implementation in a model to link extreme weather events to the concrete service life assessment of ASR, to the best of the authors' knowledge. This is our critical innovation in the modeling phase which incorporates random behavior of the environmental parameters into the ASR model.

Concentration of ASR gel is maximum on the aggregate surface which diffuses back into the mortar as the time progresses, increases the overall concrete density, and subsequently develop cracking. Concrete which is submerged in water and completely uncoated under a high degree of saturation and temperature would lead to maximum damage to the structures. This case study can be best suited for a nuclear reactor which can come up with high expansion (0.48% at 1 year). A concrete dam submerged in water from the beginning and open to high saturation and moderate temperature can also lead to high amount of expansion (0.35% at 1 year). Any concrete superstructures which are not submerged in water but still under high degree of saturation and temperature will show significant amount of expansion (0.225% at 1 year). Concretes which are considered under room temperature will have a low expansion (0.0056% at 1 year), whereas for a fully coated or insulated structure expansion can be very insignificant (8.31×10^{-12} % at 1 year). However, most interesting phenomena happens when we supply late moisture or drying to

the structure under ASR expansion. When we apply drying under low humidity to a previously uncoated structure exposed to high moisture, it stops to produce any significant expansion further, and can potentially come to a complete stop after a certain period. Unlike this, when we supply more moisture to a relatively low ASR structure, the expansion gets boosted significantly and so the damage.

Seasonal change and stochastic weather conditions confirm how non-linearly ASR expansion and damage can propagate under a real-world scenario. A mean weather condition can lead to a low expansion (0.348% at 30 years). However, stochastic weather events under global warming can produce further expansion (0.366% at 30 years), which increases the expansion content by 5.2%. Even though the expansion under relevant stochasticity looks less severe compared to the extreme constant weather cases, the associated uncertainty can potentially bring more damage to the structure due the consecutive contraction and expansion in the cement-mortar matrix.

The major findings from this work is to evaluate how ASR expansion and associated damage propagate in partially/variably saturated porous media under the impact of climate change and extreme weather events. Potential exposure to extreme weather events can greatly influence the service life of concrete and infrastructure network. Location and service condition of the existing structures can be the driving factors in defining their ASR damage. These justify the importance to anticipate the adverse impacts of climate change on ASR prone structures. This developed model can be very crucial for other concrete structures in predicting the evolution of ASR expansion as well as service life under the real world environmental conditions. Thus, this work will advance in the

field of resilience and sustainable infrastructure development by supporting on-time prediction and adaptive management to account for the weather uncertainty.

Author Contribution Statement

The authors confirm contribution to the paper as follows: study conception and design: Md. Asif Rahman, Yang Lu; model development: Md Asif Rahman; analysis and data collection: Md Asif Rahman; draft manuscript preparation: Md. Asif Rahman; approval of the final version of manuscript: Yang Lu.

Acknowledgements

Declarations of interest

None.

Funding

This research did not receive any specific grant from funding agencies in the public, commercial, or not-for-profit sectors.

References

[1]. Poole, A.B. Proceedings of the Third International Symposium on the Effect of Alkalis on the Properties of Concrete. Cement and Concrete Association, Wexham Springs, Slough, UK, 1976.

[2] Hobbs, D. W. Alkali-silica reaction in concrete. Thomas Telford, London, 1988

[3] Poole, A.B. Introduction to alkali-aggregate reaction in concrete. The Alkali Silica Reaction in Concrete. Swamy R.N. (Ed.), Van Nostrand Reinhold, New York, 1992

[4]. Diamond, S. Alkali Silica Reactions – Some Paradoxes. Cement and Concrete Composites, 1997. 19: 391-401.

[5]. Kim, T., J. Olek. Influence of Alkali Silica Reaction on the Chemistry of Pore Solutions in Mortars With and Without Lithium Ions. Brittle Matrix Composites, 2012. 10: 11-20.

[6]. Poyet, S., A. Sellier, B. Capra, G. Thèvenin-Foray, J. M. Torrenti, H. Tournier-Cognon, and E. Bourdarot. Influence of Water on Alkali-Silica Reaction: Experimental Study and Numerical Simulations. Journal of Materials in Civil Engineering, 2006. 18: 588-596.

[7]. Leger, P., P. Cote, and R. Tinawi. Finite Element Analysis of Concrete Swelling Due to Alkali-Aggregate Reactions in Dams. Computers & Structures, 1996. 60: 601-611.

[8]. Christidis, N., P. A. Stott, and S. J. Brown, 2011: The role of human activity in the recent warming of extremely warm daytime temperatures. Journal of Climate, 24, 1922-1930, doi:10.1175/2011JCLI4150.1.

[9]. Duffy, P. B., and C. Tebaldi, 2012: Increasing prevalence of extreme summer temperatures in the U.S. Climatic Change, 111, 487-495, doi:10.1007/s10584-012-0396-6.

[10]. Noah S. Diffenbaugh. Verification of extreme event attribution: Using out-of-sample observations to assess changes in probabilities of unprecedented events. Science Advances 18 Mar 2020:Vol. 6, no. 12, eaay2368. DOI: 10.1126/sciadv.aay2368.

[11]. NOAA (National Oceanic and Atmospheric Administration). 2016. National Centers for Environmental Information. Accessed February 2016. www.ncei.noaa.gov.

[12]. Dai, A., 2006: Recent climatology, variability, and trends in global surface humidity. Journal of Climate, 19, 3589-3606, doi:10.1175/JCLI3816.1.

[13]. Willett, K. M., P. D. Jones, N. P. Gillett, and P. W. Thorne, 2008: Recent changes in surface humidity: Development of the HadCRUH dataset. Journal of Climate, 21, 5364-5383, doi:10.1175/2008JCLI2274.1.

[14]. Vose, R. S. et al., 2013: Monitoring and understanding changes in extremes: Extratropical storms, winds, and waves. Bulletin of the American Meteorological Society, in press, doi:10.1175/BAMS-D-12-00162.1.

[15]. Wang, X. L., Y. Feng, G. P. Compo, V. R. Swail, F. W. Zwiers, R. J. Allan, and P. D. Sardeshmukh, 2012: Trends and low frequency variability of extra-tropical cyclone activity in the ensemble of twentieth century reanalysis. Climate Dynamics, 40, 2775-2800, doi:10.1007/s00382-012-1450-9.

[16]. Wang, X. L., V. R. Swail, and F. W. Zwiers, 2006: Climatology and changes of extratropical cyclone activity: Comparison of ERA-40 with NCEP-NCAR reanalysis for 1958-2001. Journal of Climate, 19, 3145-3166, doi:10.1175/JCLI3781.1.

[17]. Touma, W. E., D. F. Fowler, and R. L. Carrasquillo. Alkali-Silica Reaction in Portland Cement Concrete: Testing Methods and Mitigation Alternatives. Research Report ICAR 301-1F. International Center for Aggregates Research (ICAR), The University of Texas at Austin, 2001.

[18]. Bentz, D. & Garboczi, E.J. & Quenard, Daniel. (1999). Modelling drying shrinkage in reconstructed porous materials: Application to porous Vycor glass. Modelling and Simulation in Materials Science and Engineering. 6. 211. 10.1088/0965-0393/6/3/002.

[19]. Grimal, Etienne & Sellier, Alain & Le Pape, Yann & Bourdarot, Eric. (2008). Creep, shrinkage, and anisotropic damage in alkali-aggregate reaction swelling Mechanism-Part I: A constitutive model. ACI MATERIALS JOURNAL. 105. 227-235.

[20]. IvanVlahinić, Hamlin M.Jennings, Jeffrey J.Thomas. A constitutive model for drying of a partially saturated porous material. Mechanics of Materials, Volume 41, Issue 3, March 2009, Pages 319-328.

[21]. Ulm, F.J., O. Coussy, L. Kefei, and C. Larive. Thermo-Chemo-Mechanics of ASR Expansion in Concrete Structures. Journal of Engineering Mechanics, 2000. 126: 233-242.

[22]. Hobbs, D. W. The Alkali-Silica Reaction - A Model for Predicting Expansion in Mortar. Magazine of Concrete Research, 1981. 33 (117): 208 - 220.

[23]. Steffens, A., and Z. P. Bazant. Mathematical Model for Kinetics of Alkali-Silica Reaction in Concrete. Cement and Concrete Research, 2000. 30: 419-428.

[24]. Bournazel, J. P., and B. Capra. Modeling of Induced Mechanical Effects of Alkali-Aggregate Reactions. Cement and Concrete Research, 1998. 28: 251-260.

[25]. Saouma, V. E., R.A. Martin, M. A. Hariri-Ardebili, and T. Katayama. A Mathematical Model for the Kinetics of the Alkali–Silica Chemical Reaction. Cement and Concrete Research, 2015. 68:184-195.

[26]. Balbo, F. A. N., G. A. Pianezzer, L. M. Gramani, E. Kaviski, and M. R. Teixeira. An Application to the Diffusion Equation in a Model for the Damage in Concrete Due to Alkali-Silica Reaction. Applied Mathematical Sciences, 2015. 9: 4135-4147.

[27]. ASTM C1293. Standard Test Method for Concrete Aggregates by Determination of Length Change of Concrete Due to Alkali-Silica Reaction. American Society for Testing and Materials (ASTM) International.

[28]. Ichikawa, T., and M. Miura. Modified Model of Alkali-Silica Reaction. Cement and Concrete Research, 2007. 37: 1291-1297.

[29]. Rahman, Md. Asif, Yang Lu. A Time-Dependent Chemo-Mechanical Analysis of Alkali-Silica Reaction for the Disparate Geometry of Concrete Meso-Structure. Journal of Construction and Building Materials, 2019. Volume 211, 847-857.

[30]. Md. Asif Rahman, Y. Lu, A meso-scale multiphysics model for predicting concrete pavement performance subject to ASR degradation, TRB Annual Meeting Paper (2019). 19–03839R1.

[31]. Hiroaki Takiya, Naoko Watanabe, Tamotsu Kozaki & Seichi Sato (2015) Effects of water-to-cement ratio and temperature on diffusion of water in hardened cement pastes, Journal of Nuclear Science and Technology, 52:5, 728-738, DOI: 10.1080/00223131.2014.979902

[32]. Richardson, L.F. Weather prediction by numerical process. University Press, Cambridge, 1922. P: 262.

[33]. Richards, L.A. Capillary conduction of liquids through porous medium. Physics, 1931. 1:318–333.

[34]. J. Bear, Dynamics of Fluids in Porous Media, Elsevier Scientific Publishing, 1972.

[35]. J. Bear, Hydraulics of Groundwater, McGraw-Hill, 1979.

[36]. M.Th. van Genuchten. A Closed-form Equation for Predicting the Hydraulic Conductivity of Unsaturated Soils. Soil Sci. Soc. Am. J., 1980. 44:892-898.

[37]. Sébastien Schneider, Dirk Mallants, Diederik Jacques. Determining hydraulic properties of concrete and mortar by inverse modelling. Materials Research Society, 2012. Vol. 1475

[38]. L. Ruiz et al. Experimental Determination of Hydrodynamic Properties of Weathered Granite. Soil Science Society of America, 2012.

[39]. Thomas, M. D. A., B. Fournier, and K. J. Folliard. Alkali-Aggregate Reactivity (AAR) Facts Book. Publication FHWA-HIF-13-019. FHWA, U.S. Department of Transportation, 2013

[40]. Andrew Park et al. Can Boreal and Temperate Forest Management be Adapted to the Uncertainties of 21st Century Climate Change? Critical Reviews in Plant Sciences, June 2014. 33:4, 251-285.

[41]. Pedneault, A. Development of testing and analytical procedures for the evaluation of the residual potential of reaction, expansion, and deterioration of concrete affected by ASR. M.Sc. Memoir, Laval University, Québec City, Canada, 1996. P: 133.

[42]. M. Ben Haha, Mechanical Effects of Alkali Silica Reaction in Concrete Studied by SEM-Image Analysis Doctoral dissertation, École Polytechnique Fédérale de Lausanne. À La Faculté Sciences Et Techniques De L'ingénieur, France, 2006.

[43]. Pan, T., C. Chen, and Q. Yu. Three-Dimensional Micromechanical Modeling of Concrete Degradation under Multiphysics Fields. Composite Structures, 2017. 175: 7-18.

[44]. Vissarion Papadopoulos, Dimitris G. Giovanis. Stochastic Finite Element Methods: An Introduction. Springer International Publishing, 2018.

[45]. Mark G. Lawrence. The Relationship between Relative Humidity and the Dewpoint Temperature in Moist Air. American Meteorological Society, 2005. DOI: 10.1175/BAMS-86-2-225

[46]. Folliard , K. J., Ryan Barborak, Thano Drimalas, Dr. Lianxiang Du, Sabrina Garber, Jason Ideker, Tyler Ley, Stephanie Williams, Maria Juenger, Benoit Fournier, and M.D.A. Thomas. Preventing ASR/DEF in New Concrete: Final Report. Publication FHWA/TX-06/0-4085-5. FHWA, U.S. Department of Transportation, 2006.

[47]. Lu, Yang, Md. Aminul Islam, Stephen Thomas, Edward J.Garboczic. Three-dimensional mortar models using real-shaped sand particles and uniform thickness interfacial transition zones: Artifacts seen in 2D slices. Journal of Construction and Building Materials, 2020. Volume 236, 117590.

[48]. S. Thomas, Y. Lu, E. Garboczi, Improved model for three-dimensional virtual concrete: Anm model, J. Comput. Civ. Eng. 30 (2) (2016). 04015027-04015027.

[49]. Comparative Climatic Data for the United States through 2018, National Oceanic and Atmospheric Administration, US Department of Commerce.

CHAPTER 5: MITIGATION SCHEMES FOR THE ALKALI-SILICA REACTION (ASR)-INDUCED DAMAGE: A MINERALOGICAL STUDY ON CONCRETE[4]

Abstract

Alkali-silica reaction (ASR) is responsible for long-term degradation in concrete structure. In this work, a meso-scale mechanical model has been established to simulate the effects of alkali-silica reaction on the mechanical properties of concrete over time as well as the impacts of different mitigation approaches on affected concrete. The results from this study confirms that the ASR expansion significantly reduces the compressive strength, tensile strength, and modulus of elasticity of concrete. Fly ash as a supplementary material is the most effective one in minimizing ASR expansion and associated damage. A case study based on different mineral types provides with the petrographic comparison between reactive or non-reactive aggregates. Thus, this developed model can accelerate the precise prediction and optimize mitigation scheme management of ASR induced damage, as well as can be used as an alternative scope to the costly laboratory tests methods. This can potentially influence the research on cement-concrete materials for long-term damage forecasts and lead to a conclusive solution for ASR damage of concrete infrastructure.

Keywords: ASR model, 3D Anm model, Concrete damage model, ASR mitigation

[4] This chapter includes results which are under preparation for the submission to the Journal of Cement and Concrete Research titled “Mitigation Schemes for The Alkali-Silica Reaction (ASR)-induced Damage: A Mineralogical Study on Concrete”. Contribution of the coauthor is sincerely acknowledged: Rahman, M. A., and Lu, Y.

1. Introduction

Concrete infrastructure damage is more frequent nowadays. Aging and detrimental chemical reaction of concrete structure are the major sources of deterioration in the recent years, causing billions of dollars in damages every year in the United States. Alkali-silica reaction (ASR) is a significant undesirable phenomena for concrete infrastructure damage worldwide.

The concrete ASR problem is influenced by many factors: aggregate/mineral types, alkali content, surrounding environment, mechanical loadings, use of supplementary materials etc. The alkali-silica reaction takes place between silica and hydroxides. Reactive silica presents in aggregate tends to breakdown due to the high alkalinity of pore solution in concrete and subsequently react with alkali-hydroxides to form ASR gel [1-3]. This diffusion of ASR gel induces internal pressure in the cementitious matrix [4], which eventually cracks the concrete surface. The swelling behavior of ASR gel determines the extent of damage to concrete structures, and the mitigation of this damage depends solely on the preventive measures to gel formation as well as its corresponding swelling [5].

Strength is the most important property and defines the load carrying capacity of concrete. It mostly depends on the interaction between mortar and aggregate phases. Alkali-silica reaction develops micro crack in the concrete domain and weakens this interaction which can lead to the significant reduction in load carrying capacity. Several investigations have been conducted to determine the effects of ASR damage on mechanical properties of concrete. With the progression of ASR damage compressive strength of concrete gets reduced [6]. Alkali-aggregate reaction can significantly reduce the flexural capacity of concrete due to the ongoing expansion over time [7-9]. Tensile strength of

concrete is more likely to be affected by the ASR phenomena [10, 11]. ASR expansion also reduces the dynamic modulus of elasticity [9] and Young's modulus [12] of concrete. Study [13] performed a details lab tests on ASR affected concrete prism to record the mechanical damage with time. According to this study, there is a strength gaining period after which compressive strength tends to decrease with the progress of time. There is noticeable reduction in the tensile capacity of concrete which is the most under high temperature and alkali content. Young's modulus is also significantly reduced with the increase in temperature and alkali content.

The use of certain aggregates can lead to the undesirable chemical reactions. Reactivity of an aggregate is greatly influenced by its irregular crystallinity as well as the amount of energy stored in the crystal structure [14]. Aggregates containing amorphous silica are more porous, provide a large surface area, and thus, more susceptible to deleterious alkali-silica reactions [14]. It is also very difficult to incorporate the effects of ASR in the model due to the random mineral sites from where aggregates are being collected.

Mitigation of alkali silica reaction and its induced damage is also a challenging job. Many experimental research efforts have been conducted to explore the mitigation measures and their consequences [15-17]. Though these experimental studies were supported by significant findings, they are limited by testing setups, cost, and time to predict ASR-induced damage under service conditions. Given the empirical nature of available findings, a robust numerical model is highly desirable to provide a modeling-guided solution with sound theoretical basis. The researchers have been working hard to quantify chemo-mechanical damage induced by the alkali silica reaction [18-21]. However,

no existing model is available to assess the effectiveness of various mitigation measures. Because of the complexity lying in the chemo-physio-mechanical behavior of ASR, we need further development in the field of modeling framework to assess and mitigate ASR related problems.

In this work, concrete mechanical properties were linked to the ASR kinetics on the basis of a modified strength model as a function of concrete density. To visualize the mechanical deterioration in concrete under ASR expansion its compressive and tensile capacity as well as Young's modulus were analyzed on a case by case basis. A 3D Anm model of meso-structure was generated as a representative concrete prism to match with size, properties, and environmental parameters as stated in ASTM C1293 standard [22]. Finite element analysis (FEA) was done to solve partial differential equation (PDE) based governing equation sets. Material properties of 17 different coarse aggregates as presented in Table 5-1 were incorporated in the model for petrographic comparisons [23]. A mitigation scheme was implemented to evaluate the efficiency of different supplementary cementitious materials (SCMs), i.e. fly ash, slag and silica fumes, in reducing ASR expansion. ASR induced damage was combined with concrete aging to identify change in mechanical properties of damaged concrete. Finally, a density-based damage model was proposed to predict service life of concrete structure. A damage rating factor (DRF) was assigned to each aggregate type based on their ASR damage after one year. Note that the DRF was defined in this paper as a tool to evaluate the extent of ASR damage.

Table 5-1 Coarse aggregates

Aggregate ID	**Mineral Type**	**Aggregate Source**
C1	Chert and quartzite	Eagle Lake, TX
C2	Tan dolomite carbonate	Eagle Pass, TX
C3	Limestone	Elgin, OK
C4	Limestone	Helotes, TX
C5	Mixed quartz/chert	Ashtown, AR
C6	Limestone	San Antonio, TX
C7	Limestone	Ontario, CA
C8	**Mixed mineralogy gravel**	**Ontario, CA**
C9	Chert with quartz and limestone	Victoria, TX
C10	Rhyolitic volcanic rocks with quartz and granite	Albuquerque, NM
C11	Mixtures of granodiorite and metadacite	North East, MD
C12	Quartzite	Dell Rapids, SD
C13	Quartzite	New Ulm, MN
C14	Granite and Quartzite Gravel	Cheyenne, WY
C15	Ryholite/Mixed Quartz	Rockville, VA
C16	Granitic gneiss, metarhyolite	North Garden, VA
C17	Greywacke	Moscow, PA

It's a new modeling approach to track the mechanical damage in concrete with the progress of alkali-silica reaction and to offer a mitigation module based on the requirements. Table 5-2 lists the abbreviations used in this work, to improve the readability.

Table 5-2 Summary of abbreviations

Abbreviations	**Anatomy/Terms**
ASR	Alkali-silica reaction
DRF	Damage rating factor
SCMs	supplementary cementing materials
CSH	calcium silicate gel
ROH	alkali hydroxyl
CH	calcium hydroxide
FA	Fly ash
SL	slag
SF	silica fume
ITZ	interfacial transition zone
FEM	Finite element modeling
PDE	Partial differential equation

2. Model Development

2.1. Chemical Kinetics

The chemical process starts with the dissolution of silicates into the alkaline pore solution. Hydroxyl ions in the pore solution of concrete reacts with siloxane components of reactive aggregates to produce ASR gel. ASR gel further absorbs water and swells to produce expansive ASR gel. However, when calcium presents in the cement paste, it reacts with the ASR gel, and produces non expansive calcium silicate gel (CSH). In this case, abundant calcium ions (Ca^{2+}) replace the alkalis (K^+ or Na^+) from alkali-silica gel according to Eq. (1) [24]. Moreover, pozzolanic reaction, which is essentially a reaction between lime and pozzolanic materials (siliceous or aluminous), occurs in concrete over time. This is a long-term reaction which may take from months to years to manifest. In this case, excess calcium ions (Ca^{2+}) (coming from the mitigation materials, i.e. fly ash) react with the hydroxyl ions (OH^-) and silica (SiO_2) available in the concrete mix, and produce hydrated CSH gels according to Eqs. (2-3) [25]. This is the dominant hydration product with higher density and strength which was considered in this work to predict the mitigation scheme of alkali-silica reaction. Subsequently, reaction with aluminous pozzolanic materials was kept out of the consideration to minimize the complexity of the problem. The calcium silicate bond (C–S–H) forms by these ionic exchanges, is very strong by nature, and thus, it limits the ASR production.

$$\underbrace{\equiv Si\text{-}O^- + (H_2O)_n + R^+}_{\text{Expanded ASR gel}} + \underbrace{\tfrac{1}{2}Ca^{2+}}_{\text{Calcium Ions}} \rightarrow \underbrace{\equiv Si - O^- + \tfrac{1}{2}Ca + (H_2O)_n}_{\text{C-S-H gel}} + \underbrace{R^+}_{\text{Excluded Alkali}} \quad (1)$$

$$\underbrace{Ca^{2+}}_{\text{Calcium Ions}} \quad \underbrace{OH^-}_{\text{Hydroxyl Ions}} \rightarrow \underbrace{Ca(OH)_2}_{\text{Calcium Hydroxide}} \quad (2)$$

$$\underbrace{Ca(OH)_2}_{\text{Calcium Hydroxide}} + \underbrace{\equiv Si\text{-}O^-}_{\text{Silicate Ions}} \rightarrow \underbrace{\equiv Si\text{-}O^- + Ca + (H_2O)_n}_{\text{C-S-H gel}} \quad (3)$$

where R^+ denotes an alkali ion. K^+ or Na^+ can be used interchangeably.

CSH gel production in Eq. (1) would run for the whole 30 years. CH productions in Eq. (2) tends to stabilize within one year of chemical reaction [26]. It was assumed that the breaking of CH bond and CSH gel production in Eq. (3) also might get stabilized within one year as Eq. (2). Thus, if we denote the three stages of chemical reaction [27] as k_1, k_2, and k_3, the rate constants related to Eqs. (1-3) can be defined as k_4=k_1, k_5=30k_1, and k_6=30k_1, respectively.

The rate of change of concentration for the species involved in the ASR gel production are presented in study [27]. The rate of change of concentration for additional species involved in the CSH gel production can be expressed as Eq. set (4).

$$\frac{d[CSHgel]}{dt} = k_4[Expanded\ ASG][Ca] + k_6[Calcium\ Hydroxide][Siloxane]$$

$$\frac{d[Calcium\ Hydroxide]}{dt} = k_5[Ca][ROH] - k_6[Calcium\ Hydroxide][Siloxane] \quad (4)$$

where *[CSH gel]*, *[Expanded ASR gel]*, *[Ca]*, *[Calcium Hydroxide]*, *[Siloxane]*, and *[OH]* represent concentration of each species, respectively.

This is an extension to author's recent work [28] where Eqs. (1-4) have been added to the existing chemical equation sets to simulate the mitigation measures. Equations defining rate constants can be found in study [28]. In this work, we predict the alkali-silica gel production or its mitigation by accurately simulating the changing concentration of each species involved in the mechanism. PDEs were developed to formulate the governing equation sets representing chemical kinetics involved in the ASR gel and CSH gel.

There are six chemical species involved in ASR gel production [28] and three additional species involved in the CSH gel production as discussed above. Thus, for this work scope we needed nine coupled governing equations to replicate complete chemical kinetics of the alkali-silica gel production and mitigation scheme. This was done based on the principles of mass balance and momentum balance in the variably saturated porous media [28].

The values of diffusion coefficients are presented in Table 5-3. The 3D concrete prism was considered with a cement content of 420 (kg/m^3) and an alkali content of 1.25% Na_2O_{eq} to replicate ASTM C 1293 concrete prism test [29]. Initial ROH and CaO concentrations for mitigation materials were found in study [17]. A corresponding initial hydroxyl ion/Ca ion concentration as shown in Table 5-4, was calculated for each of the species, from the relationship between ROH concentration and % equivalent Alkali [30].

Initial concentration of siloxane for type C8 aggregate was considered based on the parameter estimation of study [28]. Initial concentration of siloxane for other aggregate samples can be calculated by the following equation.

$$\text{Siloxane}_i = \text{Siloxane}_{C8} \times \text{Factor}_{type} \qquad (5)$$

where, Siloxane_i is the initial concentration of siloxane (mole/m^3), Siloxane_{C8} is the initial siloxane concentration for type C8 aggregate, and Factor_{type} is a multiplication factor for different aggregate types. A simulated list of initial siloxane concentration and this type factor are presented in Table 5-8 for different aggregate samples.

Table 5-3 Diffusion coefficient of chemical species

	Mortar	**Aggregate**	**Source**
Diffusion Coefficient of ASR gel (m^2/s)	1×10^{-10}	1×10^{-12}	[31]
Diffusion Coefficient of ROH (m^2/s)	7×10^{-12}	4×10^{-14}	[28]
Diffusion Coefficient of H_2O (m^2/s)	5×10^{-10}	0	[32]
Diffusion Coefficient of CaO (m^2/s)	2.17×10^{-15}	0	Calibrated

Table 5-4 Initial concentrations of chemical species

	Value	**Source**
Initial concentration of ROH for cement, ROH_C (mole/m^3)	875	[29]
Initial concentration of ROH for FA, ROH_{FA} (mole/m^3)	1260	[23]
Initial concentration of ROH for SL, ROH_{SL} (mole/m^3)	406	
Initial concentration of ROH for SF, ROH_{SF} (mole/m^3)	530	
Initial concentration of CaO for FA, CaO_{FA} (mole/m^3)	784	
Initial Concentration of siloxane for C8 aggregate (mole/m^3)	710	[28]

2.2. Mitigation Model

In this work, application of SCMs was incorporated in the model, as an effort to evaluate their efficiency in mitigating ASR expansion and corresponding damage. A certain proportion of Fly Ash, Slag, and/or Silica Fume was used in the Mitigation Model to predict and mitigate ASR-induced damage virtually. Initial concentration of alkali hydroxyl (ROH) and CaO are greatly influenced by the application of either one or all of these materials, along with the basic Portland cement. An equation was proposed as Eq. (6) to calculate the combined ROH concentration, based on the proportion and initial ROH concentration of each of the supplementary materials.

$$ROH_{com} = \frac{P_C}{100} ROH_C + \frac{P_{FA}}{100} ROH_{FA} + \frac{P_{SL}}{100} ROH_{SL} + \frac{P_{SF}}{100} ROH_{SF} \quad (6)$$

where ROH_{com} is the combined initial concentration of ROH for Portland cement and other supplementary cementing materials. ROH_C, ROH_{FA}, ROH_{SL}, and ROH_{SF} are the initial concentration of ROH for cement, fly ash, slag, and silica fume, respectively. P_C, P_{FA}, P_{SL}, and P_{SF} are the percentage of cement, fly ash, slag, and silica fume, respectively in the total cementitious materials.

To calculate initial concentration of Calcium, Eq. (7) was proposed based on the proportion of fly ash available in the mix.

$$Ca_{com} = \frac{P_{FA}}{100} CaO_{FA} \quad (7)$$

where Ca_{com} is the combined initial concentration of Calcium, and CaO_{FA} is the initial concentration of CaO generating from the available FA in the mix. It is noteworthy, FA supplies high CaO content which can potentially reduce ASR expansion.

Initial concentration of ROH and CaO for these supplementary materials are shown in Table 5-4. Case studies on these mitigation materials' proportion are presented in Table 5-5.

With the application of these supplementary cementing materials, concrete's strength and aging behavior are also changed to some extent. To address these effects in the Mitigation Model, a strength factor was proposed through the following equations. These factors were formulated as an empirical function from the relationship between 28 days relative strength and materials proportion, presented in study [33].

$$f_{FA} = (-0.0113*P_{FA}^2 - 0.371*P_{FA} + 101.12)/100 \quad (8)$$

$$f_{SL} = (-0.0005*P_{SL}^3 + 0.0194*P_{SL}^2 + 1.0293*P_{SL} + 100.85)/100 \quad (9)$$

$$f_{SF} = (-0.1136*P_{SF}^2 + 3.9058*P_{SF} + 99.87)/100 \quad (10)$$

where f_{FA}, f_{SL}, and f_{SF} are the factors to the 28 days compressive strength of concrete under the application of FA, SL, and SF, respectively.

Figure 5-1 re-plots the % relative strength with different proportion of supplementary materials. These curves are derived based on the relationship between concrete strength and proportion of each supplementary material. The % relative strength for FA was directly found, and the % relative strength for SL and SF were calculated from the strength data [33].

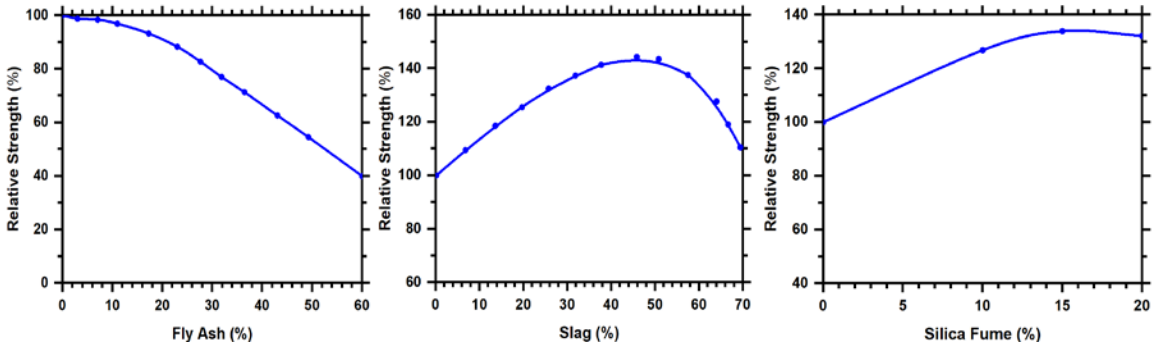

(a) (b) (c)

Figure 5-1 Influence of the proportion of supplementary materials (by mass) on strength of hardened cement paste [33]: (a) FA. (b) SL, and (c) SF

2.3. Mechanical Model

Concrete is designed to supply adequate compressive strength and durability against the sustained loads throughout its life span. Strength depicts the overall quality of concrete and an important factor in structural design. Density is also a function of compressive strength and behaves proportionally with it. An increased compressive strength ensures a denser concrete block, and, vice versa. These properties are also changing with time. The randomness depends on the concrete aging, duration of curing, mix design, porosity, compaction, material compositions etc. Concrete maturity also significantly affects the strength of concrete. Strength gain is proportional to the age of

concrete. The mechanical properties of concrete mostly depend on the density or strength and define concrete's resistance to potential damage. Thus, combined effects of mechanical properties and intensity of damage develop a complex mechanics in concrete structure. It is necessary to introduce these mechanics in ASR damaged concrete. Thus, this ASR model was analyzed under cement-concrete hydration and aging, and ambient weather conditions.

Strength Model

For concrete, the traditional practice is to consider 28-day strength as a measure to the strength of concrete. It was further factored as Eq. (11) considering the effects of mitigation materials.

$$f_{c28} = f_c' * f_{Res} \qquad (11)$$

where f_{c28} is the factored 28 days compressive strength, f_c' is 28 days compressive strength, and f_{Res} is a resultant factor of all mitigation materials. Resultant factor f_{Res} was further formulated as Eq. (12).

$$f_{Res} = f_{FA} * f_{SL} * f_{SF} \qquad (12)$$

Definition of the terms f_{FA}, f_{SL}, f_{SF} can be found in the previous section.

Density of concrete after 28 days was represented as a function of compressive strength as Eq. (13), through an empirical relation according to study [34].

$$\rho_{c28} = 8.602 * \frac{f_{c28}}{10^6} + 2110 \qquad (13)$$

where ρ_{c28} is 28 days concrete density (kg/m^3). Factored compressive strength, f_{c28} must be expressed in Pa.

Young's modulus can be calculated from Eq. (14) [35].

$$E_c = 0.043 * {\rho_{c28}}^{1.5} \sqrt{f_{c28}} \qquad (14)$$

where E_c stands for Young's modulus in concrete (Pa). Young's modulus of concrete reaches 86% of its final value after 28 days and becomes maximum after 90 days [36]. Within this context, Eqs. (11-14) were solved to determine compressive strength, density and Young's modulus of concrete after 28 and 90 days. We assumed 28 days compressive strength as 34 MPa, and thus, 28 days Young's modulus and density were calculated as 29.52 MPa and 2402 kg/m^3, respectively. Maximum Young's modulus after 90 days was determined as 34.5 MPa, and thus, maximum compressive strength and density after 90 days were calculated as 43.5 MPa and 2475.5 kg/m^3, respectively.

This work incorporated changing compressive strength and density in the model. Based on the values of 28 days and 90 days compressive strength, a piecewise function as Eq. (15) was developed to account for the dynamic compressive strength of concrete.

$$f_c = 0.00347 * (t - 28) * \left(\frac{f_{c28}}{0.86}\right) + f_{c28} \qquad (15) \qquad 0 \leq t \leq 90$$

where f_c denotes final compressive strength (Pa) and t is time (days). Figure 5-2 shows the plot of this piecewise function. Value remains constant after 90 days.

Concrete density was generated from the compressive strength as Eq. (16).

$$\rho_c = 10 * \left(\frac{f_c}{10^6}\right) + 2000 \qquad (16)$$

where ρ_c denotes final density of concrete (kg/m^3).

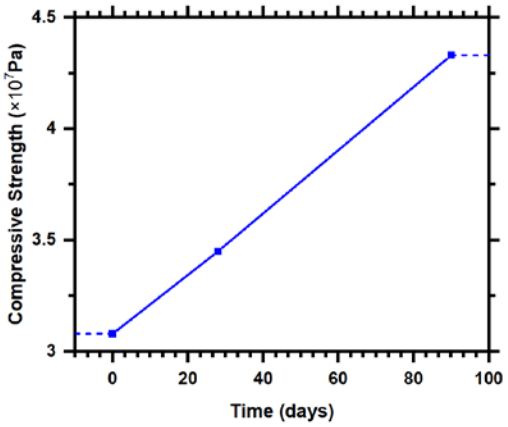

Figure 5-2: Compressive strength with time.

Damage Model

Volume change due to ASR was calculated through Eq. (17) according to study [27].

$$\varepsilon_{gel} = \frac{\rho_{gel}}{\rho_{gel}+\rho_c} \qquad (17)$$

where ε_{gel} is the volumetric strain developed from ASR expansion, ρ_{gel} and ρ_c are the mass density of alkali silica gel and concrete, respectively. The value of ρ_c can be estimated from Eq. (16). ρ_{gel} has been defined in study [27].

ASR damage can be calculated from Eq. (18) with a threshold value of 0.1% [31]

$$D_{gel} = 2.021 \times \varepsilon_{gel} - 0.195; \qquad \varepsilon_{gel} > 0.1\% \qquad (18)$$

where D_{gel} represents the ASR-damaged concrete.

Damage rating factor (DRF) was assigned to the aggregates, based on this damage model. DRF is the maximum damage at the end of the simulation period. Concrete DRF can range from 0 to 1, where 0 means no damaged state and 1 means completely damaged state.

ASR-induced damage changes the mechanical properties of concrete. This work developed a relation between ASR damage and concrete compressive strength as Eq. (19), to quantify damage in the compressive strength.

$$D_{f_c} = f_c - f_c \times D_{gel} \quad (19)$$

where D_{f_c} defines damaged portion of the compressive strength of concrete.

Damage in tensile strength of concrete was calculated from Eq. (20) as following.

$$D_{f_t} = 0.35 * \sqrt{D_{f_c}} \quad (20)$$

where D_{f_t} defines damaged portion of the tensile strength of concrete.

Damaged Young's modulus of concrete can be estimated from Eq. (14), after replacing 28 days compressive strength, f_{c28} by damaged compressive strength of concrete, D_{f_c}.

3. Numerical Modeling

In this work, a 3D meso-scale concrete prism was developed in the virtual cement-concrete testing lab based on the Anm geometric model [37]. Each sides of the prism were considered as 75mm in length following the ASTM C 1293 concrete prism test [29]. The Anm composite structure with irregular aggregate morphology were captured from real size particles using a spherical harmonic expansion method as shown in Figure 5-3(a). A details algorithm can be found in study [37-38]. A uniform-thickness shell as interfacial transition zone (ITZ) region around the aggregate particle defines the transition area of alkali silica gel. This model works based on two major phases of concrete, mortar and aggregates. Material properties such as Young's Modulus, Poisson's Ratio, and Density for mortar and aggregate domain can be found in study [27].

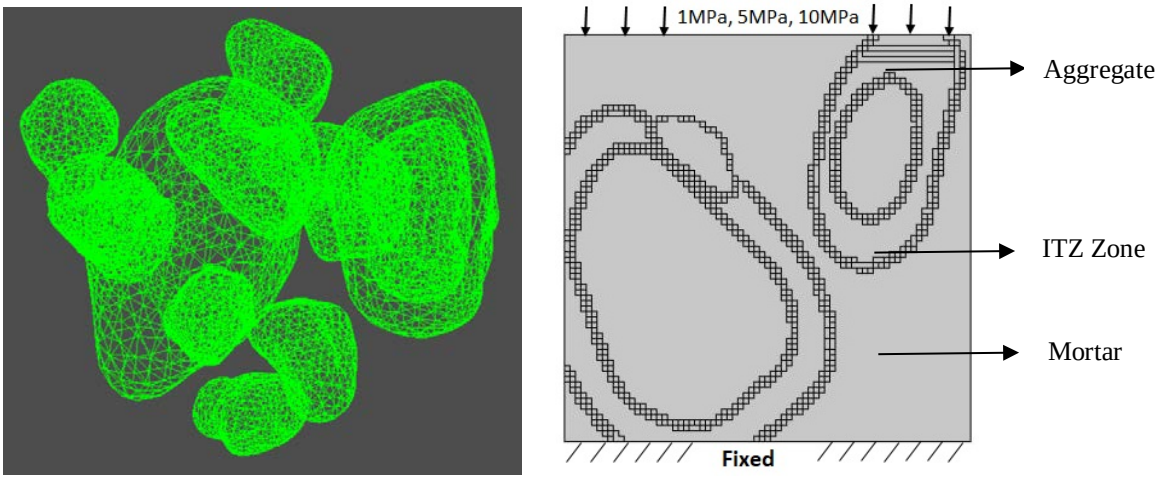

Figure 5-3 Concrete meso-scale geometry: (a) 3D Anm model, (b) Geometry under boundary conditions

A developed 3D prism was meshed using in-house MATLAB code to convert each pixel of 2D geometry into a quadrilateral element. Figure 5-3(b) shows the 2D mesh geometry of concrete prism block under loading conditions.

Case Studies of the Mitigation Materials

A case study for different proportions of the mitigation materials was also conducted, to check the efficiency of the Mitigation Model, and to guess the potential combination that can reduce the ASR expansion and damage. Mitigation scheme provided with additional benefit to the model in predicting service life and maintenance decisions. Table 5-5 shows this case study in detail.

Table 5-5 Case studies for Mitigation Model

Cases ID	Combinations	Representing Conditions
Case 1	25% FA, 75% Cement	Portland cement with moderate FA;
Case 2	50% FA, 50% Cement	Portland cement with high FA;
Case 3	30% SL, 70% Cement	Portland cement with moderate SL;
Case 4	50% SL, 50% Cement	Portland cement with high SL;
Case 5	5% SF, 95% Cement	Portland cement with moderate SF;
Case 6	10% SF, 90% Cement	Portland cement with high SF;
Case 7	25% FA, 5% SF, 70% Cement	Portland cement with moderate FA and SF;
Case 8	25% SL, 5% SF, 70% Cement	Portland cement with moderate SL and SF;
Case 9	20% FA, 10% SF, 70% Cement	Portland cement with moderate FA and high SF;
Case 10	20% SL, 10% SF, 70% Cement	Portland cement with moderate SL and high SF;

Thus, the developed mother model provides a user-friendly scheme, to run the model and simulate damage propagation in concrete. Figure 5-4 illustrates the algorithm needed to conduct the numerical analysis of the Mother Model. Table 5-6 summarizes the input parameters required by the algorithm.

Table 5-6 Input parameters for the Developed Model

Parameters	Explanations
C	Aggregate Type
RH	Ambient Relative Humidity
T	Ambient Temperature
H_20	Initial concentration based on surrounding water level
f_c'	Concrete's 28 days compressive strength
F	Boundary load
P_{FA}	% of FA (by mass) in the cementitious materials
P_{SL}	% of SL (by mass) in the cementitious materials
P_{SF}	% of SF (by mass) in the cementitious materials
P_C	% of cement (by mass) in the cementitious materials
t_{final}	Simulation time

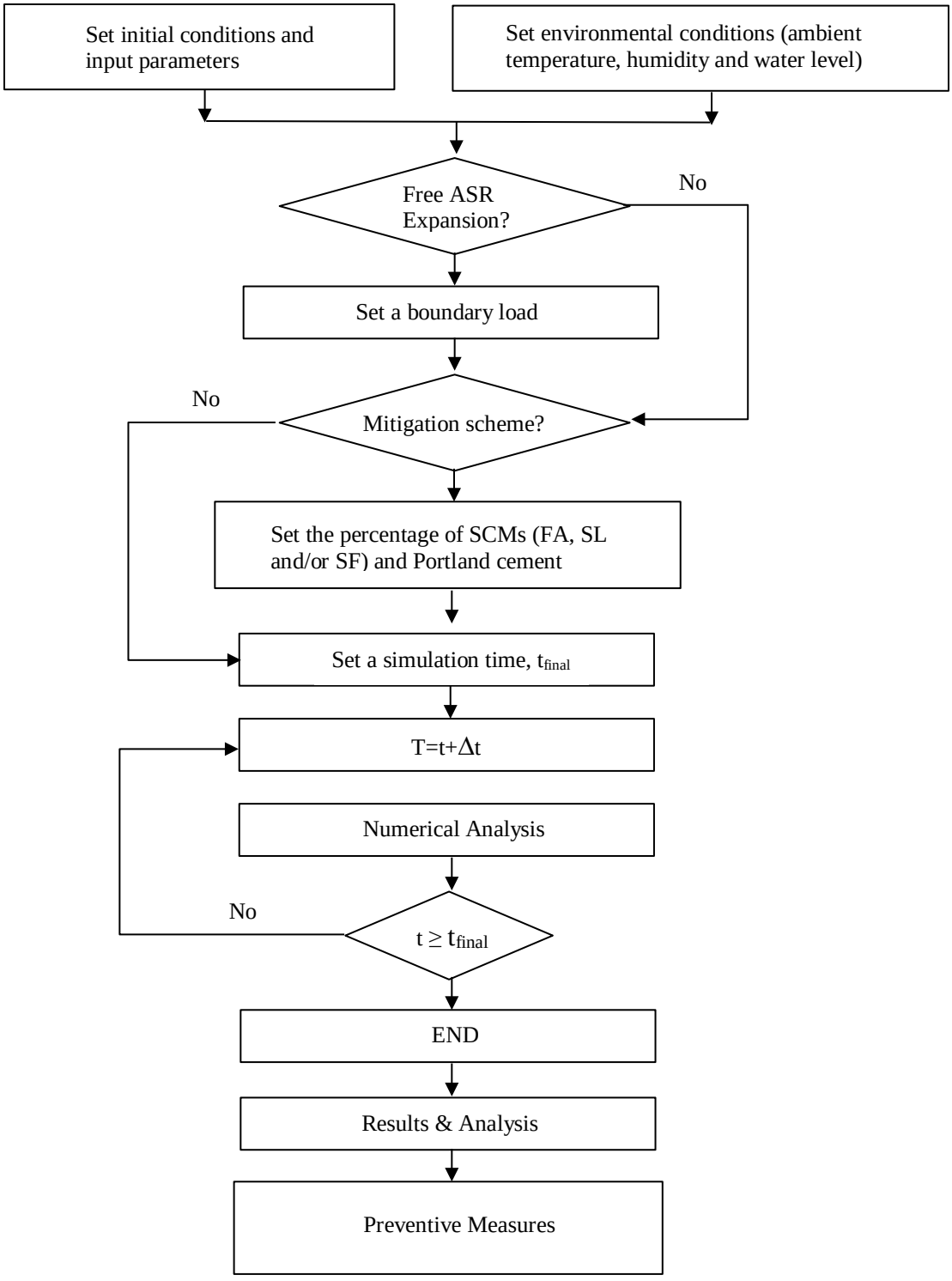

Figure 5-4 Algorithm for the numerical simulation

Here, concrete prism was considered as isotropic linear elastic material. Weather conditions considered in this study are presented in Table 5-7.

Table 5-7 Case studies for weather conditions

Case ID	Ambient Humidity (%)	Ambient Temperature (°C)	Initial Water Concentration [mole/m^3]	Representing Conditions
Case 1	100	38	0	Validation [29];
Case 2	100	60	0	Uncoated & maximum saturation; High temperature;
Case 3	80	60	0	High temperature and ambient humidity;

4. Results and Analysis

To extrapolate accurate data from the simulation results, a developed model was validated comparing with the 1 year experimental data of different aggregate types by assuming a free expansion under environmental case 1[23]. The simulated results represent the average value over the concrete domain.

The model was calibrated for different aggregate types. It was done by quantifying possible initial siloxane concentration and type factor for aggregates. Simulation was run to match with their 1 year expansions, as discussed in study [23]. Table 5-8 depicts the outcome of this study.

Table 5-8 Development of the model based on aggregate types [23]

Aggregate ID	**Initial Siloxane Concentration (mole/m^3)**	**Type Factor**
C1	608	0.856
C2	510	0.718
C3	235	0.331
C4	96	0.135
C5	367	0.517
C6	57	0.08
C7	1170	1.648
C8	**710**	**1**
C9	735	1.035
C10	808	1.138
C11	468	0.659
C12	838	1.180
C13	433	0.610
C14	430	0.605
C15	897	1.263
C16	200	0.282
C17	830	1.169

Following these values, developed models can be run as a representative model for each of the aggregate types, using their type factors.

An analytical comparison between simulated and experimental results [23] of all the aggregate types is presented in Table 5-9. The data presented in this Table defines the acceptability of the developed model.

Table 5-9 Comparison of results of the different coarse aggregates

Aggregate ID	**ASTM C 1293 1 Year Expansion (%)**	**Simulated 1 Year Expansion (%)**
C1	0.129	0.128
C2	0.112	0.110
C3	0.055	0.051
C4	0.020	0.017
C5	0.085	0.081
C6	0.010	0.008
C7	0.204	0.211
C8	**0.144**	**0.145**
C9	0.149	0.149
C10	0.159	0.161
C11	0.086	0.102
C12	0.163	0.166
C13	0.098	0.095
C14	0.097	0.094
C15	0.171	0.174
C16	0.047	0.043
C17	0.162	0.165

The 1 year simulated results lie closely with the experimental data. Thus, it is evident from the above Table that developed model is working perfectly in predicting future ASR expansions.

4.1. ASR Expansion

Figure 5-5(a) illustrates the evolution of ASR expansion with initial siloxane concentration, for different aggregate types. Siloxane, i.e. available silica defines the reactivity of each aggregate and ASR is accelerated as the concentration of it increases. Figure 5-5(b) shows the relation between ASR expansion and concrete's 28-days compressive strength. It is clear that increased strength provides more confinement to the structure, and thus, minimizes the expansion. The higher the strength, the lower the ASR expansion.

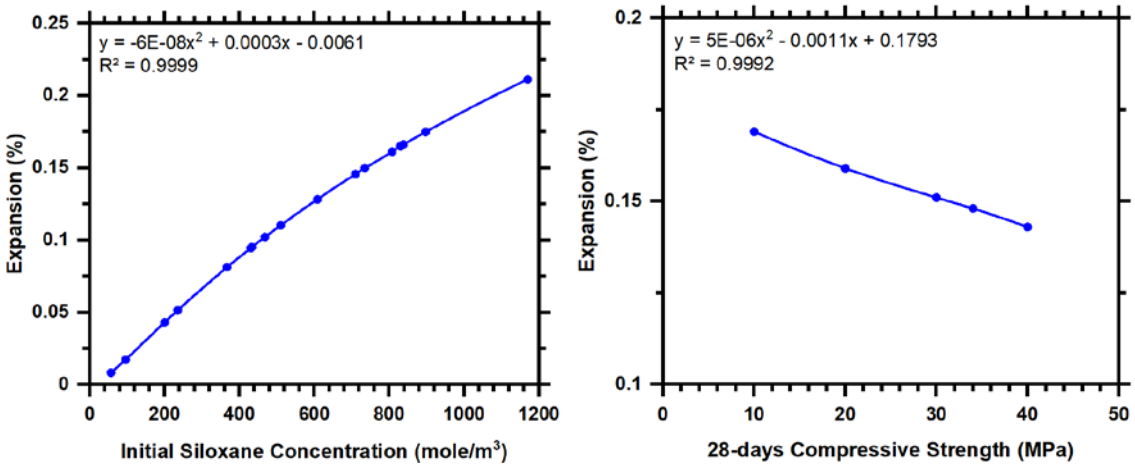

(a) (b)

Figure 5-5 Evolution of 1 year ASR expansion with: (a) initial siloxane concentration, (b) compressive strength of concrete

The expansion mechanism for different aggregate types was analyzed in this work. Figure 5-6 explains how aggregate type influences the expansion mechanisms. After 1 year ASR expansion is maximum for type C7 aggregate (0.21%) and minimum for type C6 aggregate (0.008). It is noteworthy, both aggregates are limestone material, but, they were collected from different regions. Thus, location of the gravel pit is an important factor in defining reactivity of coarse aggregates.

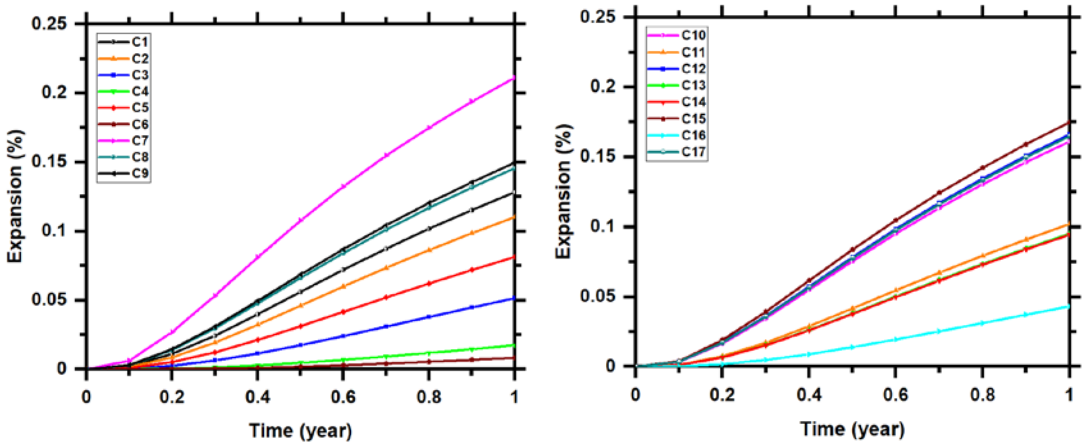

(a) (b)

Figure 5-6 Effects of aggregates on 1 year ASR expansion: (a) type C1-9, (b) type C10-17

4.2. Mechanical Impacts

This work studied how damage can potentially be evolved in concrete throughout its life cycle. Analysis was done to portray time dependent damage in the mechanical properties of concrete. Figure 5-7, 5-8, and 5-9 identify the changes in compressive strength, tensile strength, and modulus of elasticity, respectively. It is obvious that the concrete samples reached its maximum strength within around 90 days time period. This is consistent with the Strength Model discussed in section 3.5. Case 2 is the most severe case with high ASR expansion due to its extreme weather conditions, and hence, creates more damage. Case 3 has a very low ASR expansion and thus, it does't loss any strength within 1 year time period. On the other hand, type C7 is the most reactive aggregate for which concrete undergoes severe damage. Aggregate type C6 is a non-reactive aggregate and thus, its ASR damage remains minimum. It is clear that, concrete's strength reduces significantly just after that strength gaining period due to the ongoing ASR expansion. However, strength decreases with an increasing manner, and tends to stabilize by the end of 1 year.

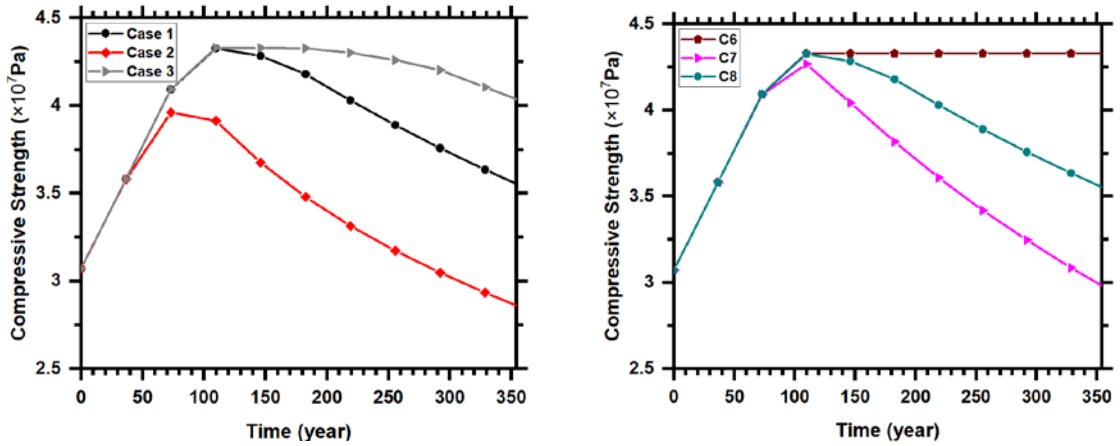

(a) (b)

Fig. 5-7 Change in the compressive strength of concrete: (a) weather case study in type C8 aggregate, (b) aggregates types study for weather case 1

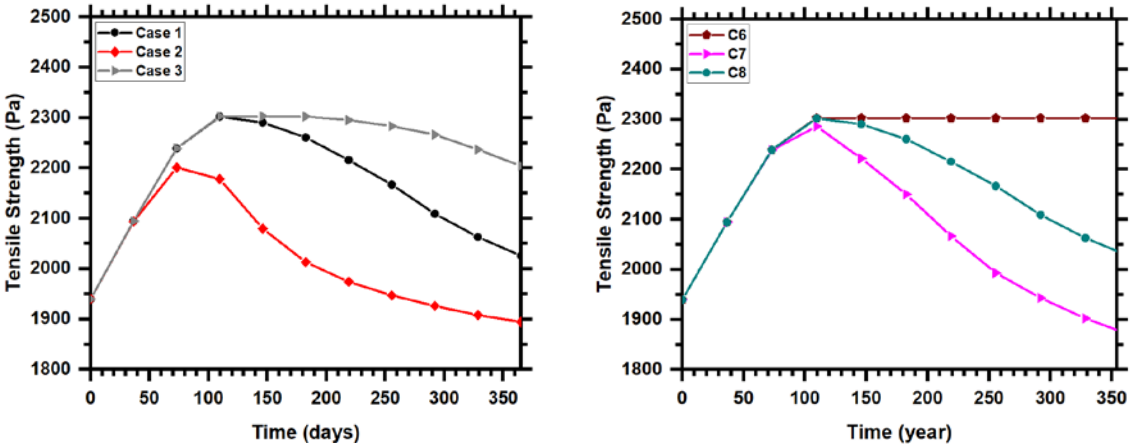

(a) (b)

Figure 5-8 Change in the tensile strength of concrete: (a) weather case study in Type C8 aggregate, (b) aggregates type study for weather case 1

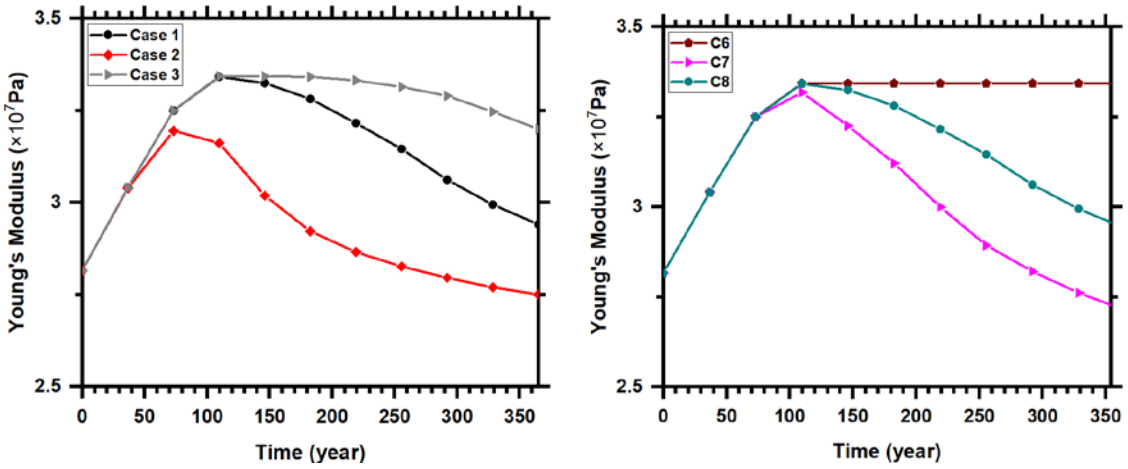

(a) (b)

Figure 5-9 Change in the Young's modulus of concrete: (a) weather case study in type C8 aggregate, (b) aggregates Type study for weather case 1

It is noteworthy that, concrete strength for case 2 and type C7 aggregate goes down beyond their initial strength at the end of 1 year. For instance, the peak of the compressive strength is 3.96×10^7 Pa and 4.27×10^7 Pa, which ends up with 2.83×10^7 Pa and 2.94×10^7 Pa, for case 2 type C8 aggregate and case 1 type C7 aggregate, respectively. If this strength reduction continues further and passes the threshold, it would damage the concrete microstructure, and subsequently, crack the surface. ASR damage can also potentially affect other related mechanical properties, i.e. modulus of rupture and reduce the fatigue and service life of concrete.

This work also analyzed the damage in concrete, generating from ASR and these mechanical changes.

Figure 5-10 depicts the aggregates damage propagation under ASR expansion. Maximum damage happens in type C7 aggregate (0.32), whereas, type C6 doesn't show any damage at the end of 1 year, because of its low ASR expansion (<0.1%).

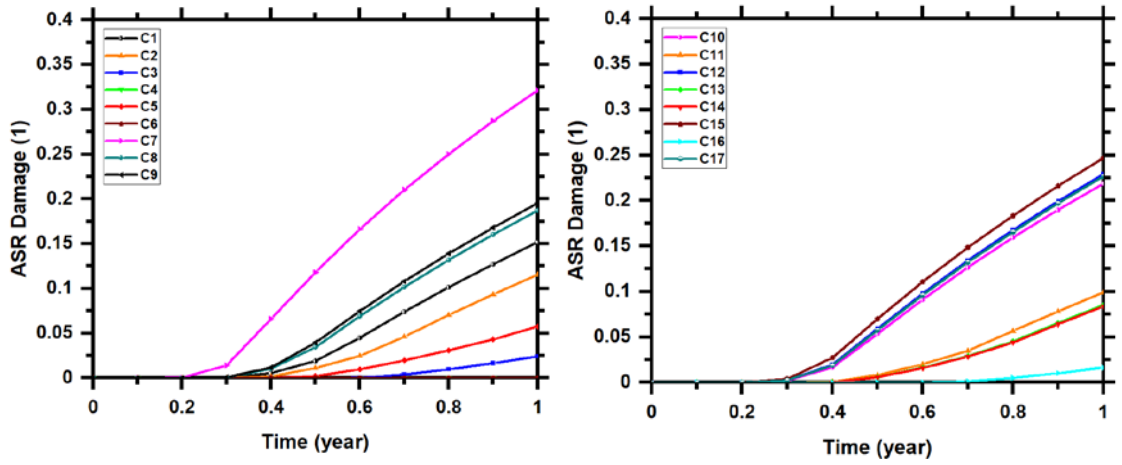

(a) (b)

Figure 5-10 ASR-induced damage for case 1 in different aggregates: (a) type C1-9, (b) type C10-17

Figure 5-11 simulates ASR damage on these aggregates for 10 years period. C7 has the maximum damage (0.91) and C6 has the minimum damage (0.09), at the end of 10 years. It is clear that damage in C6 is not zero anymore when subjected to ASR expansion for a longer period. These are consistent with their expansions and aggregate mineralogy as plotted in Figure 5-6. It is noteworthy that, coarse aggregates C4 and C6 can be considered as innocuous because of their low damage after 10 years.

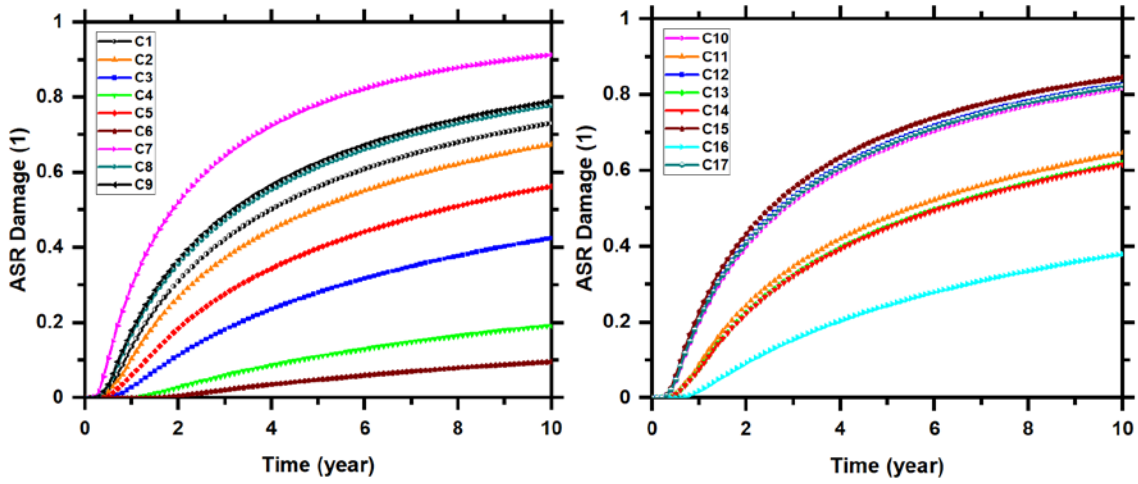

(a) (b)

Figure 5-11 ASR induced damage for aggregates under case 1 and 10 years expansion: (a) type C1-9, (b) type C10-17

Thus, a dedicated mitigation scheme is necessary to effectively minimize ASR damage in concrete.

4.3. Mitigation Scheme

Mitigation schemes were studied based on the cases presented in Table 5. Analysis was done for the most severe ASR condition (case 2 environment and type C7 aggregate). Figure 5-12(a) compares the 1 year expansion for different supplementary cementing materials. It is obvious that case 3-6, 8, and 10 can't significantly minimize the ASR expansion. Hence, SL and SF can't mitigate the ASR damage alone. On the other hand, case 1, 2, 7, and 9 significantly reduce the expansion and associated damage below 0.05% and 0.05, respectively. Hence, FA is the most effective material in mitigating ASR damage. FA reduces the ROH content through pozzolanic reaction in cement-concrete. Maximum result is found for case 2 with 50% FA content. Figure 5-12(b) presents a snapshot of all the supplementary materials used in the mitigation scheme.

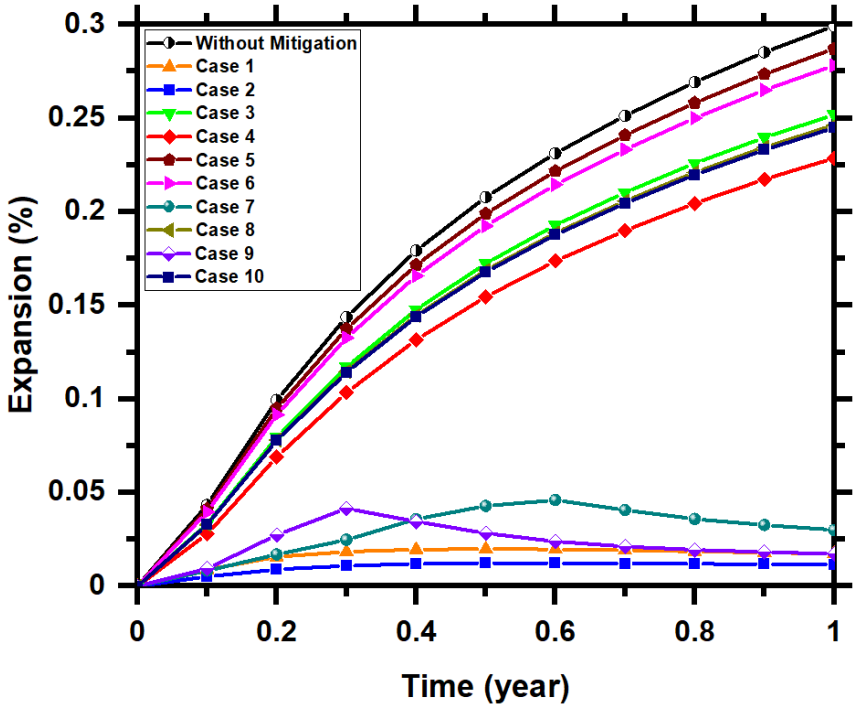

(a)

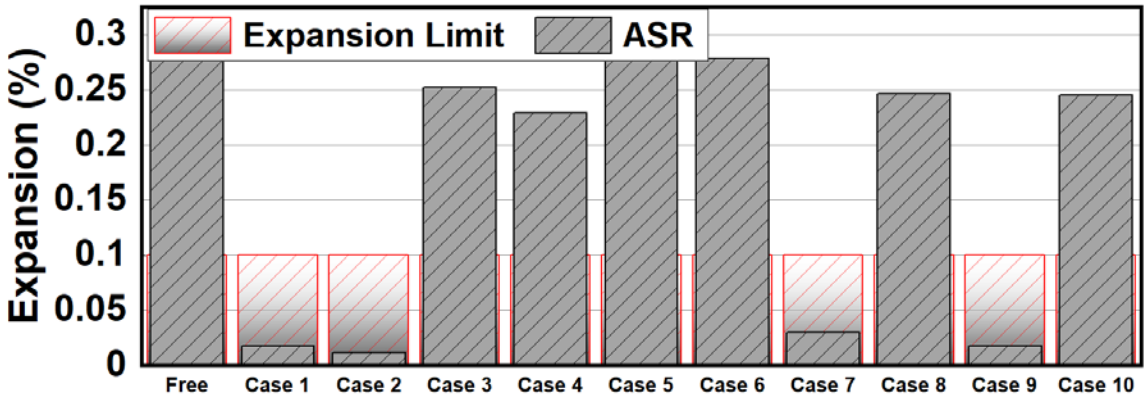

(b)

Figure 5-12 Effects of mitigation materials on 1 year expansion (a) Expansion vs time (b) Maximum expansion

Thus, high FA content is useful in minimizing ASR expansion. However, high FA content can cause low temperature problems in concrete mix during winter season. High FA also reduces the relative strength of hard concrete significantly [33]. To solve this problem, case 9 can be used (20% FA and 10% SF) instead. Furthermore, the effectiveness

of FA in reducing ASR expansions depends on the type of fly ash and its chemical composition (ROH content). That's why, FA content to be applied should be decided based on its type, reactivity of the aggregate, and weather condition around the concrete structure.

Figure 5-13 visualizes the effects of case 9 mitigation scheme on the mechanical properties of concrete. The mitigation scheme significantly improves the mechanical strength of ASR-damaged concrete. The 1 year compressive strength, tensile strength, Young's modulus before the mitigation scheme are 2.15×10^7 Pa, 1735.6 Pa, and 2.52×10^7 Pa, respectively which get boosted up to 4.48×10^7 Pa, 2300.35 Pa, and 3.42×10^7 Pa, respectively after the application of mitigation materials. Thus, case 9 effectively preserves the concrete strength under ASR susceptible environment. Thus, no further reduction in concrete's strength is possible under this combination, at least not from ASR phenomenon.

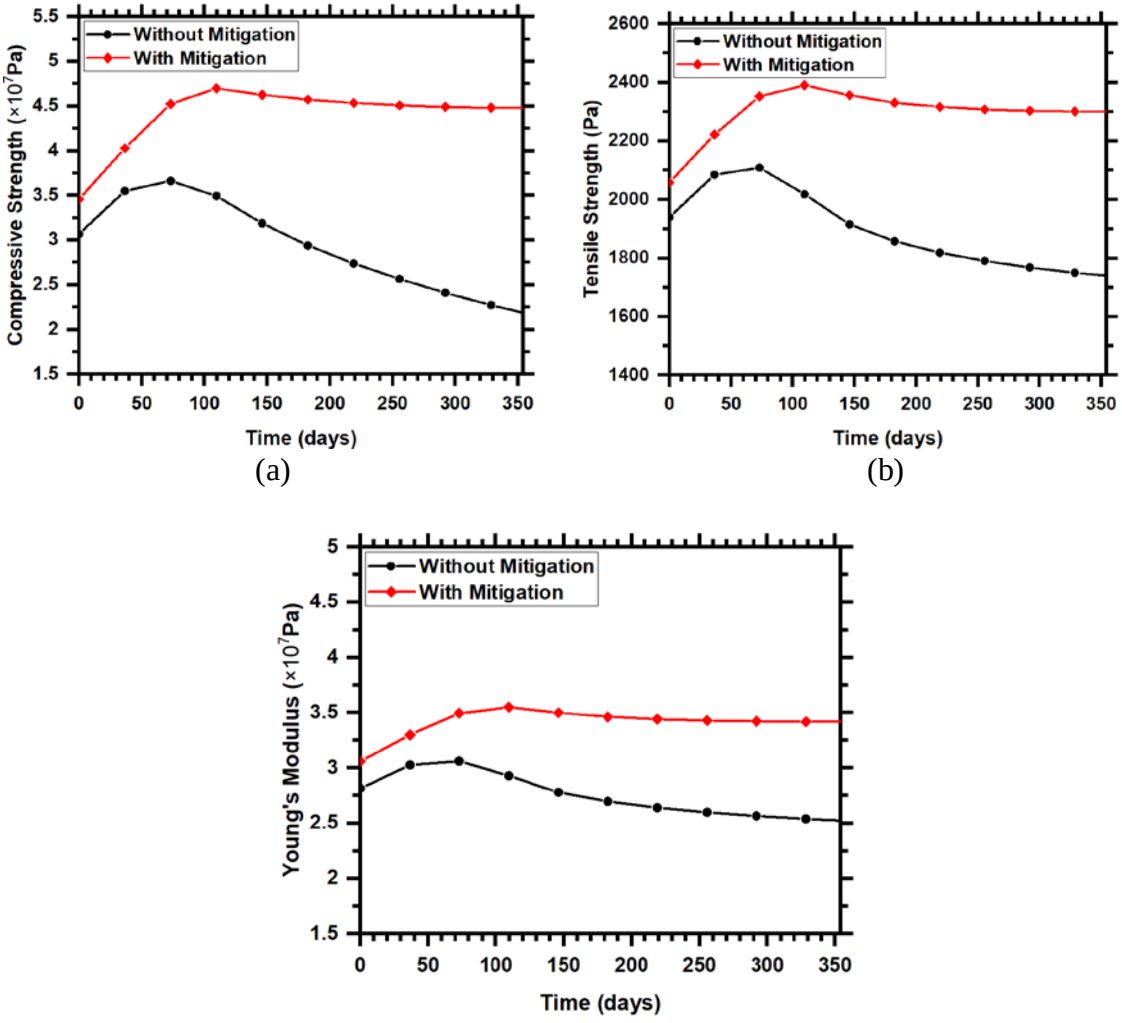

Figure 5-13 1-year strength in concrete under case 9 mitigation combination: (a) compression, (b) tension, (c) Young's modulus

This work also determined damage function-based damage rating factor (DRF) for the discussed 17 types of coarse aggregates. This is an effort to identify the reactivity of these aggregates and their possible outcomes under the mitigation scheme. Table 5-10 shows the DRF for all aggregates under case 1 weather and case 9 mitigation scheme.

Table 5-10 Comparison of 1 year DRF for different coarse aggregates

Aggregate ID	Before Mitigation	After Mitigation (Case 20)
C1	0.151797871	0.000085
C2	0.115466367	0
C3	0.024206191	0
C4	0.0000032	0
C5	0.057517002	0
C6	0	0
C7	0.321199783	0.007
C8	**0.187090331**	**0.0009**
C9	0.195295601	0.0012
C10	0.218661571	0.002
C11	0.099125814	0
C12	0.228919562	0.0024
C13	0.085169005	0
C14	0.08372523	0
C15	0.246665444	0.0032
C16	0.016391689	0
C17	0.226516951	0.00238

Finally, an extended analysis of a 30 year period was done on the developed model on a type C7 aggregate under case 1 environment and case 9 mitigation scheme, to check the effectiveness of supplementary cementing materials in minimizing long-term ASR damage. Fig. 14 shows that before the mitigation scheme ASR expansion lies mostly in the damage zone (expansion>0.1%) and maximum expansion becomes 0.54% after 30 years. However, with the application of the mitigation scheme ASR expansion remains well below the threshold limit (0.1%) throughout the 30 year simulation period.

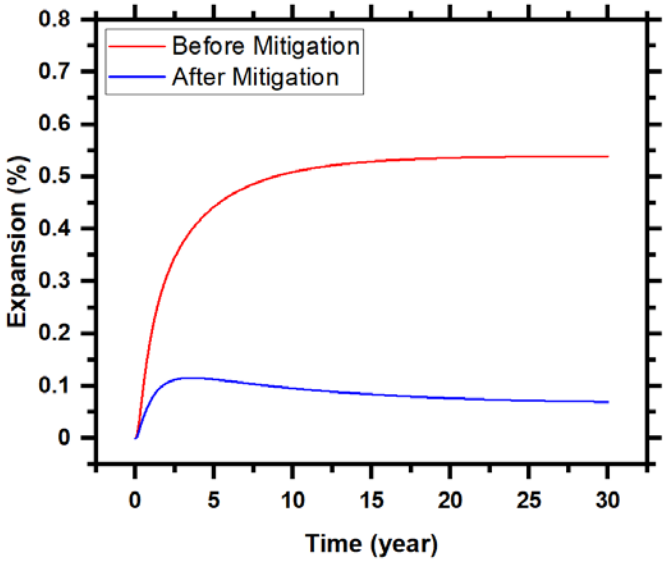

Figure 5-14 Effect of the mitigation scheme on 30 years ASR expansion

Thus, it is evident that the developed model of this work can potentially predict the ASR damage, and service life of concrete under variable environmental conditions, and can mitigate the damage with an effective combination.

5. Conclusions

This work presents the 3D concrete prism at the meso-scale and proposes a chemo-physio-mechanical model to predict and mitigate ASR damage. A processed slice from the 3D Anm model captures the composite skeleton of hardened concrete. Model construction includes time-dependent aging and mechanical damage along with a mitigation scheme for different aggregate types. Strength based governing equations formulated in the model, are the major contributions of this work. Moreover, introduction of the aggregate types and a dedicated mitigation scheme in the damage model is the first ever implementation in a model, to the best of the authors' knowledge. The simulated results from the model capture chemo-physic-mechanical processes involved in the ASR kinetics and gel production, from a close perspective. The quantitative and comparative analysis of the results magnify these phenomenon for a better understanding.

ASR expansions progress proportionally with the silica content of reactive aggregates. High initial concentration of siloxane from reactive aggregates will lead to higher ASR expansion and damage. Stress generated from the ASR expansion greatly affect the concrete mechanical strength, and ultimately crack the structure when the overall capacity reduced beyond its threshold. The 17 types of coarse aggregates considered in this work represent a wide range of mineralogical compositions. This is an effort in mapping the reactive aggregates across North America. Aggregate type C7 Limestone from Ontario, CA is highly reactive and contains high initial concentration of siloxane, i.e. silica (1170 mole/m^3). Thus, for obvious reason it comes up with the maximum damage after 10 years (0.91). On the other hand aggregate type C6 Limestone from San Antonio, TX is highly non-reactive and the maximum damage after 10 years is very low (0.09). Reactive aggregate can also significantly reduce the overall capacity of structural concrete by initiating chemical reaction to the right direction. Reactive C7 Limestone can reduce the compressive strength by 32.1%, tensile strength by 18.8%, and Young's modulus by 18.86% under a fixed environment at the end of 1 year simulation period. A damage rating factor (DRF) has also been assigned to 17 aggregates from different locations and mineralogy to facilitate the choice of materials in structural concrete design.

Ambient temperature and humidity accelerate the ASR mechanism, whereas better compressive strength of concrete can impede such type of expansion. High temperature and humidity increase the ASR expansion which further reduces the concrete strength. A 57.9% increase in temperature reduced the compressive strength by 19.6%, tensile strength by 6.48%, and Young's modulus by 6.46% for type C8 aggregate. A 25% increase in

humidity reduced the compressive strength by 29.4%, tensile strength by 14.05%, and Young's modulus by 14.06% for type C8 aggregate.

Among the many supplementary cementing material combinations case 1(25% FA), case 2 (50% FA), case 7 (25% FA, 5% SF) and case 9 (20% FA, 10% SF) are the most active in minimizing ASR expansion, and they can keep ASR damage generated from highly reactive type C7 Limestone way below the damage zone (expansion <0.1%). Thus, it is evident that the amount of fly ash in the combination mostly defines the effectiveness of the choice of SCMs in controlling ASR expansion. However, for the structures located in the cold regions, this study suggests using case 9, a combination of 20% fly ash and 10% silica fumes, to limit the gel production. Moreover, a 30 years simulation predicts that a suitable mitigation scheme (case 9) can keep the ASR expansion as well as damage below the threshold limit and thus, justifies its applicability for a long term damage prevention.

This developed model can be used further for any concrete structures by changing the input parameters, to see the evolution of ASR expansion before and after the mitigation. Mitigation scheme facilitates the application of fly ash, slag, and silica fumes in minimizing ASR-induced damage. Thus, this model can be very crucial in decision making from the management perspective, i.e. whether to replace or repair the structure, when or how to repair the structures etc. It can save huge chunk of money and guide the cement-concrete industry. There is also a great potential for this model to update in future. The analyzed and processed data from different cases studies can be fed into a machine learning algorithm to train it and develop a stand-alone software. Hence, developed model from this work seems profitable and represents a powerful tool with versatile applications.

Author Contribution Statement

The authors confirm contribution to the paper as follows: study conception and design: Md. Asif Rahman, Yang Lu; model development: Md Asif Rahman; analysis and data collection: Md Asif Rahman; draft manuscript preparation: Md. Asif Rahman; approval of the final version of manuscript: Yang Lu.

Acknowledgements

Declarations of interest

None.

Funding

This research did not receive any specific grant from funding agencies in the public, commercial, or not-for-profit sectors.

References

[1] Powers, T. C., H. H. Steinour. An Interpretation of Some Published Researches on the Alkali-Aggregate Reaction Part 1-The Chemical Reactions and Mechanism of Expansion. Journal of the American Concrete Institute, 1955. 26(6): 497-516.

[2]. Poyet, S., A. Sellier, B. Capra, G. Thèvenin-Foray, J. M. Torrenti, H. Tournier-Cognon, and E. Bourdarot. Influence of Water on Alkali-Silica Reaction: Experimental Study and Numerical Simulations. Journal of Materials in Civil Engineering, 2006. 18: 588-596.

[3] Hou, X., L. J. Struble, R. J. Kirkpatrick. Formation of ASR gel and the roles of CSH and portlandite. Cement and Concrete research, 2004. 34(9): 1683-1696

[4]. Prezzi, M., P. J. M. Monteiro, and G. Sposito. The Alkali-Silica Reaction, Part I: Use of the Double-Layer. ACI Materials Journal, 1997. January-February: 10-16.

[5]. Gholizadeh Vayghan, A. Characterization Of the Rheological and Swelling Properties of Synthetic Alkali Silicate Gels in Order to Predict Their Behavior in ASR Damaged Concrete. Doctoral dissertation, Civil and Environmental Engineering, The Pennsylvania State University, USA, 2017.

[6]. Ono K (1990). "Strength and stiffness of alkali silica reaction concrete and concrete members." structural engineering review 2: pp121-125.

[7]. Swamy R.N (1992). "Testing for alkali-silica reaction in concrete." the alkali silica reaction in concrete ed R N Swamy, Blackie, Van Nostrand Reinhold: pp54-95.

[8]. Swamy R.N, a. A.-A. M. M. (1986). "Influence of Alkali silica reaction on the engineering properties of concrete." Alkalis in concrete, ASTM STP 930, Ed, V.H. Dodson, American society for testinfg and materials Journal, Philadelphia: pp69-86.

[9]. Monette L.J, G. N. J., Grattan-Bellew P.E, (2000). "Structural effects of the alkali aggregate reactions on non-loaded and loaded reinforced concrete beams." 11th international conference on alkali aggregate reaction: pp999-1008.

[10]. Al-Asali, S. a. (1988). "Engineering properties of concrete affected by alkali silica reactions." ACI materials Journal: pp367-374.

[11]. Charlwood R.G (1992). "A review of alkali-aggregate reactions in hydro-electric plants and dams." International conference on Alkali aggregate reactions in hydro-electric plants and dams, fredericton, New brunswick, Canada.

[12]. Larive C (1998). "apports combinés de l'expérimentation et de la modélisation à la compréhension de l'alcali réaction et de ses effets mécaniques." LCPC thèse: 395pages.

[13]. M. Ben Haha, Mechanical Effects of Alkali Silica Reaction in Concrete Studied by SEM-Image Analysis Doctoral dissertation, École Polytechnique Fédérale de Lausanne. À La Faculté Sciences Et Techniques De L'ingénieur, France, 2006.

[14]. Touma, W. E., D. F. Fowler, and R. L. Carrasquillo. Alkali-Silica Reaction in Portland Cement Concrete: Testing Methods and Mitigation Alternatives. Research Report ICAR 301-1F. International Center for Aggregates Research (ICAR), The University of Texas at Austin, 2001.

[15]. Yi, C.K., C.P. Ostertag. Mechanical approach in mitigating alkali-silica reaction. Cement and Concrete Research, 2005. 35(1): 67-75.

[16]. Javier Malvar, L., Lary R. Lenke. Efficiency of Fly Ash in Mitigating Alkali-Silica Reaction Based on Chemical Composition. ACI Materials Journal, 2006. 103(5): 319-326.

[17]. Folliard , K. J., Ryan Barborak, Thano Drimalas, Dr. Lianxiang Du, Sabrina Garber, Jason Ideker, Tyler Ley, Stephanie Williams, Maria Juenger, Benoit Fournier, and M.D.A. Thomas. Preventing ASR/DEF in New Concrete: Final Report. Publication FHWA/TX-06/0-4085-5. FHWA, U.S. Department of Transportation, 2006.

[18]. L.F.M. Sanchez et al, "Comparative study of a chemo–mechanical modeling for alkali silica reaction (ASR) with experimental evidences." Construction and Building Materials 72 (2014) 301–315

[19]. Rossella Pignatelli, Claudia Comi, Paulo J.M. Monteiro, “A coupled mechanical and chemical damage model for concrete affected by alkali–silica reaction.” Cement and Concrete Research 53 (2013) 196–210

[20]. Stéphane Multon, Alain Sellier, Martin Cyr, “Chemo–mechanical modeling for prediction of alkali silica reaction (ASR) expansion.” Cement and Concrete Research 39 (2009) 490–500

[21]. Alain B. Giorla*, Karen L. Scrivener, Cyrille F. Dunant, “Influence of visco-elasticity on the stress development induced by alkali–silica reaction.” Cement and Concrete Research 70 (2015) 1–8

[22]. ASTM C1293. Standard Test Method for Concrete Aggregates by Determination of Length Change of Concrete Due to Alkali-Silica Reaction. American Society for Testing and Materials (ASTM) International.

[23]. Folliard , K. J., Ryan Barborak, Thano Drimalas, Dr. Lianxiang Du, Sabrina Garber, Jason Ideker, Tyler Ley, Stephanie Williams, Maria Juenger, Benoit Fournier, and M.D.A. Thomas. Preventing ASR/DEF in New Concrete: Final Report. Publication FHWA/TX-06/0-4085-5. FHWA, U.S. Department of Transportation, 2006.

[24]. Saouma, V. E., R.A. Martin, M. A. Hariri-Ardebili, and T. Katayama. A Mathematical Model for the Kinetics of the Alkali–Silica Chemical Reaction. Cement and Concrete Research, 2015. 68:184-195.

[25]. Sargent, P. 21 - The development of alkali-activated mixtures for soil stabilisation. Handbook of Alkali-Activated Cements, Mortars and Concretes, 2015. P: 555-604.

[26]. Papadakis, V.G. Effect of fly ash on Portland cement systems: Part II. High-calcium fly ash. Cem. Concr. Res., 2000. 30: 1647–1654.

[27]. Rahman, Md. Asif, Yang Lu. A Time-Dependent Chemo-Mechanical Analysis of Alkali-Silica Reaction for the Disparate Geometry of Concrete Meso-Structure. Journal of Construction and Building Materials, 2019. Volume 211, 847-857.

[28]. Rahman, Md. Asif, Yang Lu. A Stochastic Model to Evaluate Alkali-Silica Reaction (ASR) in Concrete Subject to Global Warming and Climate Change Impacts. Journal of Cement and Concrete Composites, 2020. (Under Review).

[29]. ASTM C1293. Standard Test Method for Concrete Aggregates by Determination of Length Change of Concrete Due to Alkali-Silica Reaction. American Society for Testing and Materials (ASTM) International.

[30]. Thomas, M. D. A., B. Fournier, and K. J. Folliard. Alkali-Aggregate Reactivity (AAR) Facts Book. Publication FHWA-HIF-13-019. FHWA, U.S. Department of Transportation, 2013

[31]. Balbo, F. A. N., G. A. Pianezzer, L. M. Gramani, E. Kaviski, and M. R. Teixeira. An Application to the Diffusion Equation in a Model for the Damage in Concrete Due to Alkali-Silica Reaction. Applied Mathematical Sciences, 2015. 9: 4135-4147.

[32]. Hiroaki Takiya, Naoko Watanabe, Tamotsu Kozaki & Seichi Sato (2015) Effects of water to-cement ratio and temperature on diffusion of water in hardened cement pastes, Journal of Nuclear Science and Technology, 52:5, 728-738, DOI: 10.1080/00223131.2014.979902.

[33]. A.M. Neville. Properties of Concrete. Pearson Education Limited, 2011.

[34]. Shohana Iffat. Relation between Density and Compressive Strength of Hardened Concrete. Concrete Research Letters, 2015. 6(4): 182-189.

[35]. Victor E. Saouma. Numerical Modeling of AAR. Taylor & Francis Group, London, UK, 2014.

[36]. M. Y. H. Bangash. Manual of Numerical Methods in Concrete: Modelling and Applications Validated by Experimental and Site-Monitoring Data. Thomas Telford Publishing, 2001.

[37]. Lu, Yang, Md. Aminul Islam, Stephen Thomas, Edward J.Garboczic. Three-dimensional mortar models using real-shaped sand particles and uniform thickness interfacial transition zones: Artifacts seen in 2D slices. Journal of Construction and Building Materials, 2020. Volume 236, 117590.

[38] S. Thomas, Y. Lu, E. Garboczi, Improved model for three-dimensional virtual concrete: Anm model, J. Comput. Civ. Eng. 30 (2) (2016). 04015027-04015027.

CHAPTER SIX: CONCLUSIONS, RECOMMENDATIONS, LIMITATIONS AND FUTURE RESEARCH SCOPE

Conclusions

This thesis work summarized four specific tasks to address in a modeling platform. The first task and associated solutions are addressed in manuscript # 1. Here concrete degradation in rigid pavement was analyzed in a three-dimensional multiphysics model. Major contribution of the work was the development of governing equation sets which integrated coupled thermo-hygro-mechanical (THM) model, material mesoscale details and damage modes in the numerical model. Simulated results confirmed that average expansion in concrete starts after the latency period and then continues to increase with a decreasing rate. When reaction starts, the ASR expansion is amplified for the initial years, and after that it tends to stabilize along with the depletion of alkali-hydroxides concentration from the porous media. Traffic loadings on the pavement play a vital role on the evolution of ASR expansion. ASR expansion and associated damage can be minimized by following three strategies: using non-reactive aggregates, limiting the maximum alkali content of concrete and limiting the moisture availability in the field structures.

The second task and associated solutions are addressed in manuscript # 2. This work analyzes the ASR chemophysics and concrete properties in a two-dimensional model. Meso-scale geometry was developed in virtual cement-concrete lab to develop concrete media with different cement-aggregate proportions and chemical species concentrations. Coupled mass and momentum balance equations and their application in the numerical

model are the major contributions of this work. ASR expansion continues as long as there are enough reactive silica, alkali hydroxide and water content in concrete structure. Depletion of any one of these contents may limit the ASR production and gel diffusion. ASR expansion is severe under concrete with high reactive aggregate proportions and high hydroxyle ion concentrations. External load or constraint has potential to mitigate ASR damage in concrete.

The third task and associated solutions are addressed in manuscript # 3. This work renders concrete prism in a two-dimensional meso-scale geometry and adds stochastic model to simulate effects of extreme weather events on the ASR evolution and expansion. This is critical innovation of this work that links random environmental conditions to the ASR mechanisms under partially/variably saturated porous media. Uncoated concrete with easy access to water is more susceptible to ASR damage. Nuclear reactors or concrete dams submerged in water can be a perfect examples of these situations. On the other hand, any concrete structure which are effectively coated or don't have easy access to water are less susceptible to ASR damage. An ASR damaged concrete can show up further expansion with late water supply to the structure. On the other hand, constant drying under low humidity can minimize further expansion significantly. Frequent expansion-contraction and non-linear change in concrete volume under the effects of extreme weather events can break the cement-aggregate chemistry and damage the structure faster.

The fourth task and associated solutions are addressed in manuscript # 4. This work processed a two-dimensional slice from the 3D Anm model to capture the composite skeleton of hardened concrete. Model construction includes time-dependent aging and mechanical damage along with a mitigation scheme for different aggregate types. Strength

based damage model along with the mitigation scheme are the major contributions of this work. This is the first ever implementation in a model, to the best of the authors' knowledge. Reactive aggregate with high silica concentration will develop faster ASR expansion and damage. This expansion will develop micro-cracks in the concrete skeleton which can significantly reduce the load carrying capacity of the structure. This work also analyzed the behavior of 17 different types of aggregate from different mineral sites to map the reactive coarse aggregate across North America. ASR expansion is reduced under the impact of creep loadings. However, a mitigation scheme with a diverse choice of supplementary materials can be the conclusive solution to ASR problems. Among the many supplementary cementing materials fly ash is most effective in minimizing ASR expansion.

Recommendations, Limitations and Future Research Scopes

The developed model from this thesis work can be very crucial for other concrete structures in predicting the evolution of ASR expansion as well as service life under the real world environmental conditions. It can be helpful in decision making from the management perspective, i.e. whether to replace or repair the structure, when or how to repair the structures etc. It can save huge chunks of money and guide the cement-concrete industry. Thus, this work will advance in the field of resilience and sustainable infrastructure development by supporting on-time prediction and adaptive management to account for the weather uncertainty.

Pressure of crystallization was not included in this developed model. The effect of crystallization and subsequent expansion is a mechanism of alkali-carbonate reaction (ACR). Thus, this model is valid for alkali-silica reaction (ASR) only. The damage model is for isotropic concrete block only.

However, the developed governing equation set can be calibrated further for any concrete structure by changing the input parameters, initial concentrations of chemical species, concrete density, and loading conditions according to the purpose, proportion or properties of concrete domain. There is also a great potential for this model to update in future. The analyzed and processed data from different cases studies can be fed into a machine learning algorithm to train it and develop a stand-alone software. Hence, developed model from this work seems profitable and represents a powerful tool with versatile applications.

.